
Electronic Thesis and Dissertation Repository

4-17-2014 12:00 AM

Peptidomimetic GHS-R1a Agonists as PET Imaging Agents for Prostate Cancer

Milan M. Fowkes
The University of Western Ontario

Supervisor
Dr. Leonard G. Luyt
The University of Western Ontario

Graduate Program in Chemistry
A thesis submitted in partial fulfillment of the requirements for the degree in Master of Science
© Milan M. Fowkes 2014

Follow this and additional works at: <https://ir.lib.uwo.ca/etd>

 Part of the [Medicinal-Pharmaceutical Chemistry Commons](#), and the [Radiochemistry Commons](#)

Recommended Citation

Fowkes, Milan M., "Peptidomimetic GHS-R1a Agonists as PET Imaging Agents for Prostate Cancer" (2014). *Electronic Thesis and Dissertation Repository*. 1972.
<https://ir.lib.uwo.ca/etd/1972>

This Dissertation/Thesis is brought to you for free and open access by Scholarship@Western. It has been accepted for inclusion in Electronic Thesis and Dissertation Repository by an authorized administrator of Scholarship@Western. For more information, please contact wlsadmin@uwo.ca.

**PEPTIDOMIMETIC GHS-R1A AGONISTS AS PET IMAGING AGENTS FOR
PROSTATE CANCER**

(Thesis format: Monograph)

by

Milan Mrázek Fowkes

Graduate Program in Chemistry

A thesis submitted in partial fulfillment
of the requirements for the degree of
Master of Science

The School of Graduate and Postdoctoral Studies
The University of Western Ontario
London, Ontario, Canada

© Milan Mrázek Fowkes 2014

Abstract

Contemporary diagnostic techniques for prostate cancer (PCa) have a limited ability to distinguish between benign and malignant disease. The ghrelin receptor has a differential expression in normal, benign and cancerous prostatic tissue. Targeting this receptor with ^{18}F -radiolabelled peptidomimetics would enable differentiation between these disease states *via* PET imaging. A series of ^{19}F -peptidomimetics were synthesized and characterized by HRMS, HPLC and ^1H -NMR spectroscopy in order to test locations for ^{18}F radioisotope insertion. Competitive receptor binding assays using HEK293/GHS-R1a cells were used to evaluate compound binding affinities. This led to the identification of two lead compounds: [1-Nal⁴,Lys⁵(4-FB)]G-7039 (IC₅₀ = 69 nM) and [Lys⁵(2-FP)]G-7039 (IC₅₀ = 19 nM). Prosthetic group radiolabelling of [1-Nal⁴,Lys⁵(4-FB)]G-7039 using N-succinimidyl 4-[^{18}F]fluorobenzoate gave radiochemical yields of 51-52%, radio-purity > 98% and specific activity of 116 MBq/ μmol after 127 minutes at end-of-synthesis. Successful ^{18}F -radiolabelling of [1-Nal⁴,Lys⁵(4-FB)]G-7039 highlights its potential for use as a PET imaging agent for early-stage PCa diagnosis.

Keywords

Molecular imaging, prostate cancer, positron emission tomography, imaging agents, growth hormone secretagogues, ghrelin receptor agonists, GHS-R1a, ghrelin, peptidomimetics, solid-phase peptide synthesis, ^{18}F -radiolabelling, G-protein coupled receptors.

Co-Authorship Statement

Chapter 2: The work presented herein was performed solely by the author. The only exception was the transfection of HEK293 cells with the GHS-R1a. This was conducted by Rebecca McGirr, a research technician in the lab of collaborator Dr. Dhanvantari, an Assistant Professor in Medical Biophysics and Medicine at the University of Western Ontario. In addition, the calcium flux assays were performed by EMD Millipore's GPCRProfiler® service.

“I have not failed. I’ve successfully discovered 10,000 things that won’t work.”

-Thomas Edison

Acknowledgments

First of all, I would like to thank my supervisor Dr. Luyt for all the help, support and guidance he gave me during the course of my master's thesis, especially his willingness to pause in the middle of his work and devote some time to help me move my project forward, whatever the time of day might have been.

Special thanks go to Dr. Lihai Yu for his extensive knowledge of chemical syntheses and especially for his help in ^{18}F -radiochemistry!

I would also like to extend my thanks to the following people: André (for teaching me peptide synthesis), Dana and Brian (for their helpful suggestions and training) and of course all other students, technicians and post-docs in our lab who kept me motivated and working hard until the very end.

Special thanks also go to Dr. Dhanvantari and Dr. Kovacs at the Lawson Health Research Institute for allowing me to carry out radioligand binding assays and ^{18}F -radiolabelling of my compound in their respective laboratories. Thanks also to Becky for providing me with materials, cell pellets and supplies for the aforementioned assays.

Finally, I would like to thank my family and close friends for supporting me during the course of my studies, despite many of them being so far away.

Table of Contents

Abstract.....	ii
Co-Authorship Statement	iii
Acknowledgments.....	v
Table of Contents	vi
List of Tables	ix
List of Figures.....	x
List of Schemes	xii
List of Appendices	xiii
List of Abbreviations and Symbols.....	xiv
Chapter 1	1
Molecular Imaging.....	1
1.1 Introduction.....	1
1.2 Prostate Cancer	2
1.3 Imaging Modalities.....	3
1.4 Fluorine-18 Positron Emission Tomography.....	4
1.5 Peptide-based Imaging Agents	6
1.6 Scope of Thesis.....	9
Chapter 2.....	11
The Design and Synthesis of Peptidomimetic GHS-R1a Agonists as PET Imaging Agents for Prostate Cancer.....	11
2.1 Introduction.....	11
2.2 Agonists and Antagonists in Molecular Imaging	14
2.3 Design of Agonist and Structure Activity Relationships	15
2.4 Initial ¹⁸ F-Radiolabelling Strategy.....	21

2.4.1	Results and Discussion	23
2.4.1.1	Synthesis of 4-FB Peptidomimetic GHS-R1a Agonists	23
2.4.1.2	4-FB Agonist Receptor-Ligand Binding Assays.....	27
2.4.1.3	4-FB Agonist Partition Coefficients	33
2.4.1.4	Calcium Flux Assay	36
2.4.1.5	¹⁸ F-Radiochemistry	38
2.4.1.6	Conclusions	45
2.5	Alternative ¹⁸ F-Radiolabelling Strategy.....	47
2.5.1	Results and Discussion	48
2.5.1.1	Synthesis of 2-FP Peptidomimetic GHS-R1a Agonists.....	48
2.5.1.2	2-FP Agonist Receptor-Ligand Binding Assays	50
2.5.1.3	2-FP Agonist Partition Coefficients.....	51
2.5.1.4	Calcium Flux Assay	52
2.5.1.5	Conclusions	53
Chapter 3	55
The Future of Prostate Cancer Imaging	55
3.1	Final Remarks	55
4	Experimental.....	58
4.1	General Information	58
4.2	Experimental Procedures	59
4.2.1	Manual Fmoc Solid-Phase Peptide Synthesis (Fmoc-SPPS)	59
4.2.2	Deprotection of the Alloc Protecting Group.....	60
4.2.3	Kaiser Test.....	60
4.2.4	Receptor-Ligand Binding Assay	60
4.2.5	Synthesis of Peptidomimetics.....	62
4.2.6	Synthesis of Small Molecule Triflate Salt.....	71

4.3 Calcium Flux Dose-Response Assay	72
4.4 Computation of Partition Coefficient ($\text{Log}P$).....	72
4.5 Radiochemistry	73
4.5.1 General Information.....	73
4.5.2 Production of [^{18}F]Fluoride	73
4.5.3 Synthesis of [^{18}F]FBA.....	73
4.5.4 Attempted Coupling of [^{18}F]FBA to [1-Nal 4]G-7039.....	74
4.5.5 Synthesis of [^{18}F]SFB	74
4.5.6 Synthesis of [1-Nal 4 , Lys 5 (4-[^{18}F]-FB)]G-7039.....	75
5 References.....	76
Appendix A: Peptidomimetic Chromatograms	87
Appendix B: Triflate Salt UHPLC Chromatogram.....	98
Appendix C: Peptidomimetic ^1H -NMR Spectra	100
Appendix D: Triflate Salt ^1H -NMR and ^{13}C -NMR Spectra.....	120
Appendix E: Peptidomimetic Displacement Curves.....	123
Curriculum Vitae.....	134

List of Tables

Table 1. Synthesized peptidomimetics and their amino acid sequences.	25
Table 2. Yields, purities and HRMS data for the synthesized GHS-R1a agonists.	26
Table 3. IC ₅₀ values of ipamorelin and a series of derivatives thereof.	28
Table 4. IC ₅₀ values of GHRPs and their derivatives.	30
Table 5. IC ₅₀ values of Genentech peptidomimetics and their derivatives.	32
Table 6. Computationally calculated log <i>P</i> values for 4-FB peptidomimetic GHS-R1a agonists.	35
Table 7. Amino acid sequences of the 2-fluoropropionyl agonists and their parent compounds.	49
Table 8. Yields, purities and HRMS data for the 2-fluoropropionyl agonists and their parent compounds.	49
Table 9. 2-Fluoropropionyl Genentech peptidomimetic derivatives and their IC ₅₀ values.	50
Table 10. Lipophilicities of Genentech peptidomimetic agonists and their 2-fluoropropionyl derivatives.	52

List of Figures

Figure 1. The key steps of a molecular imaging study.	2
Figure 2. Positron emission and the principle of PET imaging.....	5
Figure 3. a) Structure of [¹⁸ F]FDG b) whole body human PET scan using [¹⁸ F]FDG	5
Figure 4. Examples of clinically used PET imaging agents for diagnosing prostate cancer.....	6
Figure 5. The general design of an imaging agent.....	7
Figure 6. Structure of the fluorescein ghrelin(1-19) imaging probe.....	9
Figure 7. Enkephalin analogues and the most widely studied GHRPs.....	11
Figure 8. Schematic diagram of human GHS-R1a topology.....	12
Figure 9. Growth hormone secretagogues used in Feighner <i>et al</i> 's study.....	16
Figure 10. Amino acid sequence of the ghrelin receptor and residues identified for mutation in Feighner <i>et al</i> 's study.....	17
Figure 11. GH secretagogue 3D pharmacophore established by DistComp.....	19
Figure 12. Benzothiazepin compound with nanomolar <i>in vitro</i> potency.....	19
Figure 13. Representative IC ₅₀ curve for the endogenous ligand ghrelin.....	27
Figure 14. Efficacy curves for lead agonist [1-Nal ⁴ ,Lys ⁵ (4-FB)]G-7039 (circles) and the control ligand ghrelin (squares).....	37
Figure 15. Crude HPLC UV trace of the reaction between [1-Nal ⁴]G-7039 and 4-[¹⁹ F]FBA in DMF.....	38
Figure 16. A series of chromatograms resulting from the co-injection of cold standard 4-[¹⁹ F]FBA ($\lambda = 254$ nm) and crude "hot" product [¹⁸ F]FBA.....	41

Figure 17. HPLC radio-chromatogram of pure [^{18}F]SFB.....	43
Figure 18. Stacked HPLC Chromatograms for [1-Nal 4]G-7039, [1-Nal 4 ,Lys 5 (4-FB)]G-7039 (both $\lambda = 254$ nm) and [1-Nal 4 ,Lys 5 (4-[^{18}F]-FB)]G-7039.....	43
Figure 19. Stacked HPLC chromatograms resulting from the co-injection of cold standard [1-Nal 4 ,Lys 5 (4-FB)]G-7039 ($\lambda = 254$ nm) and [1-Nal 4 ,Lys 5 (4-[^{18}F]-FB)]G-7039.....	44
Figure 20. Calibration curve for cold standard [1-Nal 4 ,Lys 5 (4-[^{18}F]-FB)]G-7039.....	45
Figure 21. [^{18}F]GalactoRGD and [^{18}F]NFP.....	47
Figure 22. ^1H -NMR signature of methine proton in [Lys 5 (2-FP)]G-7039 (LCE00295).....	50
Figure 23. Efficacy curves for the peptidomimetic GHS-R1a agonist [Lys 5 (2-FP)]G-7039 (circles) and the control ligand ghrelin (squares).....	53
Figure 24. ^{18}F -radiolabelling strategies being explored for the 2-fluoropropionyl lead compound [Lys 5 (2-FP)]G-7039	54

List of Schemes

Scheme 1. Truncated ghrelin derivatives (Merck).....	13
Scheme 2. General procedure for manual Fmoc-SPPS	23
Scheme 3. Orthogonal protecting group strategy and coupling of 4-[¹⁹ F]FBA illustrated for the peptide ipamorelin.....	24
Scheme 4. Synthesis of the precursor 4-(tert-butoxycarbonyl)- <i>N,N,N</i> -trimethylbenzenammonium triflate salt.....	39
Scheme 5. Synthesis of [¹⁸ F]FBA and attempted coupling to precursor peptidomimetic [1-Nal ⁴]G-7039.	40
Scheme 6. Synthesis of the [¹⁸ F]SFB prosthetic group and subsequent ¹⁸ F-radiolabelling of [1-Nal ⁴]G-7039.....	42
Scheme 7. Orthogonal protecting group strategy and coupling of 2-[¹⁹ F]FPA illustrated for the peptidomimetic G-7039 (36).....	48

List of Appendices

Appendix A: Peptidomimetic Chromatograms	87
Appendix B: Triflate Salt UHPLC Chromatogram.....	98
Appendix C: Peptidomimetic ¹ H-NMR Spectra	100
Appendix D: Triflate Salt ¹ H-NMR and ¹³ C-NMR Spectra.....	120
Appendix E: Peptidomimetic Displacement Curves.....	123

List of Abbreviations and Symbols

[¹⁸F]FBA: 4-[¹⁸F]-fluorobenzoic acid

[¹⁸F]FDHT: [¹⁸F]fluorodihydrotestosterone

[¹⁸F]NFP: 4-nitrophenyl 2-[¹⁸F]fluoropropionate

[¹⁸F]SFB: *N*-succinimidyl-4-[¹⁸F]fluorobenzoate

¹H-NMR: proton-nuclear magnetic resonance

1-Nal: 1-naphthylalanine

2-FP: 2-fluoropropionyl

2-Nal: 2-naphthylalanine

4-[¹⁹F]FBA: 4-[¹⁹F]-fluorobenzoic acid

4-FB: 4-fluorobenzoyl

⁶⁴Cu-CB-TE2A-AR06: ⁶⁴Cu-4,11-bis(carboxymethyl)-1,4,8,11-tetraazabicyclo(6.6.2)hexadecane-PEG₄-D-Phe-Gln-Trp-Ala-Val-Gly-His-Sta-Leu-NH₂

AEEA: aminoethanolethylamine

Alloc: allyloxycarbonyl

AMBA: DOTA-CH₂CO-G-4-aminobenzoyl-QWAVGHLM-NH₂

BPH: benign prostatic hyperplasia

BSA: bovine serum albumin

CB-TE2A: cross-bridged-tetraazamacrocyclic 4,11-bis(carboxymethyl)-1,4,8,11-tetraazabicyclo [6.6.2]hexadecane

CHO cells: Chinese hamster ovary cells

CL: cytoplasmic loop

CSP: chemical shift perturbation

CT: computed tomography

c-zone: central zone

D-2-Nal: D-2-naphthylalanine

DCE-MRI: dynamic contrast enhanced MRI

DIPEA: *N,N*-diisopropylethylamine

DMF: dimethylformamide

DOTA: 1,4,7,10-tetraazadodecane-*N,N',N'',N'''*-tetraacetic acid

DPC: dodecyl-phosphocholine micelles

Dpr: diaminopropionic acid

DRE: digital rectal exam

DW-MRI: diffusion-weighted MRI

e⁻: electron

EC₅₀: half-maximal effective concentration

EDC: *N*-(3-dimethylaminopropyl)-*N'*-ethylcarbodiimide

EDTA: ethylenediaminetetraacetic acid

EK: enkephalin

EL: extracellular loop

EOS: end of synthesis

FITC: fluorescein isothiocyanate

Fmoc: fluorenylmethyloxycarbonyl

GH: growth hormone

Ghrelin receptor: GHS-R1a

GHRP: growth hormone releasing peptide

GHS-R1a/1b: growth hormone secretagogue receptor type 1a/1b

GHSs: growth hormone secretagogues

GPCR: G-protein coupled receptor

GRPr: gastrin releasing peptide receptor

HATU: 1-[Bis(dimethylamino)methylene]-1*H*-1,2,3-triazolo[4,5-*b*]pyridinium 3-oxid hexafluorophosphate

HCTU: (2-(6-Chloro-1*H*-benzotriazole-1-yl)-1,1,3,3-tetramethylamminium hexafluorophosphate)

HEK293 cells: human embryonic kidney 293 cells

HEPES: 4-(2-hydroxyethyl)piperazine-1-ethanesulfonic acid

HPLC: high-performance liquid chromatography

HRMS: high resolution mass spectrometry

IC₅₀: half-maximal inhibitory concentration

Inp: isonipecotic acid

K_a: dissociation binding constant

kDa: kiloDaltons

K_i: binding affinity

M: molar

mM: milli-molar

mpMRI: multi-parametric MRI

MRI: magnetic resonance imaging

MRSI: magnetic resonance spectroscopic imaging

NHS: *N*-hydroxysuccinimide

nM: nanomolar

NODAGA: 1,4,7-triazacyclononane,1-glutaric acid-4,7 acetic acid

PBS: phosphate-buffered saline

PCa: prostate cancer

PEG: polyethylene glycol

PET: positron emission tomography

PIN: prostate intraepithelial neoplasia

pM: picomolar

PRE: paramagnetic relaxation enhancement

PSA: prostate specific antigen

p-zone: peripheral zone

QSAR: quantitative structure activity relationship

rhGH: recombinant human growth hormone

RM1: DOTA-CH₂CO-G-4-aminobenzoyl-fWAVGH-Sta-L-NH₂

RP: reverse-phase

SCE: slow conformational exchange

SPECT: single-photon emission computed tomography

SPPS: solid-phase peptide synthesis

Sta: statin

TBMe: tert-butyl methyl ether

TFA: trifluoroacetic acid

Thi: D-2-thienylalanine

TIPS: triisopropylsilane

TM: transmembrane

TOCSY: total correlation spectroscopy

TRUS: trans-rectal ultrasound

t-zone: small transitional zone

ν_e : neutrino

β^+ : positron

The abbreviations for the common amino acids are in accordance with the recommendations of the IUPAC-IUB Joint Commission on Biochemical Nomenclature (JCBN).

Chapter 1

Molecular Imaging

1.1 Introduction

The field of molecular imaging, despite existing for only 15-20 years,¹ is enabling both researchers and clinicians to better observe and understand the intricate biochemical activities that occur inside living systems.² Defined as the real-time observation, identification, and quantification of cellular and subcellular biological and chemical events within living organisms,^{2, 3} it utilizes unique instrumentation and imaging modalities that interrogate the mechanisms of disease progression and human physiology.² Molecular imaging is considered to be a multidisciplinary field with contributions from areas such as chemistry, molecular biology, engineering, biochemistry, physics and many others.² One of its main aims is to attempt to overcome the limitations of *in vitro* biological assays by non-invasively studying intact living organisms and cellular processes without affecting the system under investigation.² Figure 1 illustrates the typical steps involved in a molecular imaging study. The first step requires the selection of a pathology or biochemical process of interest.² Having determined whether this process or disease state may be studied by molecular imaging, a molecular target which would allow either direct or indirect visualization of this phenomenon is chosen (step 2).² This may be a G-protein coupled receptor (GPCR) overexpressed in a particular cancer (e.g. the gastrin-releasing peptide receptor; GRPr, in breast cancer⁴) or a cellular event, such as glucose metabolism.⁵ Careful choice of imaging modality then ensues (step 3). These modalities include (but are not limited to) positron emission tomography (PET), single-photon emission computed tomography (SPECT) and magnetic resonance imaging (MRI).² Depending on the type of imaging method employed, the order of subsequent steps will vary. For example, development of an MRI contrast agent would require the synthesis of the probe, *in vitro* testing and an animal study (4, 5 and 7) followed by eventual imaging in humans (8). For a SPECT or PET imaging agent, synthesis would be followed by a series of *in vitro* tests to check the

stability of the probe and target specificity (5). This could result in a change in the structure of the imaging agent. In any case, labelling with a positron-emitting radioisotope would then ensue (6), along with an animal study (step 7, a murine model is the usual starting point) and finally, the image acquisition and processing step (8).²

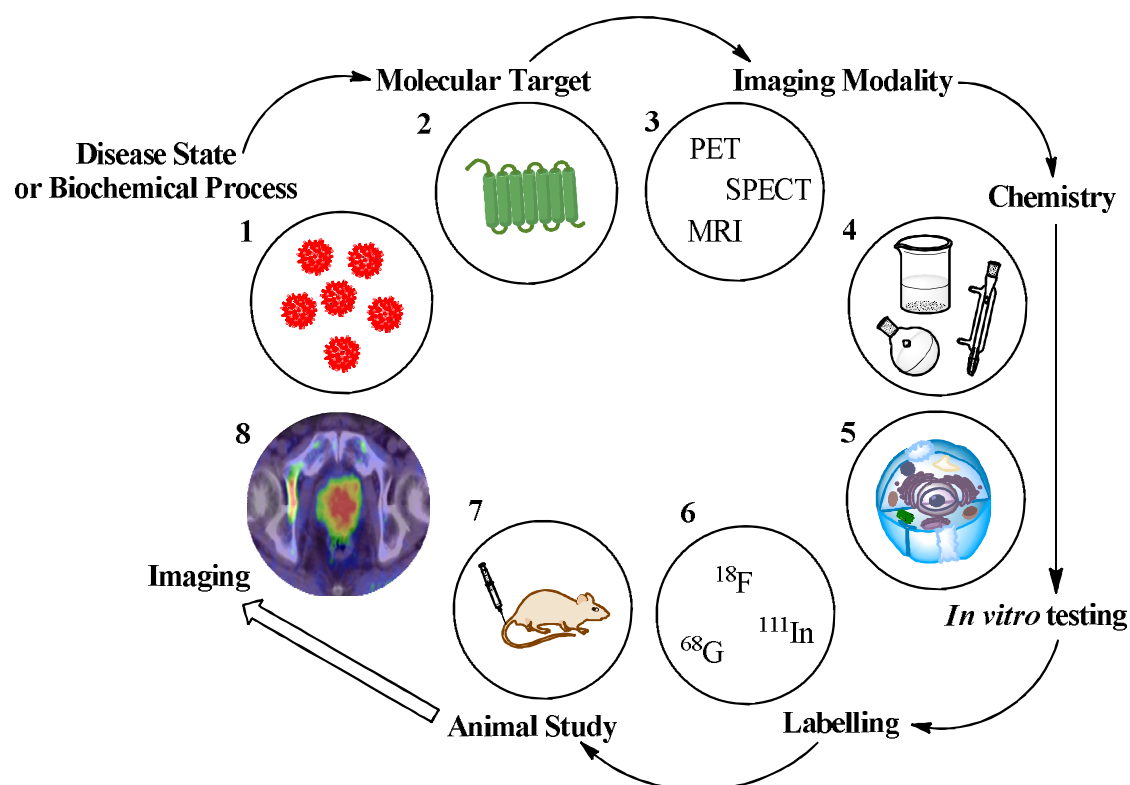


Figure 1. The key steps of a molecular imaging study.

1.2 Prostate Cancer

As can be seen in Figure 1 above, a molecular imaging study often begins with the identification of a specific disease process. A considerable variety of pathologies exist but of particular interest to this thesis is prostate cancer (PCa). This carcinoma is the foremost male malignancy in North America.⁶ In Canada in 2013 it was estimated that prostate cancer represented 25% of all new cancer cases and 10% of all cancer deaths in men.⁷ Despite the absence of a single cause for PCa, a number of potential risk factors do exist.⁸ These include inherited gene mutations⁸ and diets high in fat, processed meat and dairy products.⁸ The prostate may be divided up into three specific regions that assist in

tumour localization: the peripheral zone (p-zone), the central zone (c-zone) and the small transitional zone (t-zone).^{9, 10} Approximately 75% of malignant tumours originate in the p-zone.^{10, 11} Benign tumours (which lead to the state known as benign prostatic hyperplasia, BPH) are found exclusively in the t-zone.^{9, 10} Clinical methods currently used to diagnose PCa involve a combination of the digital rectal examination (DRE), the serum prostate-specific antigen (PSA) test and trans-rectal ultrasound (TRUS)-guided biopsy.¹⁰ These methods are not only used to predict the recurrence of tumours after radical prostatectomy¹² and the potential for cancer to spread from the prostate,¹³ but also to divide patients into groups based on the risk of PCa reappearance after localized treatment.^{14, 15} Despite the utility that these techniques provide, the presence of sampling error in TRUS-guided biopsies¹⁵ coupled with patients who have consistently elevated levels of serum PSA in spite of negative prostate biopsies,¹⁰ suggests that developing non-invasive imaging methods to improve disease identification at an earlier phase of illness is crucial.¹⁵

1.3 Imaging Modalities

There are a number of different methodologies in current use that could be applied to imaging prostate cancer. One such non-invasive technique for PCa diagnosis and staging is a combination of MRI and functional MRI methods such as diffusion-weighted MRI (DW-MRI), magnetic resonance spectroscopic imaging (MRSI) and dynamic contrast-enhanced MRI (DCE-MRI).¹⁰ Briefly, these methodologies collect information on *in vivo* diffusion coefficients for biological tissues, metabolism and tissue vascularity respectively.¹⁰ The combination of T2-weighted MRI and two or more functional techniques make up the multi-parametric prostate MRI (mpMRI) exam, which is currently a highly effective way to identify and localize PCa.¹⁵ Despite the usefulness of the data gathered by functional MRI, it tends to suffer from difficult and lengthy procedures (for MRSI),¹⁵ limited lesion detection in the central gland,¹⁶ the requirement for dedicated computer software for data analysis (DCE-MRI)¹⁵ and the inability to specify cut-off values in apparent diffusion coefficients in DW-MRI, thus making the delineation between benign and malignant tumours problematic.^{15, 17} In addition to these

factors, there are currently no guidelines available that specify which functional sequence is most appropriate in a particular clinical scenario.¹⁰

Alternative techniques for cancer imaging such as computed tomography (CT) have been in clinical use since the 1970s. This method utilizes high energy X-rays to give high resolution morphological and anatomical information about a specific region of interest, thus enabling tumour localization and identification.^{2, 18} Unfortunately, CT is not capable of differentiating between PCa and BPH and also has trouble diagnosing primary PCa.^{18, 19} In addition, CT scans expose patients to high levels of radiation, further reducing the utility of this method. This is because the quantity of scans that can be carried out on a specific patient in a set time period is limited.² It is therefore clear that additional modalities for imaging PCa (such as PET) should be considered.

1.4 Fluorine-18 Positron Emission Tomography

PET is a three-dimensional nuclear medicine imaging technique that can observe functional processes occurring in the body by detecting γ rays indirectly resulting from the decay of specific radioisotopes.^{2, 5} These radioisotopes include (amongst others): ^{18}F ($t_{1/2} = 109.8$ mins), ^{64}Cu ($t_{1/2} = 12.7$ hrs), ^{68}Ga ($t_{1/2} = 67.8$ mins) and ^{11}C ($t_{1/2} = 20.3$ mins).^{2, 4} Positron (β^+) emission occurs when one of the above nuclei starts to decay owing to the presence of a surplus of protons, which have the effect of destabilizing the nucleus.² In order to gain stability, the nucleus of the atom converts a proton into a neutron, a positron and a neutrino.² In the case of fluorine-18, this results in the formation of the stable oxygen-18 isotope and the release of the positron and neutrino.² This process is shown below (Figure 2). The positron, being highly unstable, quickly loses kinetic energy and decelerates before annihilating with an electron from the nuclei of surrounding tissue.² This event causes the release of two 511 keV photons at 180° to each other, which are picked up by a series of rings on the PET detector.² The consequent electrical signals are transformed into sinograms that make up the tomographic image after a number of processing steps (Figure 2).² The images acquired from PET have a clinical spatial and temporal resolution of 5-7 mm and seconds-minutes respectively.² This is only slightly worse than CT, where a spatial resolution of 0.5-1 mm and temporal

resolution of minutes is obtained in the clinic.² In addition, PET possesses a high level of sensitivity ($10^{-11} - 10^{-12}$ M) allowing low radiotracer concentrations to be detected.²

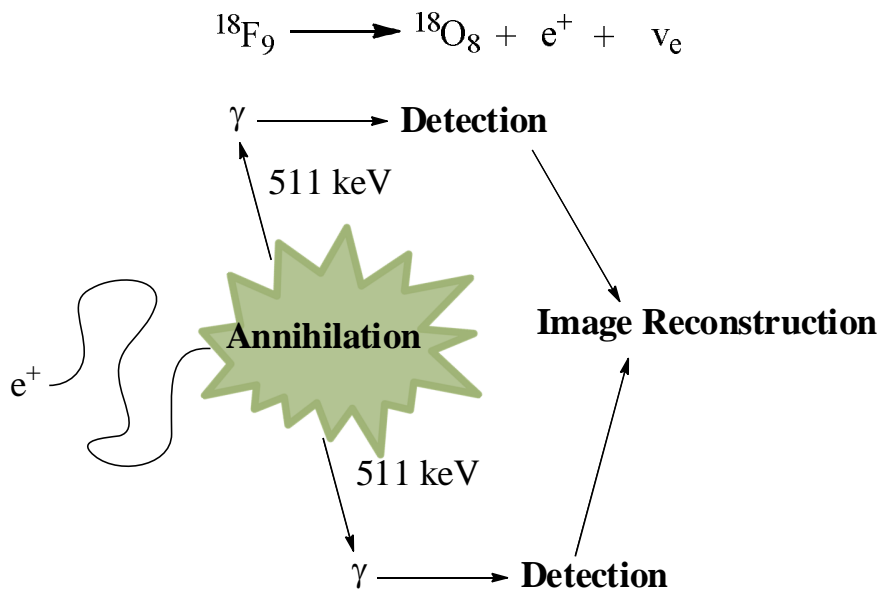


Figure 2. Positron emission and the principle of PET imaging.

The most commonly used clinical imaging probe for the identification, staging and monitoring of carcinoma is [${}^{18}\text{F}$]FDG (Figure 3a). First synthesized by Ido and co-workers,²⁰ this radioactive glucose derivative is injected into the body intravenously.²

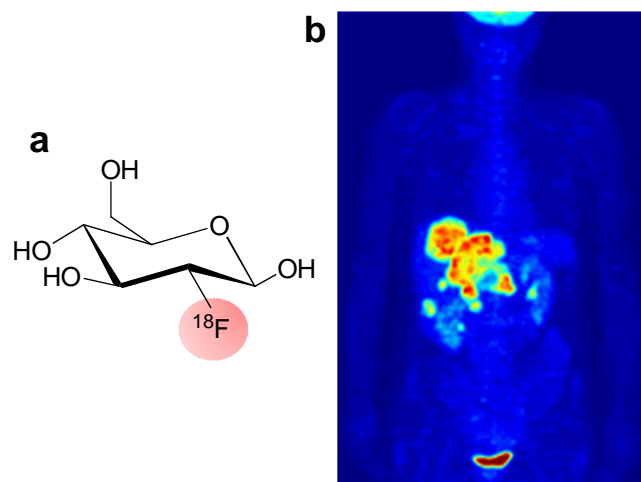


Figure 3. a) Structure of [${}^{18}\text{F}$]FDG b) whole body human PET scan using [${}^{18}\text{F}$]FDG.²¹

Due to the fact that cancer cells have a higher rate of glucose metabolism than normal cells (known as the Warburg effect²²), radiotracer accumulation differs between both cell types, ultimately leading to a difference in contrast in the PET image.⁵ A representative PET image is shown on the previous page (Figure 3b).

Unfortunately, much as in the case of MRI and CT, a number of limitations exist, especially with respect to the imaging of prostate cancer. In spite of the fact that a combination of PET/CT using the radiotracer [¹⁸F]FDG enables tumour localization *via* the Warburg effect,^{22, 23} the probe suffers from renal excretion, thus masking possible prostatic tumours due to the build-up of activity in the bladder.^{18, 24} In addition to this, PET has a limited ability to distinguish between benign and malignant disease, in spite of the use of alternative radiotracers such as [¹⁸F]fluorodihydrotestosterone (FDHT, molecule **1**)¹⁸, [¹¹C]acetate (**2**),²⁵ [¹⁸F]Choline, (**3**)¹⁸ and [¹¹C]methionine (**4**).^{18, 26} It is therefore clear that the development of novel PET imaging agents to improve differentiation between benign and malignant prostatic tumours (as well as addressing the clinical issue of over-diagnosing prostate cancer and thus over-treating potentially benign tumours) is of paramount importance.⁶

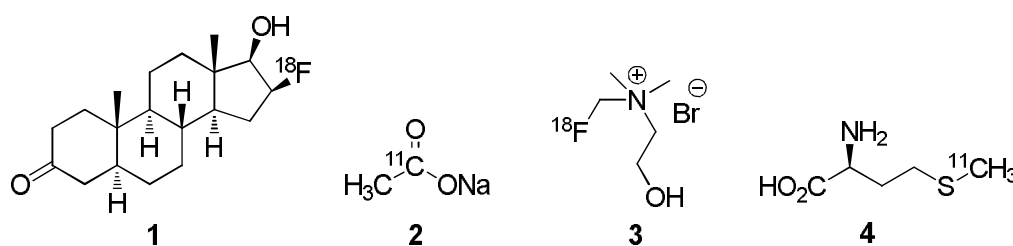


Figure 4. Examples of clinically used PET imaging agents for diagnosing prostate cancer.¹⁸

1.5 Peptide-based Imaging Agents

Molecular imaging agents generally consist of two parts: a targeting entity and a signalling entity (Figure 5, overleaf). The former component ensures that the imaging probe interacts effectively with the desired target. In the specific case of a peptide-based imaging agent binding to a G-protein coupled receptor, this represents the probe's

pharmacophore. On the other hand, the signalling entity allows the target to be detected by the imaging modality being used. For peptides that are to be detected through PET, this entity is formed *via* insertion of a positron-emitting radionuclide into the structure of the peptide. This can occur by using a chelator, which is often separated from the peptide by a linker (e.g. polyethylene glycol, PEG), so as to prevent interference between the respective entities.² This approach is mainly used for radiometals such as ^{68}Ga and ^{64}Cu .²⁷ Common chelators include 1,4,7,10-tetraazadodecane- N,N',N'',N''' -tetraacetic acid (DOTA)²⁸ for ^{68}Ga and cross-bridged-tetraazamacrocycle 4,11-bis(carboxymethyl)-1,4,8,11-tetraazabicyclo[6.6.2]hexadecane (CB-TE2A)²⁹ for ^{64}Cu . On the other hand, the radioisotope ^{18}F is introduced into peptides without the use of a chelator. Small molecules such as *N*-succinimidyl-4- ^{18}F fluorobenzoate (^{18}F SFB)³⁰ and 4- ^{18}F -fluorobenzoic acid (^{18}F FBA)³¹ are predominantly used. This is because adding the ^{18}F radioisotope directly into the main peptide sequence is frequently difficult to perform and not sufficiently regio-selective. Instead, addition of a pre-formed ^{18}F -radiolabelled small molecule (known as a “prosthetic group”)³² is more convenient. However, direct routes for ^{18}F radioisotope insertion into peptides using fluorine-19 chemistry do exist.^{2, 33, 34}

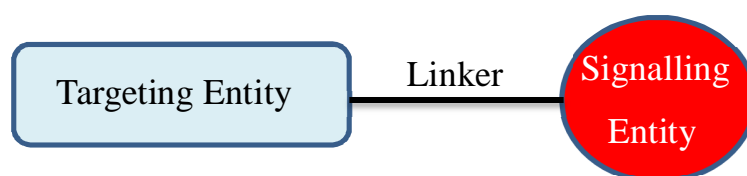


Figure 5. The general design of an imaging agent.

Once the imaging agent has been synthesized, it is tested and modified so as to establish the following favourable attributes (step 5 of the molecular imaging study described in Figure 1): high target selectivity, good *in vivo* stability, low toxicity, decreased non-specific binding, signal amplification and multiplexing potential.²

Peptides are a very versatile class of imaging agents that possess a variety of advantageous properties: facile synthesis by solid-phase peptide synthesis (SPPS), fast clearance from the body and a high degree of selectivity and specificity.^{2, 35} They also possess flexibility in terms of the type of changes that can be introduced without

significantly affecting the binding affinity.^{2, 35} In addition, despite their lower binding affinity compared to antibodies, they have a greater level of *in vivo* stability and lower likelihood of eliciting an immune response.^{2, 36} These factors play a large part in the frequent use of peptides as imaging entities.

A number of recent studies aiming to image prostatic tumours utilize peptide-based imaging agents. For example, Y. Liu *et al.*,²⁷ recently synthesized several radiolabelled bombesin analogues that targeted the gastrin-releasing peptide receptor (GRPr), which is known to be overexpressed in PCa.^{27, 37} Amongst the synthesized compounds, two of the imaging agents were ⁶⁴Cu-chelated-peptides, namely ⁶⁴Cu-1,4,7-triazacyclononane,1-glutaric acid-4,7 acetic acid-DOTA-CH₂CO-G-4-aminobenzoyl-QWAVGHLM-NH₂ (⁶⁴Cu-NODAGA-AMBA) and ⁶⁴Cu-NODAGA-DOTA-CH₂CO-G-4-aminobenzoyl-fWAVGH-Sta-L-NH₂ (⁶⁴Cu-NODAGA-RM1).²⁷ These compounds were used to image PC3 tumours in mice.²⁷ Both imaging probes exhibited good tumour-to-background ratios, with ⁶⁴Cu-NODAGA-RM1 showing persistent tumour uptake four hours post-injection.²⁷

An alternative non-radiolabelled approach was taken by the work of Lu and co-workers.⁶ This involved fluorescent imaging of the growth hormone secretagogue receptor 1a (GHS-R1a),⁶ which is known to be expressed in a number of prostate cancer cell lines such as ALVA-41, LNCaP, DU145 and PC3.³⁸ It was found that this receptor had a differential expression in normal, benign and cancerous prostatic tissue.⁶ This was indicated by the specificity of the peptidic imaging probe fluorescein-ghrelin(1–19) towards PCa, with low level association in BPH, prostate intraepithelial neoplasia (PIN) and normal prostatic tissue⁶ (compound **5**, Figure 6). By moving from the original peptide based fluorescein-ghrelin(1-19) to peptidomimetics, imaging agents with superior targeting, stability and pharmacokinetic properties should result. In addition, by using PET as the primary imaging modality over fluorescent imaging, a more clinically translatable imaging probe would result.

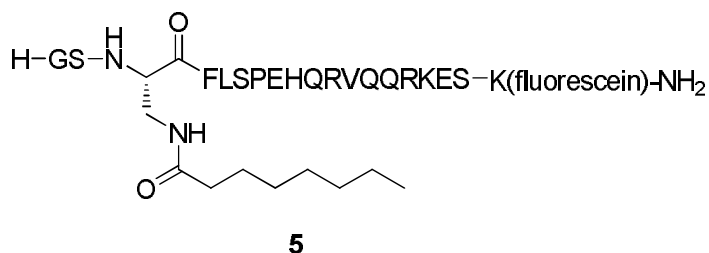


Figure 6. Structure of the fluorescein ghrelin(1-19) imaging probe.

1.6 Scope of Thesis

This thesis deals with the synthesis of a variety of peptidomimetic growth hormone secretagogue (GHS) agonists targeting the GHS-R1a, known to have a differential expression in normal, benign and malignant prostatic tissues.⁶ To begin with, an introduction is given to the field of GHSs, encompassing their initial development and use as a means to treat growth hormone deficiency (section 2.1). This is followed by a short discussion on the preference for an agonist imaging agent over an antagonist imaging probe. A number of reasons are then given for the peptidomimetic structures employed by the agonists in section 2.3, with a detailed account on the available literature that covers their interaction with the GHS-R1a. Section 2.4 deals with the strategy for modifying the peptidomimetic agonists for ¹⁸F radioisotope introduction by synthesizing a series of ¹⁹F mimics with the 4-[¹⁹F]fluorobenzoic acid (4-[¹⁹F]FBA) prosthetic group. The results and discussion begins by describing the synthesis of these ¹⁹F-fluorobenzoyl peptidomimetic GHS-R1a agonists and their characterization by high-performance liquid chromatography (HPLC), high-resolution mass spectrometry (HRMS) and proton-nuclear magnetic resonance spectroscopy (¹H-NMR). Furthermore, a description of the biological evaluation of these ¹⁹F-mimics through competitive *in vitro* receptor-ligand binding assays using human embryonic kidney 293 cells stably transfected with the GHS-R1a receptor (HEK293/GHS-R1a) and [¹²⁵I]ghrelin as the radio-ligand follows. This led to the identification of the lead compound [1-Nal⁴,Lys⁵(4-FB)]G-7039. The results of the 4-fluorobenzoyl (4-FB) modifications and their effect on the receptor binding affinity are examined. Partition coefficients are calculated for the ¹⁹F-fluorobenzoyl agonists using ACD/log*P* and XLOGP3 software and discussed. A calcium flux assay was used to check

the retention of agonist activity for [1-Nal⁴,Lys⁵(4-FB)]G-7039. Finally, ¹⁸F-radiolabelling of the lead compound's parent precursor [1-Nal⁴]G-7039 using [¹⁸F]FBA and [¹⁸F]SFB is elaborated upon. A conclusions section completes this approach.

The next section (2.5) looks briefly at an alternative way of modifying the agonists with a racemic 2-fluoropropionyl (2-FP) group and the results from that endeavour. This section covers a discussion of the computationally calculated Log*P* values of the 2-FP peptidomimetic GHS-R1a agonists, a series of receptor binding assays and a calcium flux assay. A discussion of possible ¹⁸F-radiolabelling strategies for the lead compound [Lys⁵(2-FP)]G-7039 identified by the binding assays (as well as a conclusions section) completes the chapter. The entire body of the work described above is concentrated into Chapter 2. This project was carried out in collaboration with Dr. Savita Dhanvantari, an Assistant Professor in Medical Biophysics at the University of Western Ontario and a Scientist at the Lawson Health Research Institute, London, Ontario, Canada.

Chapter 3 reviews the findings of Chapter 2 and looks at the future direction of prostate cancer imaging with PET.

Chapter 2

The Design and Synthesis of Peptidomimetic GHS-R1a Agonists as PET Imaging Agents for Prostate Cancer

2.1 Introduction

In 1977, Bowers and co-workers were studying enkephalin (EK) analogues (Figure 7, compounds **6** and **7**) in order to gain a better understanding of small peptide structure-activity relationships related to pituitary hormone secretion.³⁹ During the course of their research they found that certain enkephalin derivatives (such as DTrp²-Met-EK-NH₂ for example) released growth hormone (GH) *in vitro* from the pituitary glands of female rats.³⁹ This eventually led them to discover the hexamer H-His-D-Trp-Ala-Trp-D-Phe-Lys-NH₂ in 1984, which represented the first synthetic peptide that released GH *in vitro* in rats and *in vivo* in a number of animals including lambs, rats, monkeys⁴⁰ and humans.⁴¹ This compound was later termed growth hormone releasing peptide 6 (GHRP-6, compound **8**). In 1989, a paper by Ilson *et al*⁴² discussed the potential of these synthetic peptides to replace recombinant human growth hormone (rhGH) for the treatment of GH deficiency.⁴² This form of therapy is expensive and requires injection or inhalation of the recombinant hormone on a daily basis.⁴³

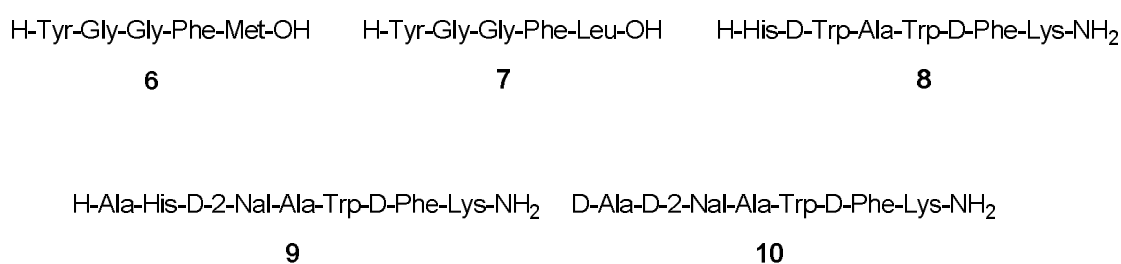


Figure 7. Enkephalin analogues and the most widely studied GHRPs.

Following the publication of this paper, interest in the field of growth hormone releasing peptides began to grow. Two second generation derivatives of GHRP-6 were synthesized in 1993, GHRP-1⁴⁴ and KP-102 (later termed GHRP-2)^{41, 45} (compounds **9** and **10** respectively). These peptides were also found to release GH *in vivo* in humans.⁴¹ Growth

hormone releasing peptides belong to a class of compounds known as growth hormone secretagogues.⁴⁶ These are compounds that are specifically defined as molecules that stimulate the secretion of pituitary GH through a route different from that of GH releasing hormone (GHRH).⁴⁶ Between 1993 and 1995 a number of GHSs were synthesized by research teams with the aim of developing orally bioavailable drugs for treating GH deficiency. These included small molecules such as L-692429, L-692585 and MK-0677 (all Merck & Co.),⁴⁷⁻⁴⁹ EP-51389 (Europeptides),⁵⁰ peptides such as hexarelin (Mediolanum Farmaceutici)⁵¹ and peptidomimetics such as G-7039, G-7143, G-7203 and G-7502 (all Genentech).⁵²

In 1996 the group of R. Smith at the Merck Sharp & Dohme Research Laboratory (USA) identified the receptor that these compounds acted on through expression cloning methods.⁵³⁻⁵⁵ This receptor belongs to the GPCR family⁵⁶ and constitutes seven transmembrane (TM) regions, 366 amino acids and has an approximate mass of 41 kDa.^{54, 55} It was termed the GHS-R1a in order to distinguish it from its splice variant, the GHS-R1b, a five TM, 289 amino acid protein with unknown biological activity.^{54, 55} A schematic diagram of the predicted GHS-R1a topology is shown in Figure 8.

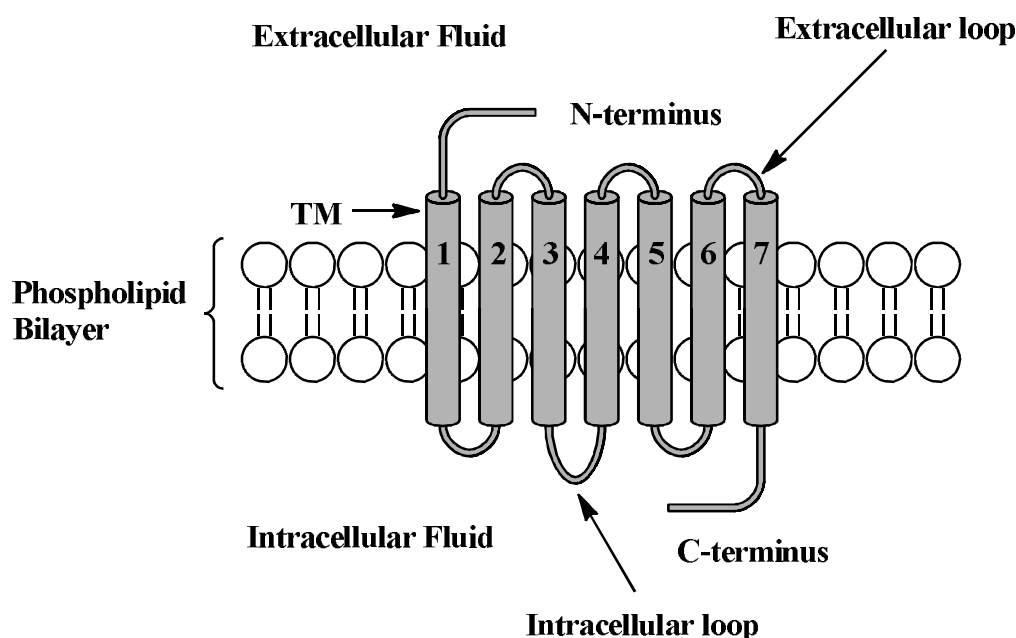
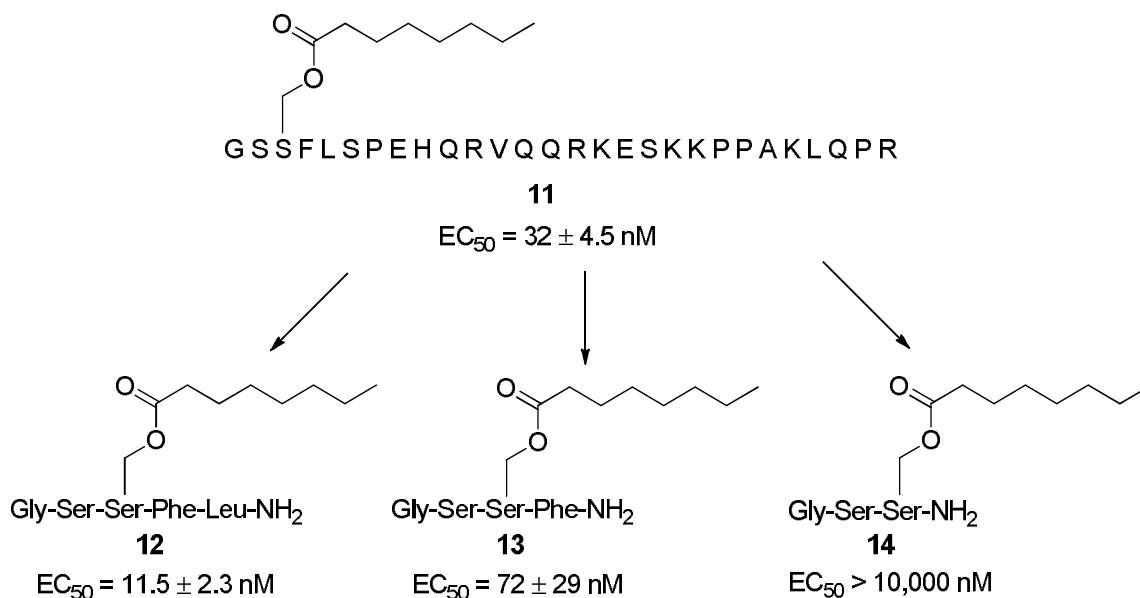


Figure 8. Schematic diagram of human GHS-R1a topology.

The GHS-R1a is predominantly expressed in the hypothalamus and pituitary, as well as in the thyroid gland, stomach, intestine, pancreas, spleen, ventricular myocardium, aorta, lung, adrenal gland, kidney, adipose tissue, testis, ovary and lymphocytes.⁵⁵

Three years later, the endogenous ligand for the GHS-R1a was isolated from the rat stomach by Kojima and co-workers,⁵⁷ thereby completing the cycle of reverse pharmacology. This ligand, termed “ghrelin” (compound **11**, Scheme 1) is a 28 amino acid peptide with an *n*-octanoyl group on the Ser 3 side-chain that is important for binding to the GHS-R1a and releasing GH *in vivo*.⁵⁷ In addition, this acylation is also responsible for ghrelin’s numerous biological activities, such as regulation of glucose metabolism,⁵⁸ insulin release,⁵⁹ gut motility,⁶⁰ and many others.⁵⁵



Scheme 1. Truncated ghrelin derivatives (Merck).

Following the isolation of ghrelin, research shifted towards truncated ghrelin derivatives. This was carried out in order to identify the active pharmacophore of the peptide that is responsible for its biological activity.⁶¹ Amongst these derivatives are peptide agonists **12-14** developed by Merck (Scheme 1). Scientists at Merck found that only the first four to five N-terminal amino acids of ghrelin (Gly-Ser-Ser-Phe/-Leu) were needed to bind to and activate the receptor.⁶¹ This is clearly indicated by the decrease in *in vitro* potency

(half-maximal effective concentration, EC_{50}) with decreasing number of N-terminal residues (Scheme 1, *cf.* **12** to **13** to **14**, $EC_{50} = 11.5 \pm 2.3$ nM, 72 ± 29 nM and $>10,000$ nM respectively).⁶¹

Unfortunately, these shortened ghrelin derivatives were incapable of releasing GH *in vivo*.⁶² This could be due to lower expression levels of the ghrelin receptor in pituitary cells compared to its overexpression in the HEK293 cells used to determine the EC_{50} values mentioned above.⁶² Up to the present day, a wide range of GH secretagogues have been synthesized since the discovery of ghrelin. These encompass (but are certainly not limited to) small molecules developed by Merck,⁶³ Bristol-Myers Squibb,⁶⁴ Sumitomo Pharmaceuticals⁶⁵ and Abbott Laboratories⁶⁶ as well as the extensive work on peptidomimetic and pseudo-peptide agonists at Novo Nordisk (DK), whose structures possess some pharmacophoric similarities to the native ligand ghrelin.⁶⁷⁻⁷⁷

The development of an imaging probe targeting the ghrelin receptor based on the extensive research in the area of GHSs involves three main steps. Firstly, the nature of the ligand is decided upon. This can be divided up into two possible candidates: an agonist or an antagonist. Secondly, the structural nature of the ligand is established, with peptidomimetic, peptide or small molecule frameworks to choose from. Finally, the location and method of radioisotope incorporation into the structure of the imaging agent is determined. The following sub-sections (2.2-2.4) address these respective challenges and explain the rationale behind the design and synthesis of the peptidomimetic GHS-R1a agonists found in this chapter.

2.2 Agonists and Antagonists in Molecular Imaging

From a historical standpoint, agonists have been most frequently used as radiolabelled peptides aimed at imaging peptide receptors overexpressed in cancerous tumours.⁴ The most well-known example of this are the somatostatin receptors which have been known to be up-regulated in a variety of neuroendocrine tumours since the 1980s.^{78, 79} In this form of oncological imaging, a radiolabelled somatostatin derivative (e.g. ¹¹¹In-OctreoScan⁴) is intravenously injected into the subject under study, where it will specifically target the highly expressed somatostatin receptors in the plasma membranes

of the cells that make up the neuroendocrine tumours.⁷⁸ As the somatostatin analogue is an agonist, a receptor-radioligand complex forms upon agonist binding.⁸⁰ This complex is then internalised into the tumour cell, which results in an increase in the amount of radioactivity in the tumour in comparison to other organs.⁷⁸ As a consequence of this accumulation of radioactivity, an increase in contrast and thus *in vivo* target visualization by PET results.^{4, 78} The ability to internalize with the receptor is believed to make radiolabelled peptide agonists better adapted to targeting tumours compared to antagonists.⁴ This is because receptor-ligand internalisation is not possible for antagonists (despite typically having a higher binding affinity than agonists⁸⁰) as they do not activate the receptor, but rather, prevent the natural ligand or agonist from interacting with it.⁴ This is the primary reason for choosing an agonist over an antagonist in the design of PET imaging agents targeting the GHS-R1a in PCa.

However, it should be noted that the development of antagonist imaging probes for cancer imaging is currently a heavily researched topic in the field of radiolabelled peptide imaging probes.^{28, 29, 81} A recent paper by Wieser *et al.*,²⁹ has shown that clinical imaging of prostate cancer using the radiolabelled GRPr antagonist ⁶⁴Cu-4,11-bis(carboxymethyl)-1,4,8,11-tetraazabicyclo(6.6.2)hexadecane-PEG₄-D-Phe-Gln-Trp-Ala-Val-Gly-His-Sta-Leu-NH₂ (⁶⁴Cu-CB-TE2A-AR06) resulted in reduced kidney and intestine uptake with a higher tumour uptake when compared to GRPr agonists.²⁹ The mechanism of action of the antagonist or the reasons behind these results is not currently known. The preference for an antagonist radiotracer does not seem to be isolated to the GRPr receptor however.^{29, 81}

2.3 Design of Agonist and Structure Activity Relationships

The decision to use peptidomimetic agonists rather than a single class of small molecule GHS-R1a agonists was based on a number of reasons. Firstly, peptidomimetic agonists tend to have a peptide-based structure that allows for facile and rapid synthesis using manual or automated fluorenylmethyloxycarbonyl SPPS (Fmoc-SPPS). This is in contrast to small molecules, where synthetic procedures can be somewhat lengthy. Secondly, given the fact that small molecule agonists mostly consist of the pharmacophore required

to interact with the receptor, addition of a radioisotope for imaging would likely have a greater effect on this pharmacophore compared to a peptide, where the pharmacophore typically forms part of the structure with the non-pharmacophoric portion acting as a supporting framework. In addition, the process of screening existing GHSs to find new small molecule “hits” would likely be a tedious and time-consuming enterprise. Most importantly of all, the wealth of previous research on GHRPs, pseudo-peptide and peptidomimetic GHSs as well as their interaction with the ghrelin receptor gives clues as to the kind of structural modifications that may be required to develop them into imaging agents. Such structure-activity relationships form the starting point for the design of peptidomimetic agonists targeting the ghrelin receptor.⁸²⁻⁸⁷

The first such study was carried out by Feighner *et al.*,⁸² who used site-directed mutagenesis⁸⁸ and molecular modelling to determine the key residues required by the ghrelin receptor in order to be activated by peptide (GHRP-6, compound **8**) and non-peptide (MK-0677, **15** and L-692585, **16**) agonists (Figure 9).⁸²

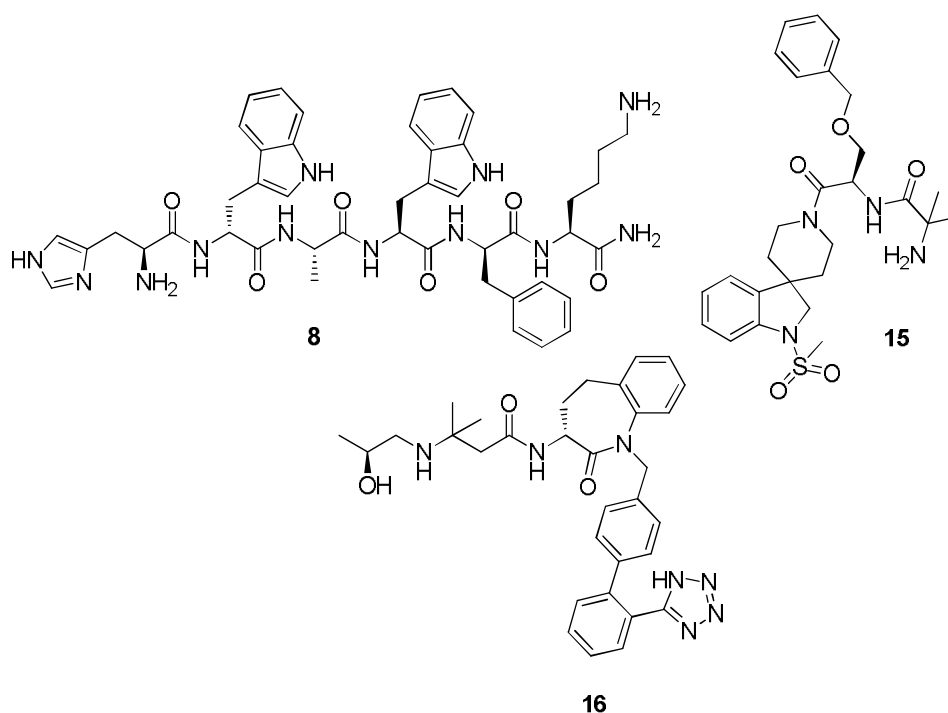


Figure 9. Growth hormone secretagogues used in Feighner *et al.*'s study.

This activation was assessed *via* an aequorin bioluminescence assay, where the degree of aequorin photoprotein luminescence (caused by intracellular calcium ions) indicated the extent of GHS-R1a activation.⁸² Using homology modelling⁸⁹ founded on the helical impression of bacteriorhodopsin as well as a two-dimensional sequence alignment of repeated motifs in a number of associated GPCRs (specifically the neurotensin, somatostatin-2, angiotensin II and β_2 -adrenergic receptors as well as human, swine and rat GHS-Rs) the importance of a number of amino acids required for successful ligand interaction was predicted.⁸² These results were then confirmed through mutagenesis studies on those residues. Figure 10 shows the 366 amino acids of ghrelin receptor along with its predicted topology (the phospholipid bilayer has been omitted for clarity). Mutated residues are highlighted in red.

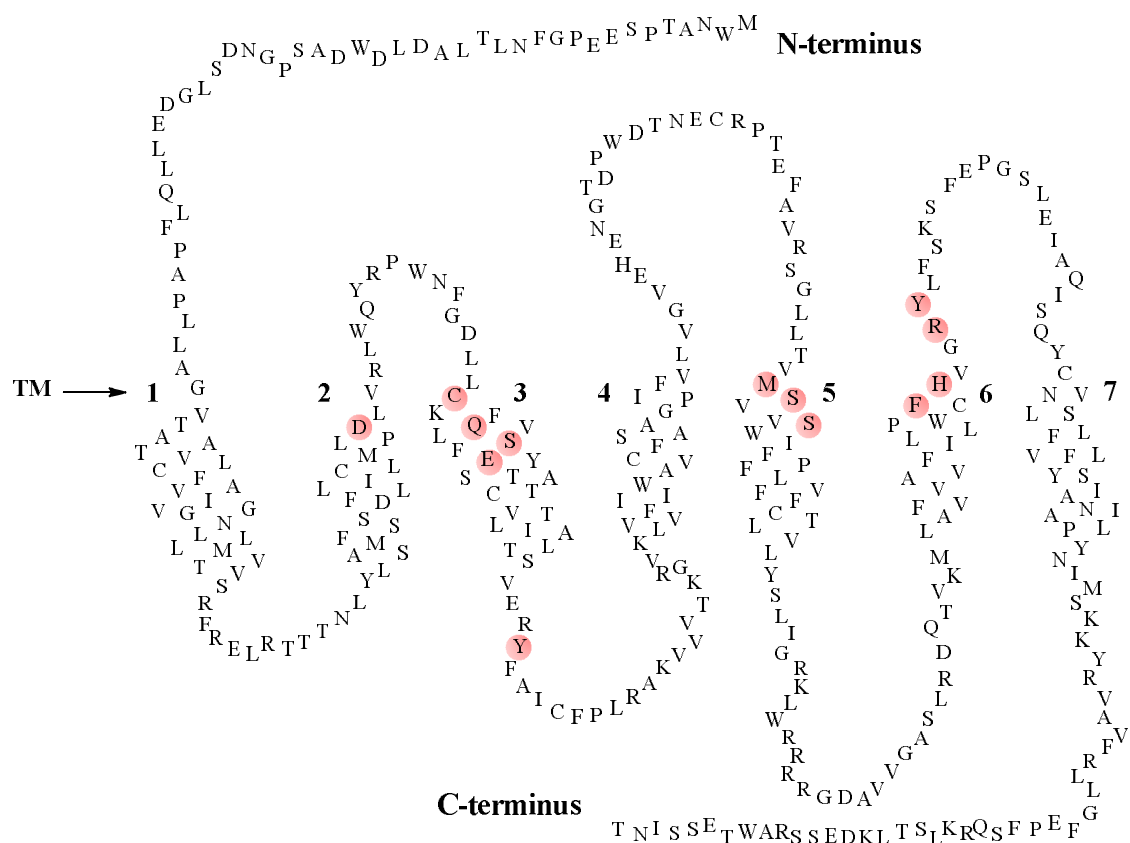


Figure 10. Amino acid sequence of the ghrelin receptor and residues identified for mutation in Feighner *et al*'s study.

By far the most significant residue for receptor activation was found to be the E124 residue in transmembrane region 3 (TM3), which is believed to form a salt bridge with the primary ammonium cation in the N-terminus of the peptide ligand, or the amino group present in both small molecules.⁸² This non-covalent interaction was initially observed in a docking model of L-629585 with the ghrelin receptor,⁹⁰ postulated to be similar to the ligand-binding interaction of the D113 residue in the β_2 -adrenergic receptor⁹¹ and finally confirmed through replacement of E124 with Q124, which deactivated the GPCR.⁸² The M213 residue was shown to be crucial for binding L-692585.⁸² In addition, mutation of the D99 residue (TM2) to N99 resulted in a more than two fold reduction in the functional activity of the receptor.⁸² The mutation of C116 (TM3) to A116 was found to destroy all agonist activity, as the thiol group is believed to form a disulfide bond with the agonists, an interaction that is retained in all GPCRs.^{82, 92} Finally, a decrease in the binding of [³⁵S]-MK-0677 to GHS-R1a was observed upon mutation of S123 to A123 and Q120 to H120 in TM3 (dissociation constant: $K_D = 0.27$ nM for wild-type ghrelin and $K_D = 0.12$ nM for both mutants respectively) thereby highlighting the importance of these residues for ligand interaction.⁸²

A second SAR study was performed by Huang and co-workers in 2001.⁸³ This involved the identification of pharmacophoric regions (A-F) in six peptidyl- and four non-peptidyl agonists of the ghrelin receptor. Using these regions, an in-house computer program (DistComp)⁹³ determined a 3D pharmacophore common to all agonists with the inactive congener [Val³]GHRP-6 used as a negative control.⁸³ This calculation was achieved by inputting a library of low-energy conformers for each compound into the DistComp software.⁸³ The three-dimensional pharmacophore represented the ensemble of functional groups necessary for successful activation of the G-protein coupled receptor and is shown in Figure 11 overleaf.⁸³

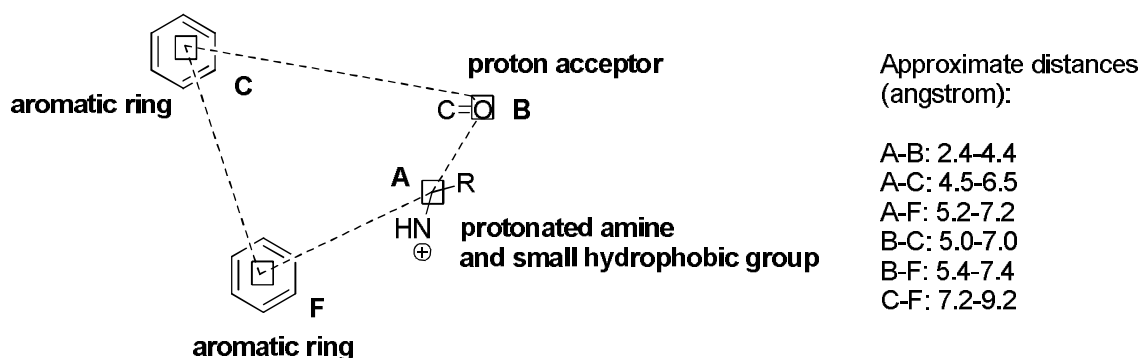


Figure 11. GH secretagogue 3D pharmacophore established by DistComp.

Having derived the pharmacophore, it was screened against a large database of compounds in order to find potential “hits” where the ensemble of moieties matched those of the pharmacophore in similar regions of space.⁸³ After the discovery of an initial lead compound, further optimization was carried out using a site-dependent fragment QSAR program.⁸³ This resulted in the synthesis of a benzothiazepin GH secretagogue **17** which was found to have low nanomolar efficacy, thereby proving the validity of both computational techniques (Figure 12).⁸³

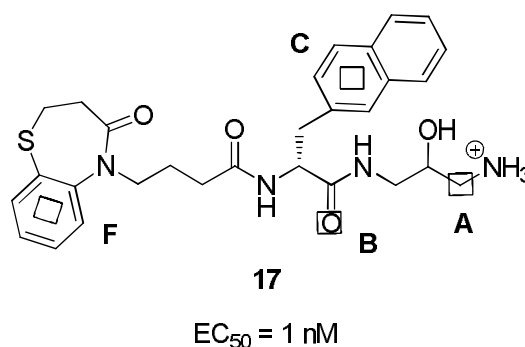


Figure 12. Benzothiazepin compound with nanomolar *in vitro* potency.

The 3D pharmacophore confirmed the importance of the protonable amine (identified in the site-directed mutagenesis study by Feighner *et al*),⁸² and also established the necessity for a core framework of aromatic amino acids and an amidated C-terminal, the latter of which also lends *in vivo* stability to peptide-based GHS-R1a agonists.⁸³ In addition, some of these computational findings supported the experimental work of Hansen and co-

workers⁶⁹ who discovered that aromatic amino acids and a C-terminal amide play an important role in binding to the receptor for tripeptide derivatives of the compound ipamorelin.⁶⁹

A second computational study was performed by Pedretti and co-workers,⁸⁴ who decided to construct a full-length model of the human ghrelin receptor in its open state through the use of a fragmental prediction strategy.⁸⁴ The first step divided up the primary structure of the transmembrane protein into a series of 15 fragments which then underwent homology modelling. The final receptor model was then constructed by overlaying each fragment backbone onto the corresponding fragment in the structure of rhodopsin.⁸⁴ Docking of the receptor with the active core of ghrelin Gly-Ser-Ser(*n*-octanoyl)-Phe-NH₂ and 35 literature peptidomimetic GH secretagogues was used to validate the model.⁸⁴ The results substantiated the existence of two separate sub-pockets located in the binding domain of the ghrelin receptor: a polar sub-pocket bordered by TM2 and TM3 and a non-polar/aromatic sub-pocket lined by TM5 and TM6.⁸⁴ These binding pockets are located far enough apart from each other that a ligand cannot interact with both concurrently.⁸⁴ However, the outcome of docking studies was that some of the most active nanomolar compounds were capable of interacting strongly with either sub-pocket, implying that there may be a co-operative effect between both binding modes.⁸⁴ It was thought that the binding of GHSs to the aromatic sub-pocket could be transitioning the receptor into an inherently active state *via* a non-competitive mechanism of partial agonism.⁸⁴ The overall GH-releasing effect could therefore be taken as a combination of full agonism in the polar cavity and partial agonism in the non-polar cavity.⁸⁴ A follow up paper by the same authors on the GHS-R1a suggested that GH secretagogues could also bind to the inactive closed state, although it was unclear whether ligands could distinguish this from the open state.⁸⁵

Experimental studies examining the interaction of ghrelin with the ghrelin receptor are also useful in determining important pharmacophoric parameters for strong receptor binding. Amongst these, the work of Martín-Pastor *et al.*,⁸⁶ and Jörg Großbauer and co-workers⁸⁷ are the most notable. In the former paper, a ¹H-NMR study was conducted on the interaction of ghrelin and its un-acylated analogue des-acyl ghrelin with stably

transfected HEK293/GHS-R1a and Chinese hamster ovary (CHO)/GHS-R1a cell lines in phosphate-buffered saline (PBS).⁸⁶ A change in the chemical shift of aliphatic protons on the *n*-octanoyl side-chain was observed in the ¹H-NMR spectrum of ghrelin.⁸⁶ Further experiments using two dimensional total correlation spectroscopy (2D TOCSY) examining chemical shift perturbations (CSP) and slow conformational exchange (SCE) effects showed that a considerable number of residues were affected by the interaction of ghrelin with the GHS-R1a receptor, including the *n*-octanoyl group.⁸⁶ This suggests that there is a significant change in the conformation of the peptide when it interacts with the receptor.⁸⁶ The absence of CSP and SCE effects for des-acyl ghrelin confirmed the importance of the *n*-octanoyl group in binding to the receptor and supports the evidence that this moiety is responsible for ghrelin's biological activity.^{57, 86}

On the other hand, the latter paper utilized dodecyl-phosphocholine (DPC) micelles as membrane-mimetics for the GHS-R1a to study the residues of ghrelin involved in receptor binding based on changes in chemical shift and paramagnetic relaxation enhancements (PRE) in ¹H-NMR spectra.⁸⁷ It was found that ghrelin binds to the micelles through its Ser3 *n*-octanoyl side-chain. This is further strengthened by hydrophobic interactions from the side-chain of Phe4.⁸⁷ Low PRE values observed for the *n*-octanoyl group indicated deep immersion in the micellar membrane suggesting that it may also behave as a membrane anchor⁸⁷ (a role observed with myristoyl and palmitoyl functionalities⁹⁴). This paper corroborates the results of Bednarek *et al*⁶¹ who showed that the first 4-5 residues of ghrelin were critical for its activity and also the results from the ¹H-NMR study of Martín-Pastor and co-workers⁸⁶ regarding the importance of the *n*-octanoyl group.

2.4 Initial ¹⁸F-Radiolabelling Strategy

The SAR studies covered in section 2.3 not only identified the classes of functional groups (small molecules) and amino acids (peptidomimetics) that were required by compounds to bind strongly to the ghrelin receptor, but also shed some light onto the types of amino acid residues that are open to modification.⁸²⁻⁸⁷ Out of the peptidomimetic GHS-R1a agonists found in the literature, the most promising amino acid for

modification appeared to be lysine, located at the C-terminus. This was because it did not appear to exhibit pharmacophoric importance in any of the pertinent experimental⁸² and computational⁸³ studies discussed in section 2.3. This residue is common to the most well-known GHRPs (GHRP-6, GHRP-2, GHRP-1) as well as ipamorelin (Novo Nordisk) and G-7039 (Genentech). As a direct consequence of this, the amino group of the lysine side-chain was targeted as the location for ¹⁸F-radioisotope insertion in the above molecules.

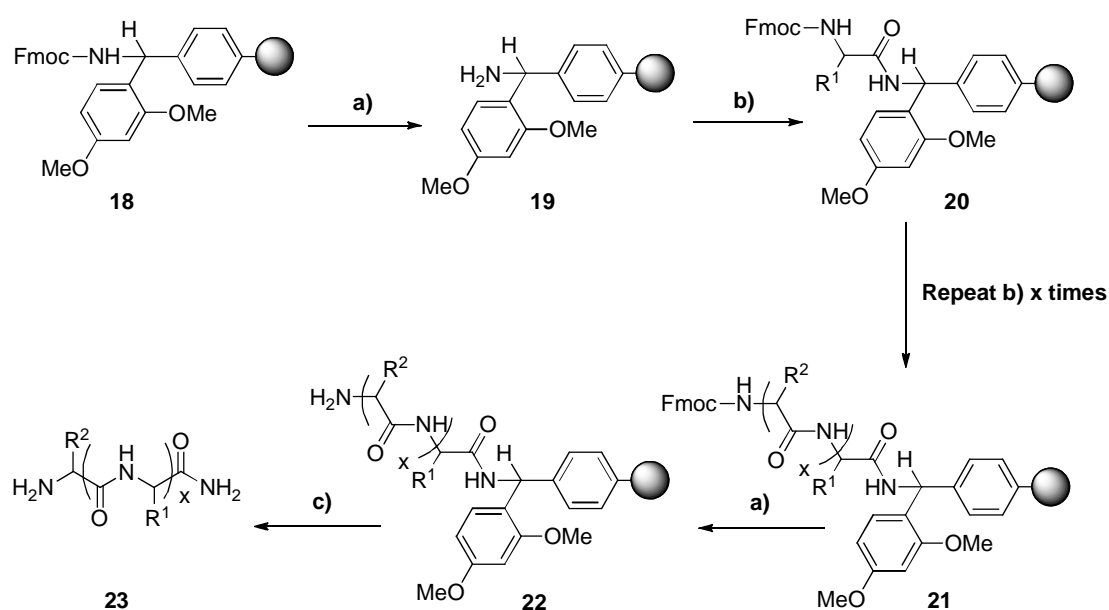
Fluorine-18 is a β^+ emitter⁵ that is frequently used in positron emission tomography, an imaging modality that was covered extensively in chapter 1. This radioisotope was chosen preferentially for insertion into the peptidomimetic agonists over a number of other radioisotopes used in nuclear medicine such as ⁶⁸Ga, ¹¹C and ⁶⁴Cu. This is because it is a small innocuous unit that can be incorporated into the agonist structure without significantly affecting receptor binding affinity. In contrast, ⁶⁸Ga or ⁶⁴Cu both require a large bulky chelator^{95, 96} which is impractical for small peptide-based agonists. Further, ¹⁸F has a half-life of 109.8 minutes⁵ which provides a good time window for carrying out imaging (*cf.* ¹¹C whose half-life is only 20.3 minutes²³). Furthermore, this shorter half-life reduces the radioactive dose experienced by the patient in the clinic.

The initial strategy for ¹⁸F radioisotope insertion into the lysine side-chain of the peptidomimetic agonists was based on common literature acylation methods of amino groups using either [¹⁸F]FBA⁹⁷ or [¹⁸F]SFB⁹⁸⁻¹⁰⁰ prosthetic groups. However, prior to incorporation of the radioisotope, it is important to test this modification in order to determine whether a significant change in agonist receptor binding would result. This was performed by utilizing 4-[¹⁹F]FBA, a “cold” non-radioactive prosthetic group mimic which was coupled to the lysine side-chain of the peptidomimetics by standard Fmoc-SPPS methodology. The principle aim of this strategy was to acquire a compound with a binding affinity of < 100 nM, owing to the low density of the GHS-R1a in prostate cancer tumours.⁶ The technique of Fmoc-SPPS, along with the synthetic scheme and the obtained characterization data of the purified peptidomimetic GHS-R1a agonists is discussed in section 2.4.1 below.

2.4.1 Results and Discussion

2.4.1.1 Synthesis of 4-FB Peptidomimetic GHS-R1a Agonists

The ghrelin receptor agonists were synthesized by standard Fmoc-SPPS manually or by using the Biotage[®] Syro Wave[™] automated peptide synthesizer. The general procedure for this process is shown in Scheme 2 below.

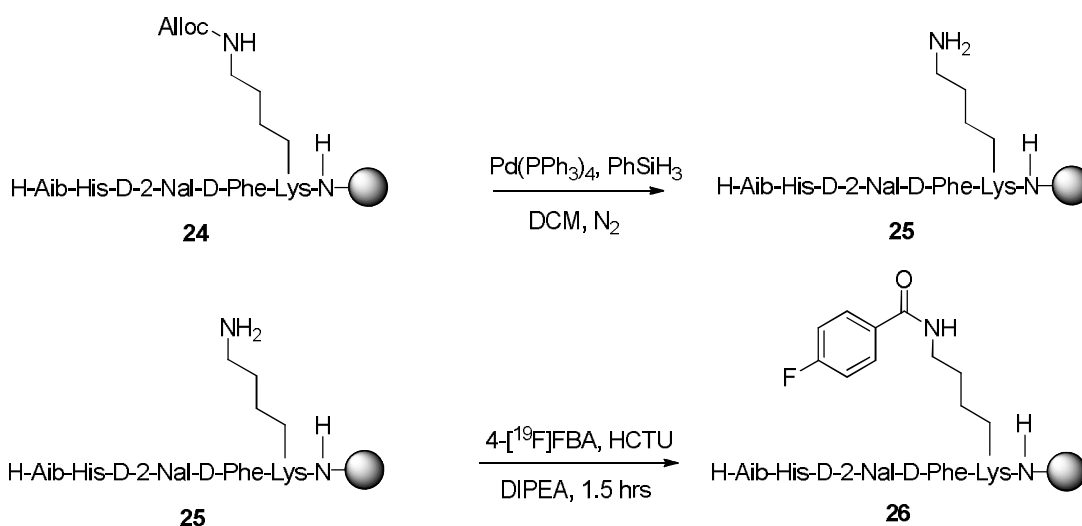


Scheme 2. General procedure for manual Fmoc-SPPS. *Reagents and Conditions:* a) 20% piperidine/DMF b) i) Fmoc-amino acid, HCTU, DMF ii) DIPEA c) 95% TFA: 2.5% H₂O: 2.5% TIPS (5-7 hours).

Briefly, the *N*-protecting Fmoc group on the resin amide resin **18** was deprotected with a solution of 20% piperidine in dimethylformamide (DMF). Coupling of the Fmoc-amino acid to the free amine **19** was performed in DMF using the coupling reagent 2-(6-chloro-1H-benzotriazole-1-yl)-1,1,3,3-tetramethylammonium hexafluorophosphate (HCTU) in the presence of diisopropylethylamine (DIPEA). This resulted in the formation of peptide **20**. The coupling step was typically carried out for a period of one hour. The successful completion of this reaction was assessed either through a micro-cleave or through the qualitative Kaiser test¹⁰¹ (see experimental section 4.2.3). After the coupling step, the resin was washed a number of times with DMF before the next cycle of coupling was

initiated (**20** to **21**). Once all of the desired amino acids had been reacted, a final removal of the N-terminal Fmoc group was performed, leading to peptide **22** with a free N-terminal amine. This peptide was then cleaved from the resin using a solution of 95% trifluoroacetic acid (TFA): 2.5% H₂O: 2.5% triisopropylsilane (TIPS) for 5-7 hours. The crude peptide **23** was purified by preparative HPLC. The full procedure for manual Fmoc-SPPS can be found in experimental section 4.2.1.

The 4-[¹⁹F]FBA moiety was introduced into the peptidomimetic agonists by way of the orthogonal allyloxycarbonyl (Alloc) protecting group present on the amino group of the lysine side-chain (Scheme 3).



Scheme 3. Orthogonal protecting group strategy and coupling of 4-[¹⁹F]FBA illustrated for the peptide ipamorelin.

Using palladium chemistry, the Alloc protecting group was selectively removed from peptide **24** with Pd(PPh₃)₄ in the presence of the PhSiH₃ allyl group scavenger.¹⁰²⁻¹⁰⁵ This resulted in the formation of compound **25** with a free amine. Amino acid coupling employing the conditions described previously delivered the final fluorobenzoylated peptide 4-FB-ipamorelin, **26**. By making use of both procedures outlined in the schemes above, 17 peptidomimetic GHS-R1a agonists were synthesized. The names, compound

identification numbers (LCE numbers) and amino acid sequences of the peptidomimetics are shown in Table 1 below.

Peptidomimetic	LCE number	Amino Acid Sequence
Ipamorelin	00210	H-Aib-His-D-2-Nal-D-Phe-Lys-NH ₂
[Lys ⁵ (4-FB)]ipamorelin	00211	H-Aib-His-D-2-Nal-D-Phe-Lys(4-FB)-NH ₂
[Lys ⁵ (AEEA-4-FB)]ipamorelin	00217	H-Aib-His-D-2-Nal-D-Phe-Lys(AEEA-4-FB)-NH ₂
GHRP-6	00239	H-His-D-Trp-Ala-Trp-D-Phe-Lys-NH ₂
GHRP-1	00240	H-Ala-His-D-2-Nal-Ala-Trp-D-Phe-Lys-NH ₂
[Lys ⁵ (4-FB)]G-7039	00243	H-Inp-D-2-Nal-D-2-Nal-Phe-Lys(4-FB)-NH ₂
[1-Nal ⁴]G-7039	00244	H-Inp-D-2-Nal-D-2-Nal-1-Nal-Lys-NH ₂
G-7039	00245	H-Inp-D-2-Nal-D-2-Nal-Phe-Lys-NH ₂
[Inp ¹ ,D-2-Thi ⁴ ,Lys ⁵ (4-FB)]ipamorelin	00246	H-Inp-His-D-2-Nal-D-2-Thi-Lys(4-FB)-NH ₂
[D-2-Thi ⁴ ,Lys ⁵ (4-FB)]ipamorelin	00267	H-Aib-His-D-2-Nal-D-2-Thi-Lys(4-FB)-NH ₂
[Inp ¹ ,Lys ⁵ (4-FB)]ipamorelin	00268	H-Inp-His-D-2-Nal-D-Phe-Lys(4-FB)-NH ₂
[Inp ¹ ,D-2-Nal ⁴ ,Lys ⁵ (4-FB)]ipamorelin	00269	H-Inp-His-D-2-Nal-D-2-Nal-Lys(4-FB)-NH ₂
[1-Nal ⁴ ,Lys ⁵ (4-FB)]G-7039	00270	H-Inp-D-2-Nal-D-2-Nal-1-Nal-Lys(4-FB)-NH ₂
[Lys ⁶ (4-FB)]GHRP-6	00272	H-His-D-Trp-Ala-Trp-D-Phe-Lys(4-FB)-NH ₂
[Dpr ⁶ (4-FB)]GHRP-6	00281	H-His-D-Trp-Ala-Trp-D-Phe-Dpr(4-FB)-NH ₂
GHRP-2	00282	H-D-Ala-D-2-Nal-Ala-Trp-D-Phe-Lys-NH ₂
[Dpr ⁶]GHRP-6	00298	H-His-D-Trp-Ala-Trp-D-Phe-Dpr-NH ₂

Table 1. Synthesized peptidomimetics and their amino acid sequences.

All final compounds were characterized by HPLC, ¹H-NMR and HRMS (ESI-TOF). The HRMS data, along with the % yields and purities are shown for the peptidomimetic agonists below (Table 2). All compounds were acquired with purities > 95% by HPLC and with HRMS data within acceptable error to computed values (± 0.003 amu).

LCE number	HRMS (calculated) [M + H] ⁺	HRMS (found) [M + H] ⁺	% Purity	% Yield
00210	712.3935	712.3959	> 97	19
00211	834.4103	834.4133	> 99	15
00217	979.4842	979.4868	> 98	8
00239	873.4524	873.4531	> 97	14
00240	955.4943	955.4964	> 99	19
00243	920.4511	920.4529	> 97	6
00244	848.4499	848.4501	> 99	23
00245	798.4343	798.4339	> 99	7
00246	866.3824	866.3850	> 99	13
00267	840.3667	840.3693	> 98	4
00268	860.4259	860.4284	> 96	6
00269	910.4416	910.4400	> 98	10
00270	970.4667	970.4693	> 96	9
00272	1017.4511 [M + Na] ⁺	1017.4522 [M + Na] ⁺	> 96	7
00281	953.4223 [M + H] ⁺	953.4237 [M + H] ⁺	> 98	14
00282	840.4204 [M + Na] ⁺	840.4173 [M + Na] ⁺	> 99	17
00298	831.4055 [M + H] ⁺	831.4070 [M + H] ⁺	> 99	3

Table 2. Yields, purities and HRMS data for the synthesized GHS-R1a agonists.

Having synthesized the 4-FB peptidomimetic agonists, competitive radioligand binding assays on HEK293/GHS-R1a cells with [125 I]ghrelin were used to assess the binding affinities of the peptidomimetics for the ghrelin receptor in terms of the half-maximal inhibitory concentration. The IC_{50} value is defined as the concentration of the agonist that prevents 50% of the radioactive ligand from being bound to the receptor⁸⁰ (in this case [125 I]-ghrelin). It is therefore an indicator of the relative binding strength of the agonist for the receptor binding site.

2.4.1.2 4-FB Agonist Receptor-Ligand Binding Assays

Before testing any novel peptidomimetics containing the 4-FB group, the endogenous ligand for the GHS-R1a (ghrelin) was tested in the receptor-ligand binding assay. This behaved as a positive control that showed whether successful overexpression of the receptor in the HEK293 cells had been achieved. The curve for ghrelin is shown in Figure 13. The obtained IC_{50} value of 7.63 nM is consistent with previous values obtained within our group, indicating that GHS-R1a expression is at a satisfactory level and initial compound testing may proceed.

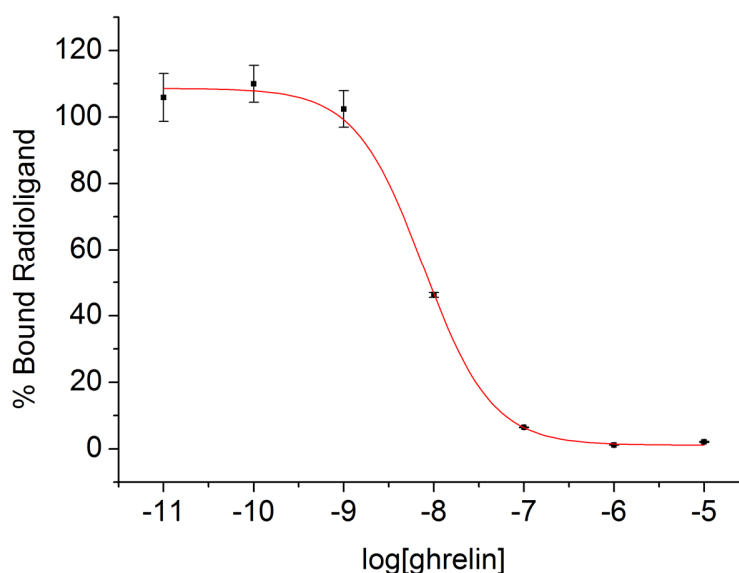


Figure 13. Representative IC_{50} curve for the endogenous ligand ghrelin.

The starting peptidomimetic compound that was chosen for ^{19}F -fluorobenzoylation was the pentapeptide ipamorelin (H-Aib-His-D-2-Nal-D-Phe-Lys-NH₂). This compound was first synthesized by K. Raun and co-workers at the Novo Nordisk A/S research facilities in Denmark.⁶⁷ Derived from GHRP-1,⁴⁴ ipamorelin displayed a low nanomolar binding affinity (K_i) in a previously reported study using HEK293 cells stably transfected with the GHS-R1a ($K_i = 240 \text{ nM}$).¹⁰⁶ It was postulated that introduction of a fluorobenzoyl moiety into the structure of ipamorelin at the lysine side-chain should not significantly affect binding to the receptor, due to the absence of this R group as a pharmacophoric site in Huang *et al*'s study.⁸³ The IC_{50} value for this modification can be found in Table 3 (LCE00211).

LCE no.	Compound Name	IC_{50} , nM
00210	Ipamorelin	483
00211	[Lys ⁵ (4-FB)]ipamorelin	170
00217	[Lys ⁵ (AEEA-4-FB)]ipamorelin	474
00246	[Inp ¹ ,D-2-Thi ⁴ ,Lys ⁵ (4-FB)]ipamorelin	1170
00267	[D-2-Thi ⁴ ,Lys ⁵ (4-FB)]ipamorelin	161
00268	[Inp ¹ ,Lys ⁵ (4-FB)]ipamorelin	688
00269	[Inp ¹ ,D-2-Nal ⁴ ,Lys ⁵ (4-FB)]ipamorelin	1920

Table 3. IC_{50} values of ipamorelin and a series of derivatives thereof.

Surprisingly, the coupling of a 4-fluorobenzoyl group to the side-chain of lysine was found to slightly improve the IC_{50} value of ipamorelin (LCE00210) from 483 nM to 170 nM (LCE00211). This could be due to the fact that the bulky fluorobenzoyl group may be decreasing ipamorelin binding to the polar sub-pocket of the GHS-R1a but increasing non-covalent interactions with aromatic residues (e.g. Phe220, Phe222 and Phe226⁸⁴) in the non-polar sub-pocket. This would then promote stronger overall binding to the

receptor. An investigation into lengthening the lysine side-chain by way of introducing a short mini-PEG linker (aminoethanoethylamine, AEEA) between it and the 4-fluorobenzoyl group (LCE00217) effectively “re-set” the IC_{50} value back to that of the parent compound ipamorelin (*cf.* 474 nM for LCE00217 to 483 nM for LCE00210). This is presumably the result of an increase in distance between the 4-fluorobenzoyl moiety and the aromatic residues in the non-polar sub-pocket mentioned previously. A compound with comparable affinity to the 4-FB-ipamorelin analogue was synthesized by replacement of the D-Phe residue with D-2-Thi, resulting in an $IC_{50} = 161$ nM ([D-2-Thi⁴, Lys⁵(4-FB)]ipamorelin, LCE00267). The rationale behind this modification was based on a paper by Hansen and co-workers which described the replacement of D-Phe with a D-2-Thi amino acid for a series of tripeptide ipamorelin derivatives.⁶⁹ This had the effect of reducing EC_{50} values by an order of magnitude.⁶⁹ By assuming that a strong efficacy is indicative of a strong binding affinity, an improvement in the IC_{50} value was predicted. Instead, binding affinity was essentially retained (*cf.* 161 nM to 171 nM for LC00210). It may be hypothesized that because the aromatic character (resonance energy) of the thiophene functionality in D-2-Thi is similar to that of benzene in D-Phe (*cf.* 36 kcal/mol to 29 kcal/mol),¹⁰⁷ π -stacking/hydrophobic interactions with the ghrelin receptor may be retained, leading to a very similar half-maximal inhibitory concentration. Next, the primary amine in the N-terminus of ipamorelin was replaced with the secondary amine isonipecotic acid (Inp) so as to make the resultant compound (LCE00268) similar to the Genetech peptidomimetic G-7039, known to have an $EC_{50} = 0.18$ nM.⁵² The increase in the IC_{50} value that resulted in moving from the primary amine (LCE00211, $IC_{50} = 171$ nM) to the secondary amine (LCE00268, $IC_{50} = 688$ nM) could be explained by the fact that the salt bridge with the Glu124 residue in TM3 (polar binding pocket) would be more difficult to form due to an increase in steric hindrance.

An order of magnitude reduction in binding affinity for the ghrelin receptor was found when the D-Phe residue and primary amine in LCE00211 were replaced with D-2-Nal and Inp respectively (LCE00269, $IC_{50} = 1920$ nM). This was carried out in order to probe the importance of the D-Phe residue in sub-pocket binding. The increase in the IC_{50} value may mean that the D-Phe residue is involved in similar π - π or hydrophobic interactions with Phe119 (TM3, polar sub-pocket) as the very same residue in the active tetrapeptide

core of ghrelin.^{84, 87} A similar reduction in binding affinity is achieved by introducing a secondary amine into the N-terminus of the peptide (Inp) along with a D-2-Thi moiety ([Inp¹,D-2-Thi⁴,Lys⁵(4-FB)]ipamorelin, IC₅₀ = 1170 nM). Both of these modifications may be making the resulting compound (LCE00246) unrecognizable to either binding domain of the GHS-R1a. In spite of the slight improvements made to the binding affinity of ipamorelin, it is clear that the 4-fluorobenzoyl modification does not yield the desired IC₅₀ of < 100 nM. Attention was therefore turned to peptidomimetic agonists with much lower initial IC₅₀ values.

Previous work on the most well-known GHRPs (GHRP-1, GHRP-2 and GHRP-6) indicated that this series of peptides could be amenable to the same amino group fluorobenzoylation that ipamorelin was subjected to. This was shown by the low nanomolar K_i values that were acquired for GHRP-6 and GHRP-2 (3.3 nM and 1.4 nM respectively) in a recent study by Pinyot *et al.*, using HEK293/GHS-R1a cells.¹⁰⁶ All three of the compounds were assayed to determine their IC₅₀ values as this is not directly comparable to the known literature binding affinity (K_i). Table 4 shows the results.

LCE no.	Compound Name	IC ₅₀ , nM
00240	GHRP-1	181
00282	GHRP-2	449
00239	GHRP-6	73
00272	[Lys ⁶ (4-FB)]GHRP-6	384
00298	[Dpr ⁶]GHRP-6	397
00281	[Dpr ⁶ (4-FB)]GHRP-6	1060

Table 4. IC₅₀ values of GHRPs and their derivatives.

It was discovered that out of the three peptides, Momany and Bowers' first GHRP⁴⁰ (GHRP-6, H-His-D-Trp-Ala-Trp-D-Phe-Lys-NH₂) was found to have the strongest

binding affinity for the ghrelin receptor ($IC_{50} = 73$ nM, LCE00239) compared to GHRP-1 ($IC_{50} = 181$ nM, LCE00240) and GHRP-2 ($IC_{50} = 449$ nM, LCE00282). This peptide was therefore transformed into the fluorobenzoylated congener [Lys⁶(4-FB)]GHRP-6 (LCE00272). Conversely, this alteration was not accepted favourably by the GHS-R1a despite the previous success achieved with ipamorelin ($IC_{50} = 384$ nM compared to $IC_{50} = 171$ nM for [Lys⁵(4-FB)]ipamorelin). One possible reason for this is that GHRP-6 only binds to the polar sub-pocket (or has a very strong selectivity for it)⁸² and thus an attempt to change its sub-pocket selectivity will simply prevent it from binding to the ghrelin receptor rather than making it preferentially bind to the non-polar sub-pocket. In an effort to increase affinity for the ghrelin receptor, the lysine side-chain of GHRP-6 was shortened by replacing it with Dpr. As a consequence of this, the IC_{50} value for both the non-fluorobenzoylated derivative ([Dpr⁶]GHRP-6, LCE00298) and the fluorobenzoylated congener ([Dpr⁶(4-FB)]GHRP-6, LCE00281) increased considerably (397 nM and 1060 nM respectively). A larger increase was observed for [Dpr⁶(4-FB)]GHRP-6 compared to [Dpr⁶]GHRP-6 indicating that the combination of a Dpr residue and a 4-fluorobenzoyl group had a more negative impact on receptor binding compared to the Dpr residue in isolation. Not only does the lysine side-chain appear to be an important pharmacophoric site for receptor binding in GHRP-6 (an observation at odds with the results from Huang *et al*'s study⁸³ and those obtained for ipamorelin), but the length of the alkyl chain also seems to play an important role. Given that the IC_{50} values for GHRP-1 (181 nM) and GHRP-2 (449 nM) were considerably higher than that of GHRP-6 (73 nM) and the subsequent failure of GHRP-6 fluorobenzoylation, further derivatization of this class of peptidomimetics agonists was not pursued.

The final peptidomimetics that were investigated in this study were two Genentech pentapeptides: G-7039 (H-Inp-D-2-Nal-D-2-Nal-Phe-Lys-NH₂) and [1-Nal⁴]G-7039 (H-Inp-D-2-Nal-D-2-Nal-1-Nal-Lys-NH₂). These compounds were chosen as a consequence of the fact that they both showed low nanomolar efficacy in a series of rat pituitary cell assays looking at GH release ($EC_{50} = 0.18$ nM for G-7039⁵² and 0.10 nM for [1-Nal⁴]G-7039,¹⁰⁸ respectively). The synthesized benzoyl congeners can be seen in Table 5.

LCE no.	Compound Name	IC ₅₀ , nM
00245	G-7039	5.2
00243	[Lys ⁵ (4-FB)]G-7039	242
00244	[1-Nal ⁴]G-7039	28
00270	[1-Nal ⁴ ,Lys ⁵ (4-FB)]G-7039	69

Table 5. IC₅₀ values of Genentech peptidomimetics and their derivatives.

A cursory glance at Table 5 shows that in both cases the coupling of 4-[¹⁹F]FBA to the lysine side-chain of the Genentech peptidomimetics results in a reduced binding affinity. What is interesting to note is that whilst blocking the lysine side-chain of G-7039 with *para*-fluorobenzoic acid has the effect of increasing the half-maximal inhibitory concentration by almost two orders of magnitude (5.2 nM for G-7039 to 242 nM for [Lys⁵(4-FB)]G-7039) only a minor increase in the IC₅₀ value is seen for [1-Nal⁴]G-7039 (28 nM to 69 nM for [1-Nal⁴,Lys⁵(4-FB)]G-7039). This is a significant finding, as both G-7039 and [1-Nal⁴]G-7039 differ only in a single residue; the former compound contains a Phe and the latter a 1-Nal. It is therefore clear that such a considerable change in binding affinity with fluorobenzoylation signifies that G-7039 may be selective for the GHS-R1a polar sub-pocket and [1-Nal⁴]G-7039 for the aromatic sub-pocket. Nevertheless, despite the decrease in the half-maximal inhibitory concentration of both compounds, [1-Nal⁴,Lys⁵(4-FB)]G-7039 represents the first lead compound to be synthesized in this study focusing on the insertion of the 4-fluorobenzoyl moiety into a number of specific peptidomimetics containing a free lysine side-chain. This is because it has a sufficiently low nanomolar IC₅₀ value (69 nM < 100 nM) to be investigated further.

In summary, the introduction of a 4-fluorobenzoyl moiety into the series of peptidomimetic GHS-R1a agonists examined here generally has the effect of weakening the binding affinity for the receptor (G-7039, [1-Nal⁴]G-7039 and GHRP-6) with the exception of ipamorelin. What is also apparent is that even minute changes to the

structure of the peptidomimetic agonists can have a significant impact on binding affinity (see previous discussion on G-7039 and [1-Nal⁴]G-7039). The 4-fluorobenzoylation approach described within this section enabled the identification of the peptidomimetic [1-Nal⁴,Lys⁵(4-FB)]G-7039 as a lead compound. This peptidomimetic will act as a “cold” standard that will be evaluated in a number of *in vitro* tests prior to ¹⁸F-radiolabelling of the parent peptidomimetic [1-Nal⁴]G-7039 with [¹⁸F]FBA or [¹⁸F]SFB. The *in vitro* assays that are to be performed include calculating partition coefficients and determining efficacy. These tests are important in anticipating the behaviour of the lead peptidomimetic [1-Nal⁴,Lys⁵(4-FB)]G-7039 *in vivo* before synthesizing the “hot” congener by ¹⁸F-radiolabelling.

2.4.1.3 4-FB Agonist Partition Coefficients

The requirement for a lead peptidomimetic GHS-R1a agonist to have a binding affinity of < 100 nM for the ghrelin receptor is not the only factor that is crucial in developing it into an imaging agent. One of these additional factors is the compound’s lipophilicity.

Generally speaking, the lipophilicity (or hydrophobicity) of a compound is expressed as a ratio of the molecule’s distribution in a mixture of *n*-octanol and water. This distribution is known as the “partition coefficient,” P (Eqn 1).⁸⁰

$$P = \frac{[\text{compound in } n - \text{octanol}]}{[\text{compound in water}]} \quad (1)$$

Hydrophilic molecules tend to have a higher concentration in water, thereby resulting in low P values. The opposite is true for hydrophobic compounds.⁸⁰ The partition coefficient is usually expressed as the logarithm of P (logP), a dimensionless quantity where favourable values for drugs or imaging agents are in the range of 1-3,¹⁰⁹ implying that hydrophobicity is preferred. This propensity for hydrophobicity can be explained based on the fact that as it increases, lead compounds are better able to cross biological barriers and interact with target receptors.⁸⁰ In other words, an improvement in biological activity often results.⁸⁰ On the one hand, this increase is especially important for imaging agents, as a rise in hydrophilicity is more likely to lead to non-specific binding.² This would in

turn result in reduced target visualization, increased background image contrast as well as higher toxicity *in vivo*.⁸⁰ On the other hand, if the $\log P$ value is too high, the imaging probe suffers from solubility issues and fast clearance from the body.⁸⁰ Finding the correct range for $\log P$ is therefore critical in predicting the behaviour of lead compounds in the body.

The lipophilicity of a specific compound can be determined in two ways: experimentally or computationally. The most accurate way of determining the $\log P$ value is through the “shake-flask” method.¹¹⁰ This technique essentially involves dissolution of the compound in a pre-equilibrated 1:1 mixture of *n*-octanol and water, taking aliquots after a specified period of time and finding the concentration of the compound in each phase using HPLC.¹¹⁰ Unfortunately this particular method suffers from a number of drawbacks. Firstly, it is labour intensive, expensive and frequently time-consuming as each sample has to be run in triplicate.¹¹¹ Secondly, complete dissolution of the sample is required, which is often difficult to observe when only small quantities are available. In addition, many of the hydrophobic peptidomimetics synthesized in this chapter have solubility issues in water. For these reasons a computational approach for determining lipophilicity was taken.

The $\log P$ values for the 4-FB peptidomimetic GHS-R1a agonists were thus determined using ACD/Log P ^{112, 113} and XLOGP3¹¹⁴ computer software. These programs were chosen based on a study by Thompson and co-workers,¹¹¹ where a comparison was made between seven fragment-based computational programs and their degree of accuracy in predicting $\log P$ within ± 0.5 to ± 1.0 log units of an experimentally determined value.¹¹¹ The experimental database was exclusively composed of peptides of varying length and type (blocked, unblocked and cyclic).¹¹¹ Both programs scored highest with blocked peptides, which as a class of compounds most accurately represent the 4-fluorobenzoyl growth hormone secretagogues synthesized here.¹¹¹

In terms of calculating lipophilicity, ACD/Log P uses an experimental data set of over 18,000 $\log P$ measurements and predicts lipophilicity using an additive-constitutive algorithm.^{112, 113} This algorithm takes into consideration contributions from individual

atoms as well as fragments.^{112, 113} XLOGP3 computes the $\log P$ value of the desired compound by using a knowledge-based atom-additive model and is calibrated using a training set of 8199 organic compounds.¹¹⁴ Table 6 lists the results of the computational calculations for the 4-FB peptidomimetic ghrelin receptor agonists.

LCE number	Peptidomimetic	LogP (ACD/LogP)	LogP (XLOGP3)
00210	Ipamorelin	1.72 ± 0.85	1.76
00211	[Lys ⁵ (4-FB)]ipamorelin	3.97 ± 0.89	3.78
00217	[Lys ⁵ (AEEA-4-FB)]ipamorelin	2.80 ± 0.93	2.83
00239	GHRP-6	1.51 ± 0.88	1.92
00240	GHRP-1	2.60 ± 0.90	2.79
00243	[Lys ⁵ (4-FB)]G-7039	7.53 ± 0.88	7.20
00244	[1-Nal ⁴]G-7039	6.51 ± 0.82	6.44
00245	G-7039	5.28 ± 0.82	5.19
00246	[Inp ¹ ,D-2-Thi ⁴ ,Lys ⁵ (4-FB)]ipamorelin	3.60 ± 0.89	3.84
00267	[D-2-Thi ⁴ ,Lys ⁵ (4-FB)]ipamorelin	3.65 ± 0.90	3.50
00268	[Inp ¹ ,Lys ⁵ (4-FB)]ipamorelin	3.92 ± 0.89	4.13
00269	[Inp ¹ ,D-2-Nal ⁴ ,Lys ⁵ (4-FB)]ipamorelin	5.15 ± 0.89	5.38
00270	[1-Nal ⁴ ,Lys ⁵ (4-FB)]G-7039	8.76 ± 0.88	8.45
00272	[Lys ⁶ (4-FB)]GHRP-6	3.76 ± 0.92	3.93
00281	[Dpr ⁶ (4-FB)]GHRP-6	3.86 ± 0.93	2.86
00282	GHRP-2	3.41 ± 0.86	3.27
00298	[Dpr ⁶]GHRP-6	1.61 ± 0.89	0.84

Table 6. Computationally calculated $\log P$ values for 4-FB peptidomimetic GHS-R1a agonists. ACD/ $\log P$ states $\log P$ values as \pm standard deviation.

A number of general trends can be seen from the table above. Firstly, the difference between the computed $\log P$ of both programs is small (≤ 1.0 log units), resulting from the fact that both use a fragment-based approach to calculate lipophilicity. Secondly, the introduction of a 4-fluorobenzoyl functionality into a “parent” peptidomimetic (e.g. [1-Nal⁴]G-7039) leads to an increase in hydrophobicity for all derivatives (+ 2.25 for ACD/Log P and +2.01/2.02 for XLOGP3). Thirdly, most of the parent peptidomimetics possess a favourable $\log P$ value in the 1-3 unit range mentioned previously. The only exception to this is G-7039 (5.28 ± 0.82 , 5.19) and [1-Nal⁴]G-7039 (6.51 ± 0.82 , 6.44), which can be attributed to the smaller size of the peptidomimetics and prevalence of strongly hydrophobic aromatic residues (D-2-Nal, 1-Nal, Phe).

Unfortunately, the lead compound [1-Nal⁴,Lys⁵(4-FB)]G-7039 possesses a very high $\log P$ value (8.76 ± 0.88 for ACD/Log P and 8.45 for XLOGP3). This suggests that it is not suited for *in vivo* PET imaging because it may cause a high degree of non-specific binding as well as suffering from potential solubility issues. Nevertheless, the $\log P$ value is not an exact predictor of compound behaviour *in vivo*, owing to criticism for the use of *n*-octanol as an organic phase.¹¹¹ *N*-octanol does not adequately isolate hydrophobic interactions from different non-covalent interactions as it still retains a high degree of water.¹¹¹ In addition, [1-Nal⁴,Lys⁵(4-FB)]G-7039 possesses a considerably lower IC₅₀ value compared to the next best compound [D-2-Thi⁴,Lys⁵(4-FB)]ipamorelin (*cf.* 69 nM to 161 nM) and therefore, despite its unfavourable lipophilicity, it was still carried forward for further *in vitro* assays.

2.4.1.4 Calcium Flux Assay

The second *in vitro* assay performed on the 4-fluorobenzoyl lead agonist was a calcium flux dose-response assay. This experiment allows the determination of the half-maximal effective concentration (EC₅₀) for [1-Nal⁴,Lys⁵(4-FB)]G-7039, a measure of the concentration of the agonist required to produce 50% of the maximum biological effect resulting from ghrelin receptor activation.⁸⁰ In this particular case, the biological effect of the peptidomimetic [1-Nal⁴,Lys⁵(4-FB)]G-7039 is the release of intracellular calcium ions, a process which is detected by fluorescence using a FLIPR^{TETRA} instrument (see

experimental section 4.3 for more details). Endogenous ghrelin was used as a control in this assay, which was performed by EMD Millipore's GPCRProfiler® service. The data acquired is presented in Figure 14.

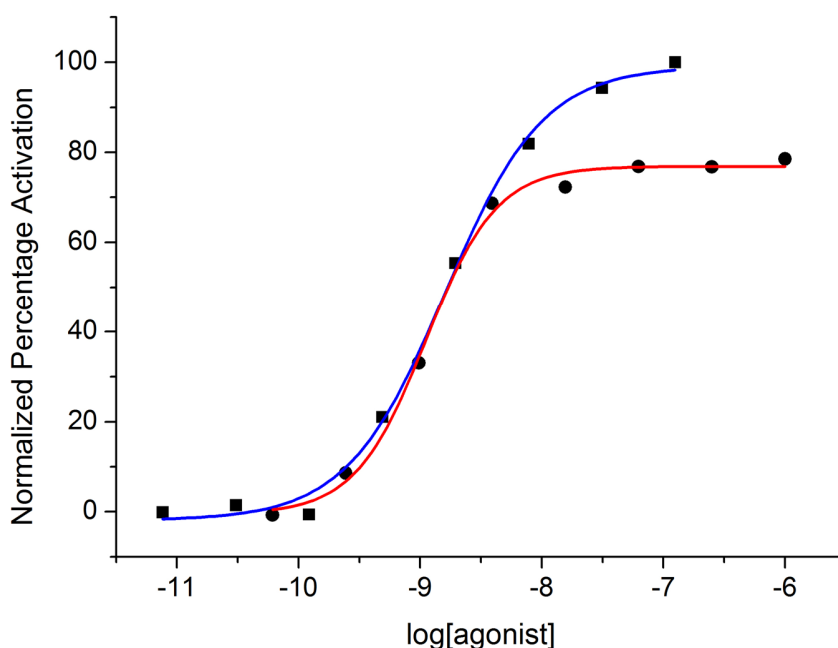


Figure 14. Efficacy curves for lead agonist [1-Nal⁴,Lys⁵(4-FB)]G-7039 (circles) and the control ligand ghrelin (squares).

The control ligand ghrelin was found to have a low *in vitro* potency ($EC_{50} = 1.6$ nM), which is expected for the endogenous ligand of the GHS-R1a. The EC_{50} value of [1-Nal⁴, Lys⁵(4-FB)]G-7039 was found to be 1.1 nM. This demonstrates that the presence of the 4-fluorobenzoyl group still results in a low nanomolar efficacy. This is in spite of the slight increase in the IC_{50} value compared to the parent compound [1-Nal⁴]G-7039 ($IC_{50} = 69$ nM *vs* 28 nM respectively). The low *in vitro* potency acquired for [1-Nal⁴,Lys⁵(4-FB)]G-7039 indicates that it is a potent ghrelin receptor agonist.

2.4.1.5 ^{18}F -Radiochemistry

The initial approach to radiolabelling the precursor compound [1-Nal⁴]G-7039 employed the radioactive compound [^{18}F]FBA. This prosthetic group has been used to radiolabel resin-bound peptides in the solid-phase,^{97, 100} but literature evidence for radiolabelling in solution appears to be sparse. In order to couple [^{18}F]FBA to a peptide, pre-activation using a coupling reagent such as 1-[bis(dimethylamino)methylene]-1*H*-1,2,3-triazolo[4,5-*b*]pyridinium 3-oxid hexafluorophosphate (HATU) or HCTU is required. This enables formation of the active ester of [^{18}F]FBA (through the same mechanism as for an amino acid) that can then be nucleophilically attacked by the desired group on the peptide.

Past attempts at solution-phase radiolabelling of GLP-1 analogues with [^{18}F]FBA in our laboratory were met with limited success.¹¹⁵ Despite these drawbacks, solution-phase coupling of 4- [^{19}F]FBA to the lysine side-chain of [1-Nal⁴]G-7039 using the coupling reagent HATU in DMF resulted in fluorobenzoylated product after 5 minutes. This can be seen in the crude HPLC UV trace (Figure 15).

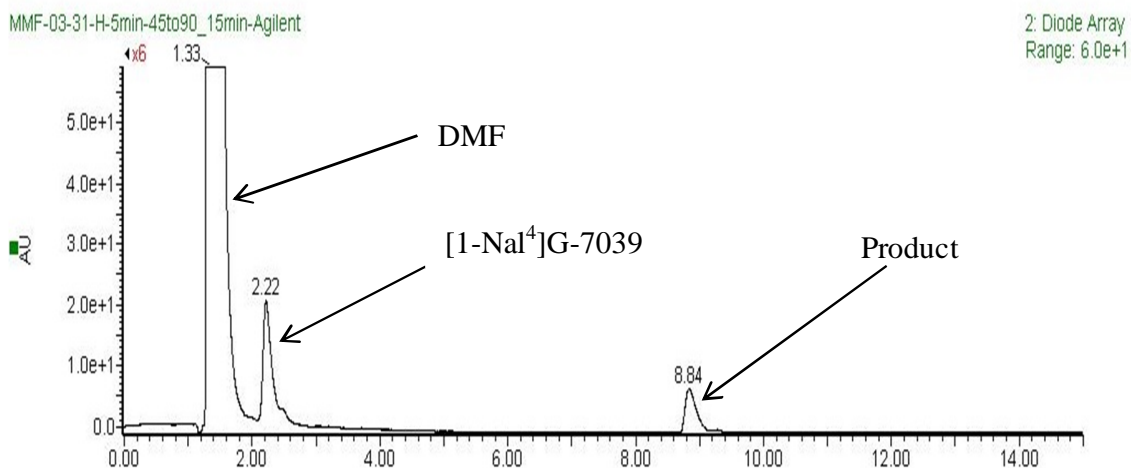
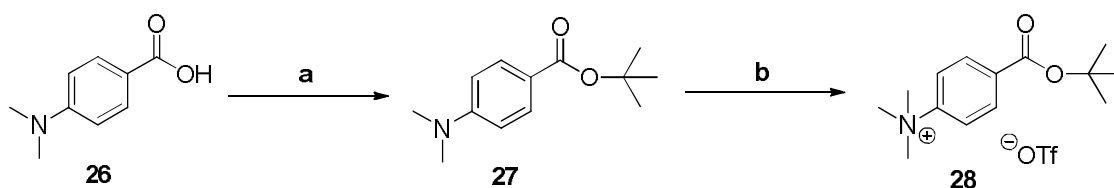


Figure 15. Crude HPLC UV trace of the reaction between [1-Nal⁴]G-7039 and 4- [^{19}F]FBA in DMF.

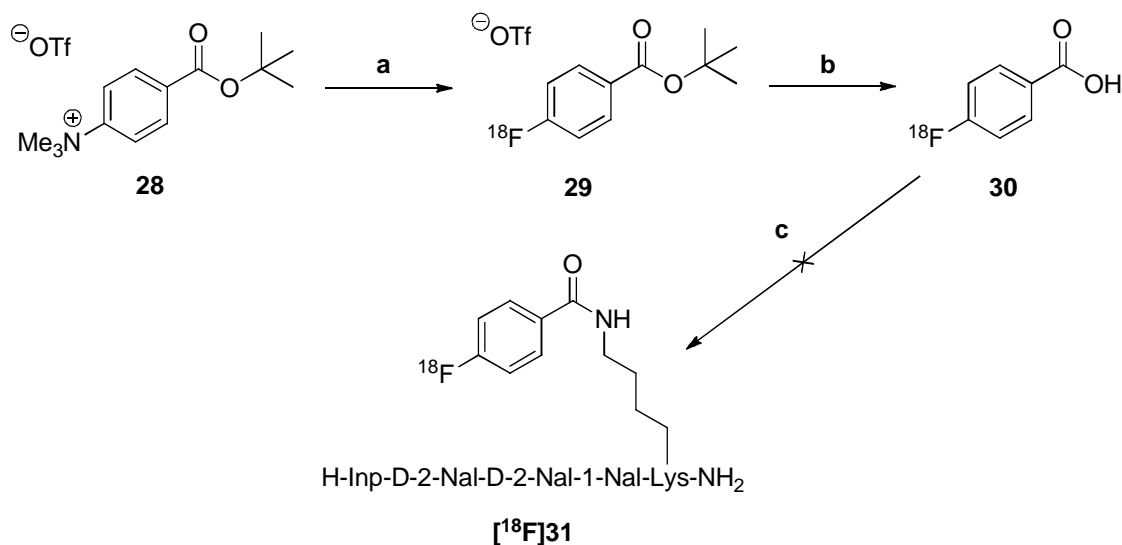
The retention time and mass of the product at 8.84 minutes corresponds to that of [1-Nal⁴, Lys⁵(4-FB)]G-7039 made by solid-phase peptide synthesis, thereby confirming that site-selective fluorobenzoylation has occurred at the side-chain of lysine as opposed to the N-terminus of the secondary amine. This is because the retention time of the N-terminally fluobenzoylated species would be different. As a consequence of the successful formation of the cold lead compound [1-Nal⁴,Lys⁵(4-FB)]G-7039, coupling of [¹⁸F]FBA to the lysine side-chain of the precursor [1-Nal⁴]G-7039 was pursued.

In order to synthesize the [¹⁸F]FBA prosthetic group, the cold precursor triflate salt was first obtained by the synthetic pathway shown below (Scheme 4). Acid catalysed esterification of the 4-dimethylaminobenzoic acid starting material **26** afforded the intermediate t-butyl ester **27**. The tertiary amine of this compound was then methylated with MeOTf (under a blanket of nitrogen) to give the final product triflate salt **28**. This compound was acquired in a yield of 38% and > 95% purity by UHPLC.



Scheme 4. Synthesis of the precursor 4-(tert-butoxycarbonyl)-*N,N,N*-trimethylbenzenammonium triflate salt. *Reagents and Conditions:* a) i) trifluoroacetic anhydride, THF, 0°C ii) ^tBuOH, room temperature, 2 hrs b) MeOTf, N₂, 0°C, 1 hour.

Having synthesized the precursor salt **28**, ¹⁸F-radiolabelling was initiated. The pathway to the [¹⁸F]FBA prosthetic group is outlined in Scheme 5. The first step in this procedure involved nucleophilic aromatic substitution of the triflate salt **28** with the [¹⁸F] anion acquired from the PET cyclotron by irradiation of [¹⁸O]H₂O (the so-called ¹⁸O(p,n)¹⁸F nuclear reaction). This led to the formation of radioactive compound **29**. Acid-catalysed de-esterification furnished the prosthetic group [¹⁸F]FBA **30** after 5 minutes. This was then reacted with the peptidomimetic precursor agonist [1-Nal⁴]G-7039 for 20 minutes *via* the solution-phase coupling procedure previously used with 4-[¹⁹F]FBA. After 20 minutes, an analytical HPLC was run in order to check the progress of the reaction.



Scheme 5. Synthesis of $[^{18}\text{F}]\text{FBA}$ and attempted coupling to precursor peptidomimetic $[1\text{-Nal}^4]\text{G-7039}$. *Reagents and Conditions:* a) K 222, K_2CO_3 , $[^{18}\text{F}]^-$, DMSO, 120°C , 10 minutes; b) 5M HCl, 120°C , 5 minutes; c) $[1\text{-Nal}^4]\text{G-7039}$, 0.023 M HATU/DMF, 4.8 % DIPEA/DMF, DMF, room temperature, 20 minutes.

As no product was observed in the radio-chromatogram, an additional aliquot of DIPEA/DMF and HATU/DMF were added. This failed to yield a fluorobenzoylated product after a further 20 minutes. Co-injection of the cold standard 4- $[^{19}\text{F}]\text{FBA}$ and $[^{18}\text{F}]\text{FBA}$ showed that formation of the latter “hot” prosthetic group was successful (Figure 16, overleaf) in spite of the failure of the coupling reaction with $[1\text{-Nal}^4]\text{G-7039}$. Seeing as the coupling strategy employing pre-activation of $[^{18}\text{F}]\text{FBA}$ with HATU did not succeed, no further attempts were made.

Following the failure of the preceding ^{18}F -radiolabelling strategy, an alternative method involving $[^{18}\text{F}]\text{SFB}$ was exploited. This molecule is by far the most commonly used ^{18}F -radiolabelled prosthetic group for functional group acylation in the literature. It is typically used to acylate N-terminal and side-chain amino groups of peptide residues as well as small molecules.¹¹⁶⁻¹¹⁸ One of the main advantages of $[^{18}\text{F}]\text{SFB}$ is that unlike $[^{18}\text{F}]\text{FBA}$, it does not require pre-activation with HATU or HCTU as it is already present as an active *N*-hydroxysuccinimide (NHS) ester. In addition, $[^{18}\text{F}]\text{SFB}$ may be prepared in a short period of time (1 hour) and in a facile manner using only three synthetic steps.⁹⁹

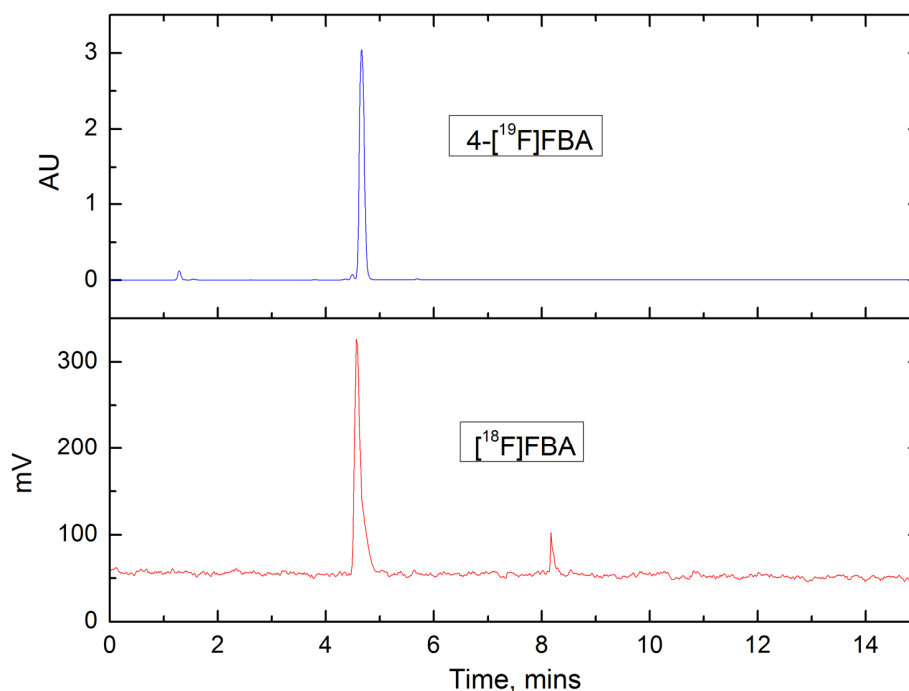
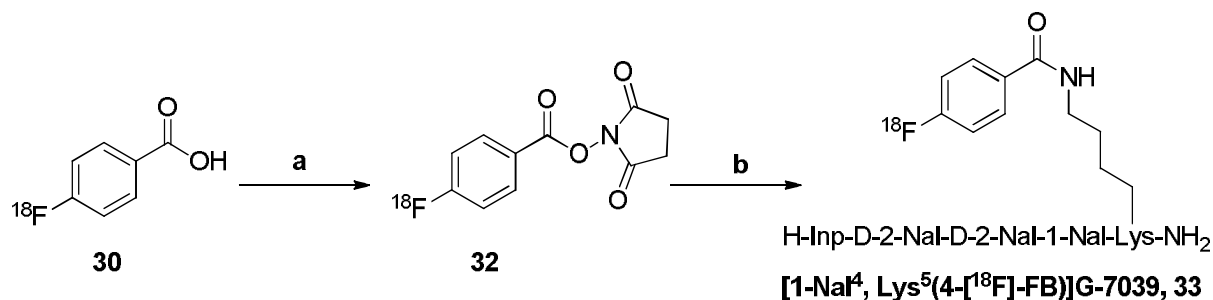


Figure 16. A series of chromatograms resulting from the co-injection of cold standard 4- $[^{19}\text{F}]\text{FBA}$ ($\lambda = 254 \text{ nm}$) and crude “hot” product $[^{18}\text{F}]\text{FBA}$.

Furthermore, the synthesis of $[^{18}\text{F}]\text{SFB}$ was recently optimised to a short reaction time (68 minutes) and reproducible radiochemical yields (34-38 %) through the use of a remotely controlled synthesis module.⁹⁹ This enabled the production of large quantities of $[^{18}\text{F}]\text{SFB}$ which would otherwise be dangerous by manual radiosynthesis. The synthetic pathway herein was initiated by $[^{18}\text{F}]\text{FBA}$ synthesis utilizing the procedure outlined in Scheme 5 above. This was followed by coupling of the crude fluorobenzoyl group to NHS (step a, Scheme 6).

The $[^{18}\text{F}]\text{FBA}$ (**30**) was coupled to NHS using the coupling reagent *N*-(3-dimethylaminopropyl)-*N'*-ethylcarbodiimide (EDC) which led to the formation of the $[^{18}\text{F}]\text{SFB}$ prosthetic group **32**. The NHS leaving group pre-activates the radiolabelled product towards nucleophilic attack when coupling with $[1\text{-NaI}^4]\text{G-7039}$.



Scheme 6. Synthesis of the [¹⁸F]SFB prosthetic group and subsequent ¹⁸F-radiolabelling of [1-Nal⁴]G-7039. *Reagents and Conditions:* a) EDC, NHS, MeCN, room temperature, 10 minutes; b) [1-Nal⁴]G-7039, DIPEA, MeCN/H₂O 1:1, 50-70°C, 15 minutes.

The crude ¹⁸F-radiolabelled prosthetic group **32** was purified by reverse-phase HPLC (35-60 % MeCN + 0.1% TFA gradient system, with retention time $R_t = 9.3$ mins) to give a decay-corrected radiochemical yield of 59%. An analytical HPLC (25-90% MeCN + 0.1% TFA) was performed to check the radio-purity of the final compound, which was found to be > 99%. The radio-chromatogram for pure [¹⁸F]SFB can be seen in Figure 17.

The pure [¹⁸F]SFB was finally added to the peptide precursor [1-Nal⁴]G-7039 in a 1:1 mixture of MeCN/H₂O using a small quantity of the hindered base DIPEA. After 15 minutes, the crude [1-Nal⁴,Lys⁵(4-[¹⁸F]-FB)]G-7039 lead compound was obtained. This was then purified using the same gradient system as for [¹⁸F]SFB (35-60 % MeCN + 0.1% TFA, $R_t = 12.3$ mins). The final radiolabelled peptide [1-Nal⁴,Lys⁵(4-[¹⁸F]-FB)]G-7039 (**33**) was obtained in a decay-corrected radiochemical yield of 52% with a radiochemical purity of > 98% and reaction time of 127 minutes after the end-of-synthesis (EOS). Figure 18 displays a series of stacked chromatograms including the cold standard [1-Nal⁴,Lys⁵(4-FB)]G-7039, the peptidomimetic precursor [1-Nal⁴]G-7039 as well as the radiolabelled [1-Nal⁴,Lys⁵(4-[¹⁸F]-FB)]G-7039 lead peptidomimetic. The retention times of the cold standard and hot peptide are almost identical ([1-Nal⁴,Lys⁵(4-FB)]G-7039, $R_t = 6.70$ mins compared to $R_t = 6.65$ mins for the hot peptide), indicating that the precursor [1-Nal⁴]G-7039 has been selectively radiolabelled at the amino group of the lysine side-chain.

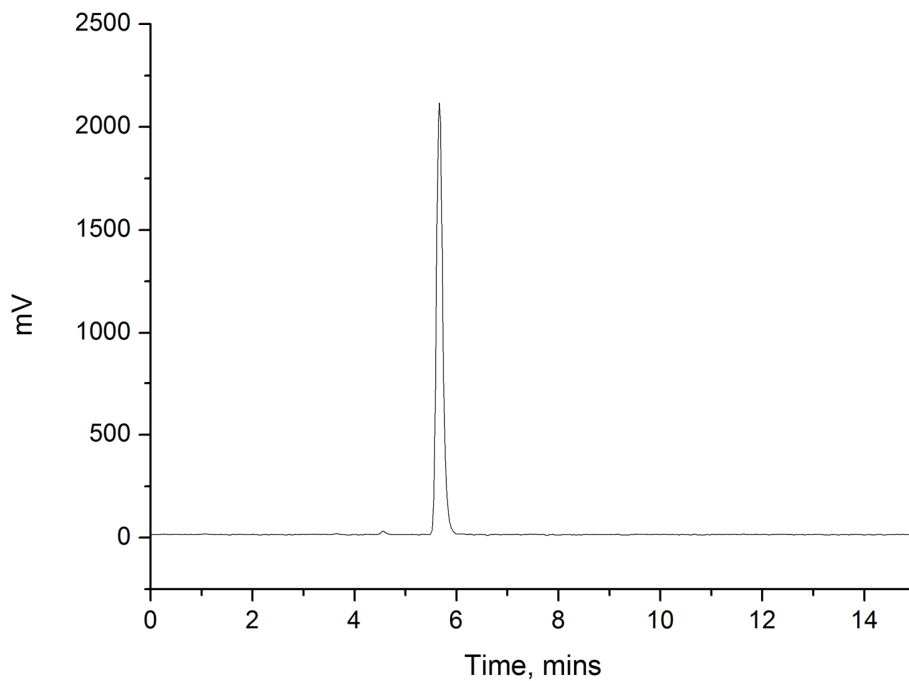


Figure 17. HPLC radio-chromatogram of pure $[^{18}\text{F}]\text{SFB}$.

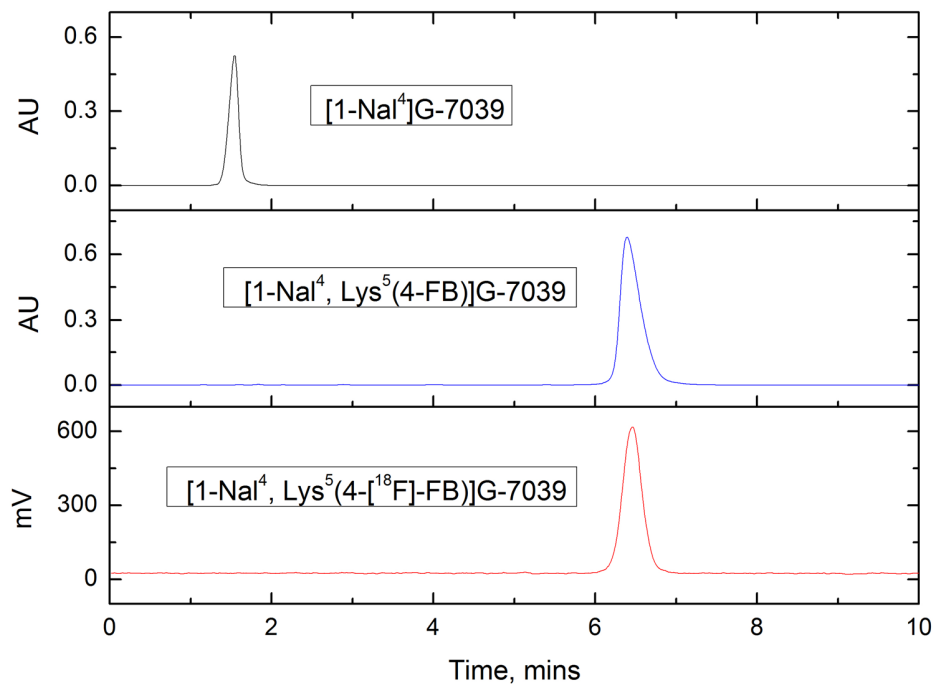


Figure 18. Stacked HPLC Chromatograms for $[1\text{-NaI}^4]\text{G-7039}$, $[1\text{-NaI}^4, \text{Lys}^5(4\text{-FB})]\text{G-7039}$ (both $\lambda = 254 \text{ nm}$) and $[1\text{-NaI}^4, \text{Lys}^5(4\text{-}^{18}\text{F}\text{-FB})]\text{G-7039}$.

Further evidence for successful coupling of [^{18}F]SFB to [1-Nal 4]G-7039 *via* the lysine side-chain was provided by a co-injection of a pre-mixed solution with a 1:1 ratio of the cold standard and “hot” peptidomimetic. This was carried out in order to make sure that minor changes in HPLC pressure between analytical runs were not causing accidental alignment of [1-Nal 4 ,Lys 5 (4-[^{18}F]-FB)]G-7039 with any by-products present in [1-Nal 4 ,Lys 5 (4-FB)]G-7039 (Figure 19 overleaf). The co-injection again showed very similar retention times between the two peptidomimetic species ([1-Nal 4 ,Lys 5 (4-FB)]G-7039 R_t = 6.26 mins and [1-Nal 4 ,Lys 5 (4-[^{18}F]-FB)]G-7039 R_t = 6.17 mins) lending further credence to regioselective ^{18}F -fluorobenzoylation at the lysine side-chain. One possible reason for this selectivity may be the increase in steric crowding afforded by the secondary amine of isonipecotic acid in the N-terminus of [1-Nal 4]G-7039. This factor, coupled with the steric bulk of [^{18}F]SFB (as well as the fact that the lysine side-chain is quite far removed from the core of the peptidomimetic) could explain why regioselective coupling of [^{18}F]SFB appears to be selective for the lysine side-chain of [1-Nal 4]G-7039.

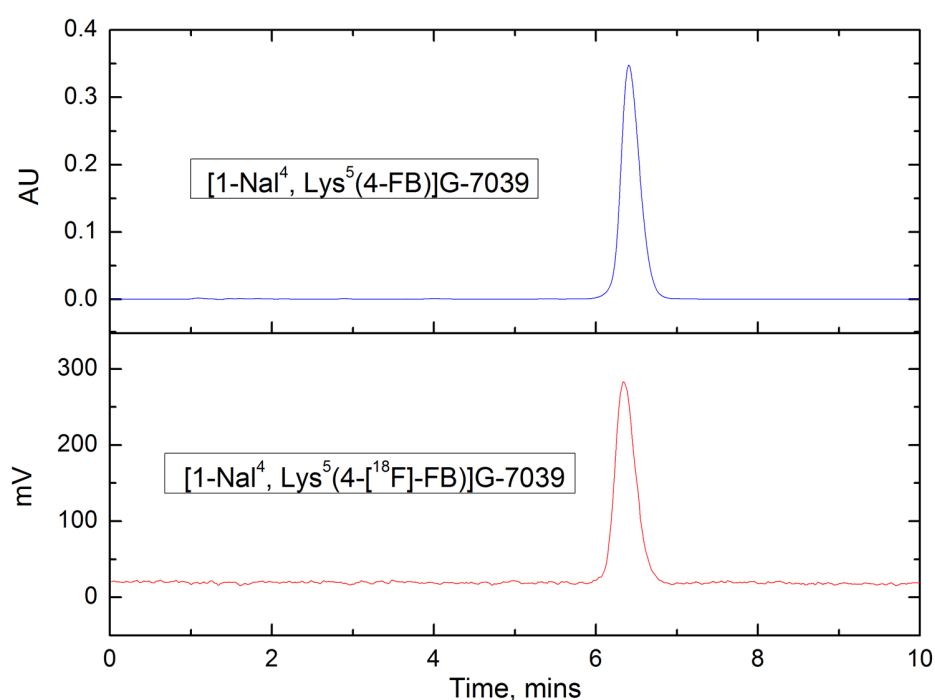


Figure 19. Stacked HPLC chromatograms resulting from the co-injection of cold standard [1-Nal 4 ,Lys 5 (4-FB)]G-7039 (λ = 254 nm) and [1-Nal 4 ,Lys 5 (4-[^{18}F]-FB)]G-7039.

Finally, a calibration curve was set-up at four different concentrations (0.46 μM , 0.92 μM , 4.6 μM and 9.2 μM) for the cold standard [1-Nal⁴,Lys⁵(4-FB)]G-7039. For each concentration, an analytical HPLC was run a minimum of two times in order to achieve area under the curve (AUC) values within 5% of each other. This curve is shown in Figure 20 and enables determination of the specific activity of the radioactive lead compound [1-Nal⁴,Lys⁵(4-[¹⁸F]-FB)]G-7039. By solving the equation for a straight line for x (the concentration of the cold lead compound [1-Nal⁴,Lys⁵(4-FB)]G-7039), and knowing the final volume of the hot peptide acquired (3 ml) the specific activity was found to be equal to 116 MBq/ μmol .

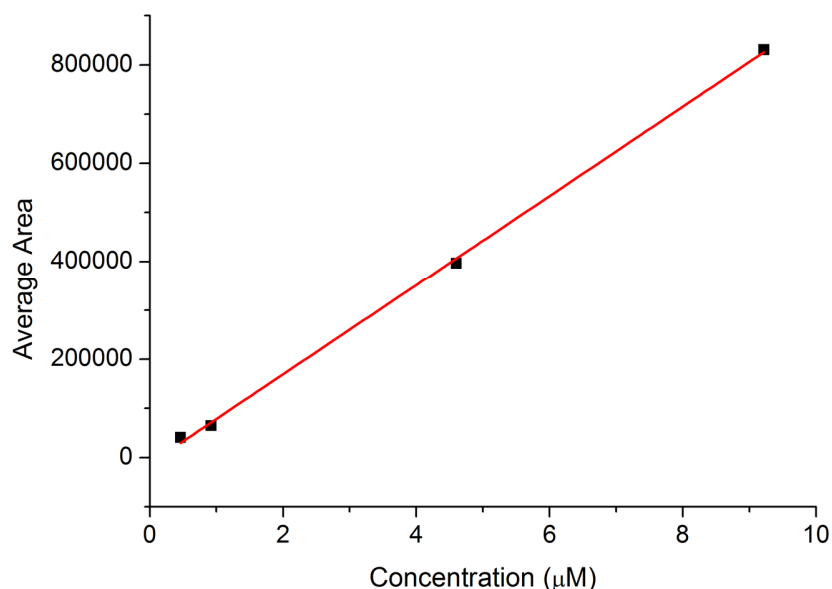


Figure 20. Calibration curve for cold standard [1-Nal⁴,Lys⁵(4-[¹⁸F]-FB)]G-7039.

2.4.1.6 Conclusions

In summary, the 4-[¹⁹F]-FBA prosthetic group was inserted into the lysine side chain of a number of peptidomimetic GHSs (ipamorelin, GHRP-6, G-7039 and [1-Nal⁴]G-7039) in order to investigate possible sites for ¹⁸F-radiolabelling of these compounds. The primary aim of this strategy was to identify a GHS with an IC₅₀ < 100 nM and secondly, to radiolabel the subsequent compound with fluorine-18. A series of receptor binding assays

utilizing HEK293/GHS-R1a cells with [125 I]ghrelin as a competitive radioligand were performed in order to fulfil the primary aim. This resulted in the identification of the lead compound [1-Nal⁴,Lys⁵(4-FB)]G-7039 with an IC₅₀ = 69 nM and a partition coefficient of 8.76 ± 0.88 (ACD/log*P*) and 8.45 (XLOGP3). A calcium flux assay established that agonist activity had been retained after blocking of the lysine side-chain with 4-[19 F]-FBA (EC₅₀ = 1.1 nM). 18 F-radiolabelling of the precursor parent compound [1-Nal⁴]G-7039 with [18 F]SFB led to the synthesis of [1-Nal⁴,Lys⁵(4-[18 F]-FB)]G-7039 in a radiochemical yield of 52% and radiochemical purity of > 98% in a reaction time of 127 minutes after EOS. The specific activity of the final radiotracer was 116 MBq/μmol. Both Figures 18 and 19 strongly imply successful regioselective coupling of the [18 F]SFB to the lysine side-chain of the peptidomimetic GHS-R1a agonist [1-Nal⁴]G-7039. The lead compound [1-Nal⁴,Lys⁵(4-[18 F]-FB)]G-7039 represents (to the best of our knowledge) the first 18 F-radiolabelled ghrelin receptor agonist to be synthesized. With this radioactive compound, a significant step has been made towards PET imaging of the ghrelin receptor in prostate carcinoma, an achievement that should eventually lead to a clinically useable radiotracer that would also enable differentiation between BPH and PCa and play a vital role in early-stage PCa diagnosis

2.5 Alternative ^{18}F -Radiolabelling Strategy

A second approach for adding a ^{18}F radioisotope into the lysine side-chain of the peptidomimetic GHS-R1a agonists was also explored. This involved the racemic 2-fluoropropionyl moiety. This particular strategy was devised on the basis of a recent paper by Haskali and co-workers.¹¹⁹ They prepared the [^{18}F]galacto-Arg-Gly-Asp radiotracer **34** (Figure 21) by prosthetic group radiolabelling of galacto-Arg-Gly-Asp with 4-nitrophenyl 2- ^{18}F fluoropropionate ([^{18}F]NFP, **35**) in a decay corrected radiochemical yield of 20%.¹¹⁹ This compound is currently the gold standard for PET imaging of the alpha-v beta-3 ($\alpha_v\beta_3$) integrin receptor.¹¹⁹

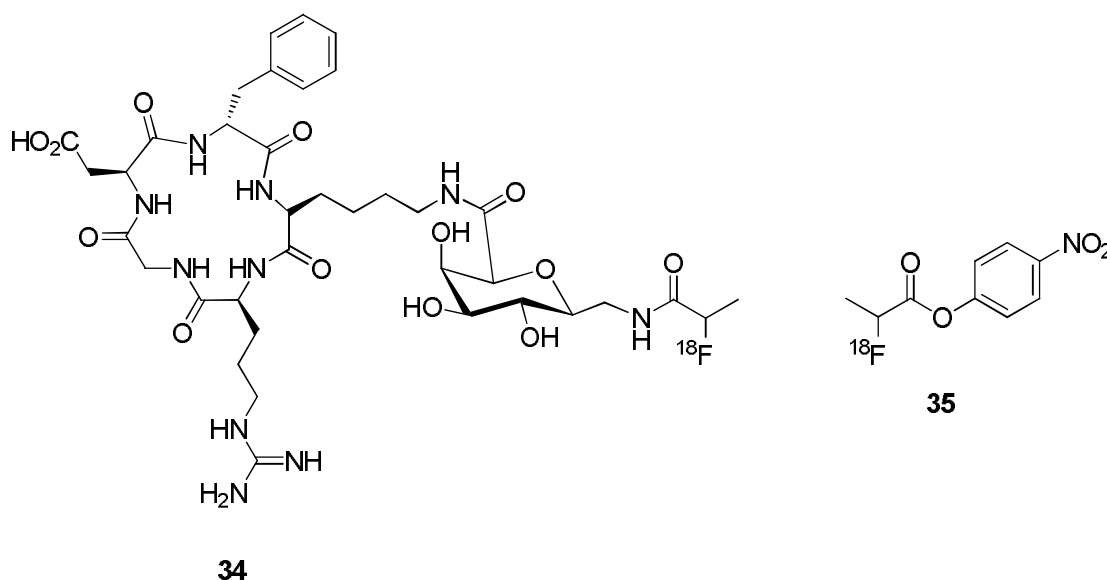


Figure 21. [^{18}F]GalactoRGD and [^{18}F]NFP.

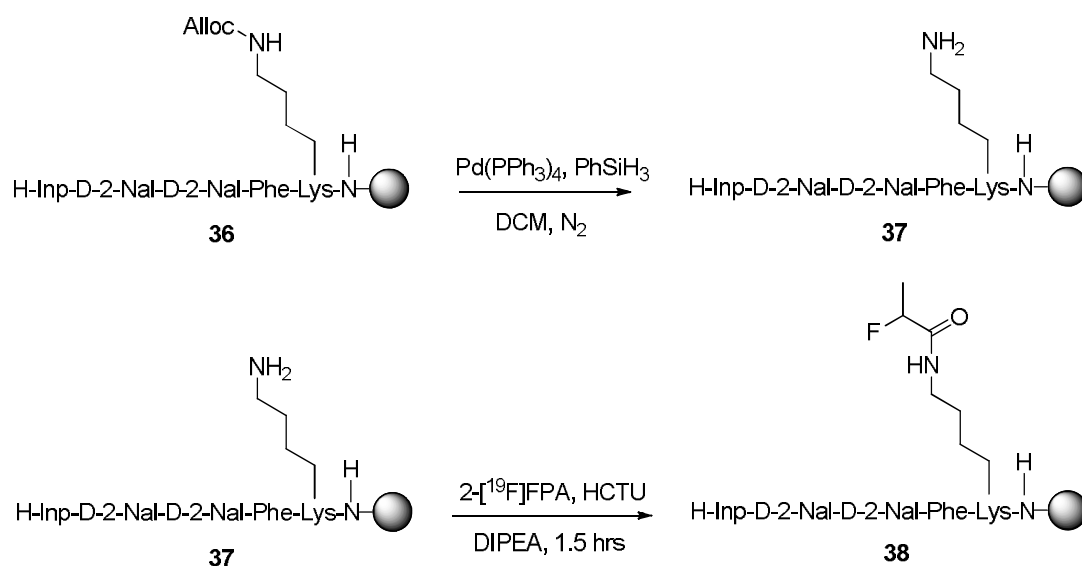
When a comparison is made between the 4-fluorobenzoyl and 2-fluoropropionyl functionalities, the latter group is much more in line with the concept of the small innocuous ^{18}F subunit that was discussed in section 2.4. As a consequence of this, it was hypothesized that the acetylation of the lysine side-chain of the peptidomimetic agonists with the ^{18}F prosthetic group mimic 2- ^{18}F fluoropropionic acid (2- ^{18}F FPA) should not affect GHS-R1a binding in the same manner as the 4- ^{18}F FBA prosthetic group. In other words, a smaller increase in the IC_{50} value would occur as the 2-fluoropropionyl group is smaller in size, less sterically hindered and therefore more likely to fit into one of sub-

pockets of the ghrelin receptor that these peptidomimetics are selective for. The primary goal of this alternate lead compound identification strategy was to obtain a peptidomimetic GHS-R1a agonist with an IC_{50} value < 20 nM.

2.5.1 Results and Discussion

2.5.1.1 Synthesis of 2-FP Peptidomimetic GHS-R1a Agonists

The Genetech peptidomimetics G-7039 and $[1-Nal^4]G-7039$ were chosen to be modified with 2- $[^{19}F]FPA$ as they both have low nanomolar IC_{50} values (5.2 and 28 nM respectively) and should therefore be less prone to losing binding affinity for the ghrelin receptor by introducing a sterically less-crowded functionality. These compounds were synthesized by Fmoc-SPPS using the same protocol outlined previously. The strategy for insertion of the 2-fluoropropionyl group was identical to that of the 4-fluorobenzoyl group, with the Alloc group being deprotected by palladium (see compound **36**, Scheme 7). Coupling of racemic 2- $[^{19}F]FPA$ was conducted for 1.5 hours and furnished a racemic mixture of the final peptidomimetic **38**.



Scheme 7. Orthogonal protecting group strategy and coupling of 2- $[^{19}F]FPA$ illustrated for the peptidomimetic G-7039 (**36**).

The 2-FP peptidomimetic GHS-R1a agonists were characterized by $^1\text{H-NMR}$, HRMS (ESI-TOF) and HPLC. Detailed characterization data is presented in Tables 7 and 8.

Peptidomimetic	LCE number	Amino Acid Sequence
G-7039	00245	H-Inp-D-2-Nal-D-2-Nal-Phe-Lys-NH ₂
[Lys ⁵ (2-FP)]G-7039	00295	H-Inp-D-2-Nal-D-2-Nal-Phe-Lys(2-FP)-NH ₂
[1-Nal ⁴]G-7039	00244	H-Inp-D-2-Nal-D-2-Nal-1-Nal-Lys-NH ₂
[1-Nal ⁴ ,Lys ⁵ (2-FP)]G-7039	00297	H-Inp-D-2-Nal-D-2-Nal-1-Nal-Lys(2-FP)-NH ₂

Table 7. Amino acid sequences of the 2-fluoropropionyl agonists and their parent compounds.

LCE number	HRMS (calculated) [M + H] ⁺	HRMS (found) [M + H] ⁺	% Purity	% Yield
00245	798.4343	798.4339	> 99	7
00295	872.4511	872.4516	> 99	13
00244	848.4499	848.4501	> 99	23
00297	922.4667	922.4651	> 99	7

Table 8. Yields, purities and HRMS data for the 2-fluoropropionyl agonists and their parent compounds.

The 2-fluoropropionyl peptidomimetic GHS-R1a agonists were obtained with purities > 99 % by HPLC and yields of > 5%. Unlike the 4-fluorobenzoyl modification, fluoropropionylation of the lysine side-chain has a unique $^1\text{H-NMR}$ signature. This consists of a doublet of quartets (dq) between 4.76-4.96 ppm resulting from the coupling of the methine proton to ^{19}F and the methyl group on the α -carbon atom respectively (Figure 22). This particular downfield signal further confirms the successful coupling of the 2-fluoropropionyl group to the lysine side-chain and hence the synthesis of the peptidomimetic agonists [1-Nal⁴,Lys⁵(2-FP)]G-7039 and [Lys⁵(2-FP)]G-7039.

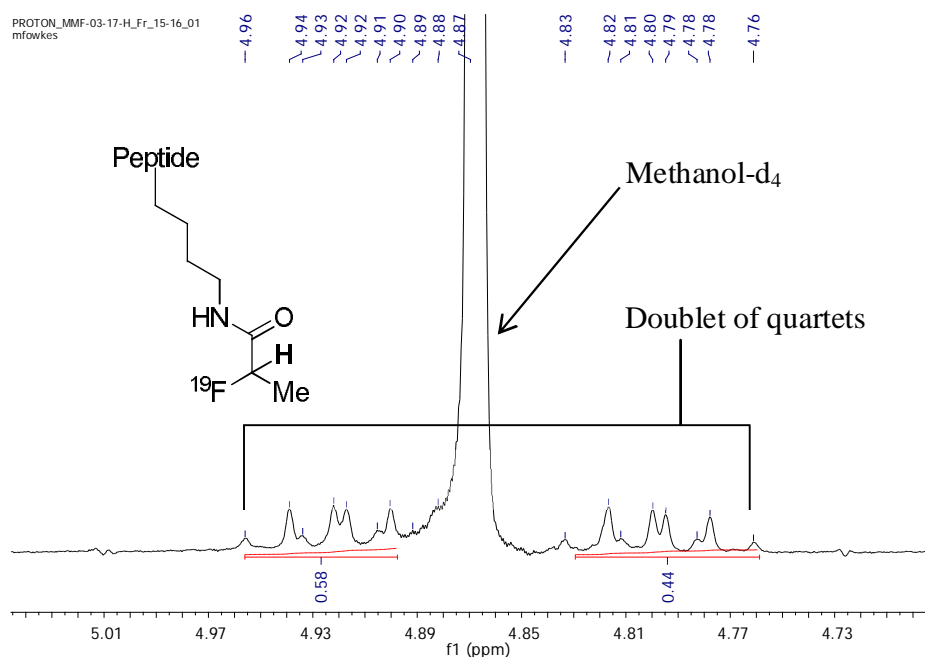


Figure 22. $^1\text{H-NMR}$ signature of methine proton in $[\text{Lys}^5(2\text{-FP})]\text{G-7039}$ (LCE00295).

2.5.1.2 2-FP Agonist Receptor-Ligand Binding Assays

The binding assays were performed using the same procedure as was presented in section 2.4.1.2. The results are tabulated below.

LCE no.	Compound Name	IC ₅₀ , nM
00245	G-7039	5.2
00295	$[\text{Lys}^5(2\text{-FP})]\text{G-7039}$	19
00243	$[\text{Lys}^5(4\text{-FB})]\text{G-7039}$	242
00244	$[1\text{-Nal}^4]\text{G-7039}$	28
00297	$[1\text{-Nal}^4, \text{Lys}^5(2\text{-FP})]\text{G-7039}$	105
00270	$[1\text{-Nal}^4, \text{Lys}^5(4\text{-FB})]\text{G-7039}$	69

Table 9. 2-Fluoropropionyl Genentech peptidomimetic derivatives and their IC₅₀ values.

As can be seen from the table above, the introduction of the 2-fluoropropionyl group into lysine side-chain of G-7039 increased the IC₅₀ value only by ~14 nM compared to ~200 nM for the 4-fluorobenzoyl group (*cf.* 19 nM for LCE00295 to 242 nM for LCE00243). This indicates that fluoropropionylation of the lysine side-chain enables G-7039 to retain binding affinity for the polar sub-pocket of the ghrelin receptor, possibly because of the lower steric hindrance afforded by this moiety. Conversely, the opposite applies to [1-Nal⁴]G-7039. Whilst the 4-fluorobenzoyl congener ([1-Nal⁴,Lys⁵(4-FB)]G-7039) has an IC₅₀ = 69 nM, the 2-fluoropropionyl derivative possesses a higher IC₅₀ value (105 nM, LCE00297) suggesting that the parent compound [1-Nal⁴]G-7039 has a strong selectivity for the non-polar sub-pocket of the ghrelin receptor.

To conclude, the 2-fluoropropionyl functionalization strategy has provided a second lead compound warranting further investigation ([Lys⁵(2-FP)]G-7039). This peptidomimetic possesses an IC₅₀ = 19 nM. In addition, it was shown that this moiety (whilst being less sterically encumbered than the 4-fluorobenzoyl group) did not necessarily improve interactions between the parent compound and the GHS-R1a receptor binding pocket. An excellent example of this is functionalization of [1-Nal⁴]G-7039 to [1-Nal⁴,Lys⁵(2-FP)]G-7039, where the IC₅₀ value increased from 28 nM to 105 nM respectively. Finally, the fact that the 2-fluoropropionyl analogue of [1-Nal⁴]G-7039 ([1-Nal⁴,Lys⁵(2-FP)]G-7039) had reduced binding to the ghrelin receptor, but the fluorobenzoyl analogue of the same parent compound ([1-Nal⁴,Lys⁵(4-FB)]G-7039) had a higher receptor binding affinity (with the opposite argument applying to G-7039) suggests that G-7039 and [1-Nal⁴]G-7039 have a preference for the polar and non-polar GHS-R1a sub-pockets respectively.

2.5.1.3 2-FP Agonist Partition Coefficients

The hydrophobicity of the 2-fluoropropionyl analogues was evaluated using ACD/LogP and XLOGP3 computer software. The results are displayed in Table 10. In stark contrast to the 4-fluorobenzoyl agonist congeners ([Lys⁵(4-FB)]G-7039 and [1-Nal⁴,Lys⁵(4-FB)]G-7039), the ACD/logP values of the 2-fluoropropionyl Genentech derivatives decrease from 5.28 ± 0.82 to 5.19 ± 0.88 for G-7039 and 6.51 ± 0.82 to 6.42 ± 0.88 for [1-Nal⁴]G-7039.

LCE number	Peptidomimetic	LogP (ACD/LogP)	LogP (XLOGP3)
00245	G-7039	5.28 ± 0.82	5.19
00295	[Lys ⁵ (2-FP)]G-7039	5.19 ± 0.88	6.22
00243	[Lys ⁵ (4-FB)]G-7039	7.53 ± 0.88	7.20
00244	[1-Nal ⁴]G-7039	6.51 ± 0.82	6.44
00297	[1-Nal ⁴ ,Lys ⁵ (2-FP)]G-7039	6.42 ± 0.88	7.47
00270	[1-Nal ⁴ ,Lys ⁵ (4-FB)]G-7039	8.76 ± 0.88	8.45

Table 10. Lipophilicities of Genentech peptidomimetic agonists and their 2-fluoropropionyl derivatives.

The reverse appears to be true for $\log P$ values computed by XLOGP3, where an increase in lipophilicity is observed for G-7039 and [1-Nal⁴]G-7039 (in both cases an increase of + 1.03). This could be a consequence of the different computational approaches taken to calculating $\log P$, where XLOGP3 uses a more knowledge-based pathway requiring the input of compounds of similar structure to those being analysed.¹¹⁴ Regardless, the computed $\log P$ values are both still higher than the accepted range of 1-3.¹⁰⁹ However, the $\log P$ value of the 2-fluoropropionyl lead compound [Lys⁵(2-FP)]G-7039 (5.19 ± 0.88, 6.22) represents a small improvement compared to the 4-fluorobenzoyl lead compound [1-Nal⁴,Lys⁵(4-FB)]G-7039 (8.76 ± 0.88, 8.45), suggesting that the former agonist could be better suited to *in vivo* PET imaging as it would benefit from enhanced solubility and reduced non-specific binding.

2.5.1.4 Calcium Flux Assay

Analogously to the 4-fluorobenzoyl lead compound [1-Nal⁴,Lys⁵(4-FB)]G-7039, the [Lys⁵(2-FP)]G-7039 lead was evaluated in a calcium flux assay for its *in vitro* potency (Figure 23).

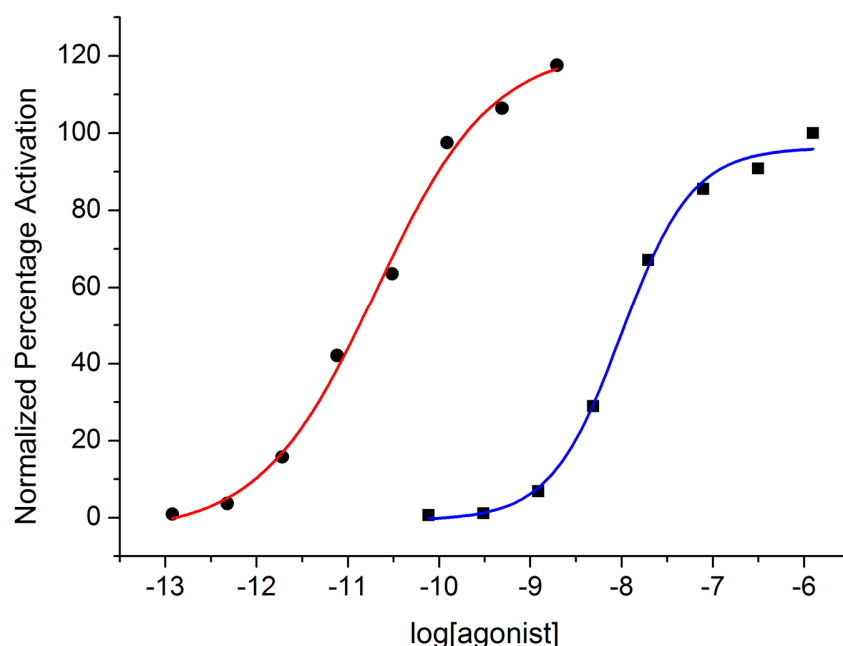


Figure 23. Efficacy curves for the peptidomimetic GHS-R1a agonist [Lys⁵(2-FP)]G-7039 (circles) and the control ligand ghrelin (squares).

The EC₅₀ value was found to be 20 pM, which is an exceptionally low efficacy for this peptidomimetic agonist. This correlates well with the reported half-maximal efficacy of the parent compound G-7039 (EC₅₀ = 0.18 nM⁵²) despite the different mode of potency determination (Ca²⁺ release for [Lys⁵(2-FP)]G-7039 but GH release for G-7039).

2.5.1.5 Conclusions

In this alternative ¹⁸F radiolabelling strategy, an aliphatic 2-fluoropropionyl prosthetic group was incorporated into the lysine side-chain of the peptidomimetic GHS-R1a agonists. This process resulted in the identification of a second lead peptidomimetic with a low nanomolar binding affinity (LCE00295, [Lys⁵(2-FP)]G-7039, IC₅₀ = 19 nM). The computation of the log*P* value of this agonist using ACD/log*P* and XLOGP3 furnished partition coefficients of 5.19 ± 0.88 and 6.22 respectively. The differences in the log*P* values could be a consequence of the contrasting computational approaches taken by each piece of software in computing hydrophobicity. Further evaluation of [Lys⁵(2-FP)]G-

7039 by an *in vitro* calcium flux assay indicated that blocking of the amino group of the lysine side-chain with the 2-fluoropropionyl group gave a peptidomimetic with picomolar efficacy ($EC_{50} = 20$ pM). This value was found to be lower than the endogenous control ligand ghrelin ($EC_{50} = 9.92$ nM) and confirmed that $[Lys^5(2-FP)]G-7039$ still behaves as an agonist. Research into an ^{18}F -radiolabelling strategy *via* direct nucleophilic displacement of a bromine or tosylate leaving group in place of the ^{19}F atom is currently underway.

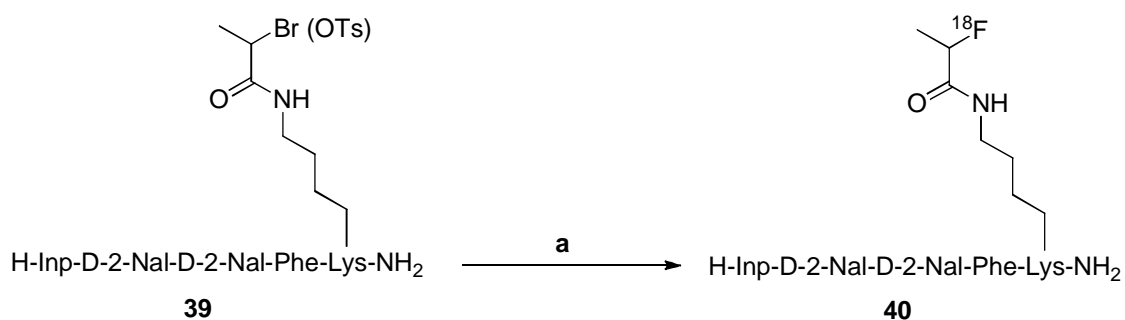


Figure 24. ^{18}F -radiolabelling strategies being explored for the 2-fluoropropionyl lead compound $[Lys^5(2-FP)]G-7039$. *Reagents and Conditions:* a) K 222, K_2CO_3 , $[^{18}F]$, DMSO, $120^\circ C$.

Chapter 3

The Future of Prostate Cancer Imaging

3.1 Final Remarks

Prostate cancer is the second most prevalent cancer in men, with an estimated 1.1 million new cases diagnosed worldwide in 2012.¹²⁰ Excluding non-melanoma skin cancer, this represents a staggering 15% of all male cancer cases.¹²⁰ Despite recent improvements in the diagnosis and staging of this carcinoma, the World Health Organization predicted about 7% of all deaths from cancer to be due to PCa in the year 2012.¹²⁰ The introduction of the mpMRI exam utilizing functional magnetic resonance imaging, PET/MRI multimodality imaging and the development of novel PET/CT probes for imaging prostate cancer (e.g. ⁶⁴Cu-CB-TE2A-AR06) have all aided in the identification and localization of cancerous tumours.¹⁵ In addition, these advancements have enabled clinicians to find treatment programs best suited to patients' diagnoses. However, in spite of these successes and achievements, several problems still remain: the ability to detect recurrent prostate cancer after radical prostatectomy, limited tumour detection in the c-zone of the prostate gland (which is not accessible by conventional diagnostic techniques such as the DRE exam) and most importantly of all, efficiently distinguishing between BPH and PCa.

The area of molecular imaging possesses the potential to continually improve and develop imaging probes that would aid in the early-stage imaging of prostate cancer at a time when it is critical to decide between an aggressive treatment plan or to monitor prostate health through active surveillance and prostatic biopsies. One of the ways in which molecular imaging does this is in the synthesis of molecular probes (peptides, peptidomimetics and small molecules for example) that specifically target peptide receptors up-regulated in prostate cancer. There are a considerable number of these GPCRs overexpressed in PCa, but some of the main ones are the luteinizing hormone-releasing hormone receptor (LHRH-R), the GRPr and the GHS-R1a.⁴ Recent papers by Wieser *et al*²⁹ and Kroll and co-workers²⁸ look at more advanced means of targeting these

receptors rather than using a traditional agonist approach. One of the ways in which these GPCRs are now being targeted is through the use of antagonist imaging probes that in some cases are known to give better imaging results *in vivo* when compared to agonists. For example, the PET/CT imaging probe ^{64}Cu -CB-TE2A-AR06 developed by Wieser *et al.* that targets the GRPr had a higher prostate tumour uptake when compared to agonists of the same receptor in initial clinical studies.²⁹ This probe also gave a more favourable image contrast.²⁹ A hybrid ligand approach has also been developed by Kroll and co-workers which combines the best aspects of an antagonist (strong receptor binding) and agonist (internalisation) into a single imaging entity.²⁸ The subsequent ^{68}Ga radiolabelled ligand benefits from an optimised distance between both targeting elements which led to excellent prostate tumour uptake and tumour retention in pre-clinical murine PET/CT studies.²⁸

In this thesis, an ^{18}F -radiolabelled peptidomimetic GHS-R1a agonist imaging agent targeting the GHS-R1a expressed in prostate cancer was developed. This process began with the modification of a number of literature GHSs with the 4- ^{19}F FBA prosthetic group which eventually led to the synthesis and identification of a cold lead compound with a strong affinity for the ghrelin receptor ([1-Nal⁴,Lys⁵(4-FB)]G-7039, $\text{IC}_{50} = 69$ nM). This peptidomimetic was evaluated for lipophilicity as well as retention of agonist activity. In the former case, a high $\log P$ value was found (8.76 ± 0.88 for ACD/ $\log P$ and 8.45 for XLOGP3) and in the latter an $\text{EC}_{50} = 1.1$ nM. This initial strategy culminated with the successful synthesis of the ^{18}F -radiolabelled congener [1-Nal⁴,Lys⁵(4- ^{18}F -FB)]G-7039 in radiochemical yields of 51-52%, a radiochemical purity > 98% and specific activity of 116 MBq/ μmol in 127 mins at EOS.

The second pathway to a PET imaging agent targeting the GHS-R1a involved modification of two Genentech peptidomimetics with the 2- ^{19}F FPA moiety. This resulted in the formation of the second lead [Lys⁵(2-FP)]G-7039 with an $\text{IC}_{50} = 19$ nM. Investigation into the $\log P$ value of this peptidomimetic showed that it has a lower value than [1-Nal⁴,Lys⁵(4-FB)]G-7039 (*cf.* 5.19 ± 0.88 and 6.22 for [Lys⁵(2-FP)]G-7039 to 8.76 ± 0.88 and 8.45 for ACD/ $\log P$ and XLOGP3 respectively). The calcium flux assay

also showed that the final peptidomimetic GHS-R1a agonist still maintained its agonist behaviour.

Further evaluation of the peptidomimetic GHS-R1a agonist [1-Nal⁴,Lys⁵(4-[¹⁸F]-FB)]G-7039 in pre-clinical PET mouse imaging will move this probe closer to clinical evaluation. The most important factors that will allow the development of a clinically useable probe for PET imaging of prostate cancer is absence of toxicity, lack of non-specific binding, low background contrast ratio, fast-clearance and stability *in vivo*. Although these steps are yet to be carried out, the [1-Nal⁴,Lys⁵(4-[¹⁸F]-FB)]G-7039 probe described in this thesis was developed through a rigorous series of evaluations which began with the identification of the ghrelin receptor as a meaningful target for PCa imaging, careful design of the probe by consideration of structure activity relationships, biological evaluation through receptor-ligand binding assays and final radiolabelling with ¹⁸F.

The lead peptidomimetic GHS-R1a agonist [1-Nal⁴,Lys⁵(4-[¹⁸F]-FB)]G-7039 is the first ¹⁸F PET imaging agent designed to target the ghrelin receptor overexpressed in prostate cancer. The synthesis of this compound represents a significant step towards solving the clinical dilemma of over-diagnosis and overtreatment of PCa, as well as distinguishing between malignant and benign disease.

4 Experimental

4.1 General Information

All reagents were obtained from commercial suppliers and used without further purification. Peptides were either synthesized manually or through the use of a Biotage[®] Syro Wave[™] automated peptide synthesizer. Peptide vessels were shaken using an IKA[®] Vibrax VXR basic shaker with centrifugation performed on a Beckman Coulter[™] Allegra X-30R or Fisher GS-6R centrifuge. In order to aid peptide dissolution, sonication of solutions was accomplished *via* a Branson[®] 2510R-MTH or Fisher F5-14 ultrasonic cleaner. A Fisher 2052 Isotemp[®] machine was used to heat test tubes in the Kaiser Test. Peptides were cryodessicated using a Labconco[®] FreeZone Freeze Dry System. Accurate weighing was carried out on a Mettler-Toledo[®] XP6 microbalance. UV traces were obtained with a Waters 2487 UV/Vis Dual λ Absorbance Detector (170-900 nm) and low-resolution mass spectra with a Micromass[®] Quattro *micro*[™] API mass spectrometer (ESI-LC-MS). Peptide purification was achieved through HPLC (MeCN + 0.1% TFA, H₂O + 0.1% TFA solvent system). All peptides and small molecules obtained had a purity \geq 95% as determined by HPLC or UHPLC analysis. A reverse-phase (RP) preparative C-18 column (SunFire[™] OBD[™], 19 x 150 mm or Agilent[™] Zorbax[®] 21.2 x 150 mm) was used for preparative HPLC, whilst a C-18 RP column (SunFire[™], 4.6 x 150 mm or Agilent[™] Zorbax[®], 4.6 x 150 mm) was used for analytical HPLC. Accurate mass spectrometry (HRMS) was carried out on a Finnigan[™] MAT 8400 mass spectrometer (EI) for small molecules and on a Micromass LCT mass spectrometer (ESI-TOF) for peptides. ¹H NMR and ¹³C NMR spectroscopy were performed on a Mercury VX 400 machine at 400 and 100 MHz respectively. Chemical shifts are referenced to residual solvent, reported in ppm on a δ scale and all coupling constants quoted in hertz (Hz).

4.2 Experimental Procedures

4.2.1 Manual Fmoc Solid-Phase Peptide Synthesis (Fmoc-SPPS)

Rink amide MBHA resin (192 mg, 0.1 mmol, 1.0 eq., 0.52 mmol g⁻¹ loading) was vortexed in DCM (2.0 ml, 1 min.), allowed to swell (15 mins) and solvent removed. This was followed by addition of DMF (2.0 ml), vortexing (1 min.) and removal of solvent. Deprotection of the Fmoc group was then performed. A solution of 20% piperidine/DMF (1.5 ml, v/v) was added to the resin and the subsequent mixture vortexed (2 mins) and solvent removed. This was then repeated a second time with vortexing for 15 minutes. After solvent had been removed, the resin was washed of any unreacted by-products with DMF six times (2.0 ml, vortex 30 s). The desired amino acid or small molecule (0.3 mmol, 3.0 eq.) and coupling reagent (HCTU, 0.12 g, 0.3 mmol, 3.0 eq.) were then dissolved in DMF (1.5 ml) and added to the deprotected resin. After vortexing (30 s), DIPEA (111 μ l, 0.6 mmol, 6.0 eq.) was added and the final mixture vortexed (1-2 hrs). The resin was then washed with DMF (2.0 ml, 30 s vortex) a final four times. The deprotection/coupling cycle was then repeated unless the final amino acid in the sequence had been added, in which case the peptide was washed with DCM five times (2.0 ml, 30 s vortex) after washing with DMF and stored in a refrigerator. Removal of the N-terminal Fmoc-group was carried out in the same fashion as the deprotection cycle described previously, with resin washing occurring six times with DMF (2.0 ml, 30 s vortex) and four times with DCM (2.0 ml, 30 s vortex). Successful synthesis of the desired peptide was then ascertained *via* a microcleave prior to full cleavage of the peptide from the solid-support. This was carried out as follows: a solution of 95% TFA: 2.5% (ⁱPr)₃SiH: 2.5% H₂O (300 μ l) was added to a small number of resin beads (< 5 mg) and the subsequent mixture vortexed (3 hrs). The clear liquid was then evaporated under a stream of N₂. Analytical HPLC was then performed to determine whether the correct peptide had been synthesized. If the correct peptide had been obtained, a full cleavage was performed using a mixture of 95% TFA: 2.5% (ⁱPr)₃SiH: 2.5% H₂O (2.0 ml) for 5-7 hrs. The subsequent solution was cooled in an ice-bath alongside tert-butyl methyl ether (TBMe, 40 ml). After 10 minutes, TBMe (20 ml) was added to the peptide solution, leading to the formation of a white precipitate. The precipitate was cooled further (10 mins) and then

centrifuged (7 mins). Decanting of the supernatant was followed by addition of a second aliquot of TBMe (20 ml), vortexing (30 s) and final centrifugation (7 mins). After decanting, a white solid was obtained. This was then freeze-dried (20 mins) to furnish crude peptide. Preparative HPLC was then used to purify the product peptide.

4.2.2 Deprotection of the Alloc Protecting Group

The resin-bound peptide was vortexed in DCM (4.5 ml, 30 s) and allowed to swell (10 mins). Deprotection was carried out under a blanket of N₂. The swollen resin-bound peptide was stirred (5 mins) before addition of PhSiH₃ (296 µl, 2.4 mmol, 24.0 eq.). Further stirring (5 mins) ensued prior to treating with Pd(PPh₃)₄ (120 mg, 0.01 mmol, 0.1 eq.). The reaction mixture changed colour from yellow to orange to brown to dark brown. After 5 minutes, the solution was vortexed (5 mins), solvent removed and the brown-coloured resin washed four times with DCM (2.0 ml, 30 s vortex). The procedure was then repeated *ab initio*, with final resin washing occurring in the following order: DCM, DMF, MeOH, DMF and DCM (all 2.0 ml, 30 s vortex).

4.2.3 Kaiser Test

The Kaiser test¹⁰¹ was used as a qualitative test to determine the success of amino acid coupling. A small number of resin beads (< 5 mg) were taken and treated with phenol: EtOH (200 µl, 8:2 v/v), 0.001 M KCN_(aq): pyridine (200 µl, 2:98 v/v, 0.001 M aqueous KCN) and ninhydrin in EtOH (200 µl, 5% w/v) respectively. Tentagel resin (< 5 mg) was used as a control in this test. Both test tubes were heated to 70 °C. The presence of free amine was indicated by blue resin beads whilst yellow or clear resin beads showed protected amine groups to be present.

4.2.4 Receptor-Ligand Binding Assay

Competitive binding assays were run at the Lawson Health Research Institute at St. Joseph's Health Care in London Ontario, Canada. These were carried out in triplicate using HEK293/GHS-R1a cells (prepared by our collaborator Becky McGirr) with [¹²⁵I]ghrelin as a competitive radioligand. To begin with, a fresh solution of binding

buffer (50 ml) was made up by adding 4-(2-hydroxyethyl)piperazine-1-ethanesulfonic acid, N-(2-hydroxyethyl)piperazine-N'-(2-ethanesulfonic acid (HEPES, 0.3 g, 25 mM), MgCl₂ (0.051 g, 5 mM), CaCl₂ (7.4 x 10⁻³ g, 1 mM), ethylenediaminetetraacetic acid (EDTA, 0.015 g, 2.5 mM) and bovine serum albumin (BSA, 0.2 g, 0.4%) to distilled water. The resultant solution was mixed over gentle heat (< 100 °C). The pH was then adjusted to 7.4 and the solution filtered through a 0.22 µm syringe filter. Two miniature complete protease inhibitor tablets were then added and the final buffer solution kept on ice.

After the buffer had been made, plastic assay test tubes were labelled and kept on ice during the setup. To assay tubes 1-21, 25-27 and 28-30 was added binding buffer (200 µl, 230 µl and 300 µl respectively). No buffer was added to tubes 22-24. An aliquot of frozen cells was thawed to room temperature, centrifuged (3000 xg, 10 mins, room temperature) and the subsequent cell pellet re-suspended in binding buffer (2 ml) and placed on ice. Cells (50 µl) were then added to test tubes 1-21 and 25-27. Cold peptide was then prepared. This was carried out by adding pre-prepared stock peptide in water (20 µl, 10⁻³ M) to binding buffer (180 µl) to make a peptide solution of 10⁻⁴ M concentration. Binding buffer (180 µl) was then added to assay tubes labelled 10⁻⁵ to 10⁻¹¹. A series of dilutions were then performed in order to acquire 10⁻⁵ to 10⁻¹¹ M concentrations. Cold peptide (30 µl) was then added to assay tubes 1-21 in triplicate.

[¹²⁵I]-ghrelin was then prepared by adding 10 µl to binding buffer (3 ml) and vortexing the resultant solution. An aliquot of this [¹²⁵I]-ghrelin solution (20 µl) was added to an empty assay tube and counted on a Cobra™ II Auto-Gamma® gamma counter using protocol 3. The volume of [¹²⁵I]-ghrelin or binding buffer was adjusted as needed in order to get 14 000 – 17 000 cpm for every 20 µl aliquot. Having achieved the correct range of cpm, the [¹²⁵I]-ghrelin (20 µl) was pipetted into assay tubes 1-27. All assay tubes were then vortexed, capped and immediately agitated (550 rpm, 20 mins, 37°C). After 20 minutes, tubes 1-21 and 25-27 were spun in a large centrifuge (2800 rpm, 2 mins, 4°C). The solution in all of the assay tubes was then transferred to numbered Eppendorf tubes. Further binding buffer (200 µl) was added to wash out residual radioactivity from the plastic test tubes, and transferred to the Eppendorf tubes. These tubes were then spun

again (13 000 xg, 5 mins, 4°C) and placed on ice. The supernatant was removed and the cell pellet rinsed with ice-cold Tris-HCl (200 µl, 50 mM, pH 7.4). The Eppendorf tubes were then mixed by inversion and spun a final time (13,000 xg, 5 mins, 4°C), cooled on ice and supernatant removed a second time. After removing the caps from the Eppendorf tubes, they were placed in 12 x 75 mm plastic test tubes and counted using a Cobra™ II Auto-Gamma® gamma counter (protocol 3). The binding assay may be summarized as follows:

- 1) Tubes 1-21: 200 µl binding buffer, 50 µl cells, 30 µl cold peptide, 20 µl [¹²⁵I]-ghrelin.
- 2) Tubes 22-24: 20 µl [¹²⁵I]-ghrelin.
- 3) Tubes 25-27: 20 µl [¹²⁵I]-ghrelin, 50 µl cells, 230 µl binding buffer.
- 4) Tubes 28-30: 300 µl binding buffer.

4.2.5 Synthesis of Peptidomimetics

All peptidomimetics were synthesized by the same general procedure as described in section 4.2.1 unless otherwise noted.

LCE00210: H-Aib-His-D-2-Nal-D-Phe-Lys-NH₂ (Ipamorelin)

The product was purified by preparative HPLC (5-80% MeCN + 0.1% TFA). This furnished a white powder (20.5 mg, 19%): ¹H-NMR (400 MHz, CD₃OD); **D-2-Nal, D-Phe, His:** δ 7.99 (s, 1H, ArH), 7.80-7.76 (m, 1H, ArH), 7.71 (d, *J* = 8.6 Hz, 2H, ArH), 7.56 (s, 1H, ArH), 7.44-7.37 (m, 2H, ArH), 7.32-7.17 (m, 6H, ArH), 6.92 (s, 1H, His H_δ), 4.58 (m, 3H, H_α), 3.30-3.21 (m, 1H, D-2-Nal H_β), 3.15-3.00 (m, 2H, H_β), 2.96-2.72 (m, 3H, H_β), **Lys:** 4.11 (dd, *J* = 9.7, 4.2 Hz, 1H, H_α), 2.96-2.72 (m, 2H, H_ε), 1.75-1.64 (m, 1H, H_β), 1.54-1.40 (m, 3H, H_β, 2H_δ), 1.05-0.93 (m, 2H, H_γ), **Aib:** 1.48 (s, 3H, CH₃) 1.44 (s, 3H, CH₃) ppm. ESI-LC-MS *m/z* 356.9 [M + 2H]²⁺; HRMS (ESI-MS) calcd. for C₃₈H₅₀N₉O₅ [M + H]⁺ 712.3935, found 712.3959.

LCE00211: H-Aib-His-D-2-Nal-D-Phe-Lys(4-FB)-NH₂ (4-FB-Ipamorelin)

Purification by preparative HPLC (20-70% MeCN + 0.1% TFA) yielded a white powder (15.4 mg, 15%): ¹H-NMR (400 MHz, CD₃OD); **D-2-Nal, D-Phe, His, 4-FB**: δ 7.91 (s, 1H, ArH), 7.85-7.77 (m, 3H, ArH, 2F-ArH), 7.70 (d, *J* = 7.9 Hz, 2H, ArH), 7.54 (s, 1H, ArH), 7.45-7.40 (m, 2H, ArH), 7.29-7.19 (m, 6H, ArH), 7.14-7.07 (m, 2H, 2F-ArH), 6.93 (s, 1H, His H_δ), 4.65-4.52 (m, 3H, H_α), 3.30-3.27 (m, 1H, H_β), 3.23 (d, *J* = 4.0 Hz, 1H, H_β), 3.10 (dd, *J* = 13.5, 7.8 Hz, 1H, H_β), 3.04-2.74 (m, 3H, H_β), **Lys**: 4.12 (dd, *J* = 9.8, 4.2 Hz, 1H, H_α), 3.04-2.74 (m, 2H, H_ε), 1.77-1.67 (m, 1H, H_β), 1.58-1.42 (m, 3H, H_β, 2H_δ), 1.14-1.03 (m, 2H, H_γ), **Aib**: 1.50 (s, 3H, CH₃), 1.46 (s, 3H, CH₃) ppm. ESI-LC-MS *m/z* 418.0 [M + 2H]²⁺; HRMS (ESI-MS) calcd. for C₄₅H₅₃FN₉O₆ [M + H]⁺ 834.4103, found 834.4133.

LCE00217: H-Aib-His-D-2-Nal-D-Phe-Lys(4-FB-AEEA)-NH₂ (4-FB-AEEA-Ipamorelin)

Peptide purification by preparative HPLC (20-60% MeCN + 0.1% TFA) delivered an off-white powder (9.2 mg, 8%): ¹H-NMR (400 MHz, CD₃OD); **His, D-2-Nal, D-Phe, 4-FB**: δ 7.93 (s, 1H, ArH), 7.86-7.77 (m, 3H, ArH, 2F-ArH), 7.71 (d, *J* = 8.0 Hz, 2H, ArH), 7.55 (s, 1H, ArH), 7.46-7.41 (m, 2H, ArH), 7.31-7.18 (m, 6H, ArH), 7.17-7.10 (m, 2H, F-ArH), 6.94 (s, 1H, His H_δ), 4.65-4.58 (m, 2H, H_α), 4.55 (t, *J* = 7.5 Hz, 1H, H_α), 3.16-2.76 (m, 6H, H_β), **Lys**: 4.10 (dd, *J* = 9.7, 4.2 Hz, 1H, H_α), 3.16-2.76 (m, 2H, H_ε), 1.72-1.62 (m, 1H, H_β), 1.52-1.43 (m, 1H, H_β), 1.41-1.30 (m, 2H, H_δ), 1.07-0.97 (m, 2H, H_γ), **AEEA linker**: 3.93 (s, 2H, NHCOCH₂O), 3.65-3.61 (m, 6H, CH₂), 3.53 (t, *J* = 5.6 Hz, 2H, CH₂), **Aib**: 1.50 (s, 3H, CH₃), 1.47 (s, 3H, CH₃) ppm. ESI-LC-MS *m/z* 490.4 [M + 2H]²⁺; HRMS (ESI-MS) calcd. for C₅₁H₆₄FN₁₀O₉ [M + H]⁺ 979.4842, found 979.4868.

LCE00239: H-His-D-Trp-Ala-Trp-D-Phe-Lys-NH₂ (GHRP-6)

Purification by preparative HPLC (15-80% MeCN + 0.1% TFA) gave a white powder (19.7 mg, 14%): ¹H-NMR (400 MHz, CD₃OD); **His, D-Trp, Trp, D-Phe:** δ 8.46 (s, 1H, His H_ε), 7.54 (d, *J* = 7.8 Hz, 1H, ArH), 7.46 (d, *J* = 7.8 Hz, 1H, ArH), 7.28 (t, *J* = 7.7 Hz, 2H, ArH), 7.23-7.13 (m, 4H, ArH), 7.12-6.92 (m, 8H, 7ArH, His H_δ), 4.47 (t, *J* = 7.4 Hz, 2H, Trp H_α), 4.35 (t, *J* = 6.7 Hz, 1H, H_α), 4.28 (t, *J* = 7.9 Hz, 1H, H_α), 3.22-3.14 (m, 3H, H_β), 3.14-3.02 (m, 3H, H_β), 2.83 (d, *J* = 8.6 Hz, 2H, H_β), **Lys:** 4.03 (dd, *J* = 10.3, 3.9 Hz, 1H, H_α), 2.75 (t, *J* = 6.8 Hz, 2H, H_ε), 1.76-1.63 (m, 1H, H_β), 1.51-1.39 (m, 3H, H_β, 2H_δ), 0.97-0.88 (m, 2H, H_γ), **Ala:** 3.91 (q, *J* = 7.2 Hz, 1H, H_α), 0.86 (d, *J* = 7.3 Hz, 3H, CH₃) ppm. ESI-LC-MS *m/z* 437.4 [M + 2H]²⁺; HRMS (ESI-MS) calcd. for C₄₆H₅₇N₁₂O₆ [M + H]⁺ 873.4524 found 873.4531.

LCE00240: H-Ala-His-D-2-Nal-Ala-Trp-D-Phe-Lys-NH₂ (GHRP-1)

The product was purified by preparative HPLC (15-80% MeCN + 0.1% TFA). This yielded a white powder (26.4 mg, 19%): ¹H-NMR (400 MHz, CD₃OD); **His, D-2-Nal, Trp, D-Phe:** δ 8.41 (s, 1H, His H_ε), 7.81-7.71 (m, 3H, ArH), 7.65 (s, 1H, ArH), 7.49 (d, *J* = 7.8 Hz, 1H, ArH), 7.46-7.40 (m, 2H, ArH), 7.35 (dd, *J* = 8.4, 1.7 Hz, 1H, ArH), 7.31 (d, *J* = 8.1 Hz, 1H, ArH), 7.24-7.13 (m, 3H, ArH), 7.10-7.04 (m, 4H, ArH), 7.00 (t, *J* = 7.5 Hz, 1H, ArH), 6.89 (d, *J* = 0.8 Hz, 1H, His H_δ), 4.67-4.60 (m, 2H, H_α), 4.38 (t, *J* = 7.4 Hz, 1H, H_α), 4.32 (t, *J* = 7.7 Hz, 1H, H_α), 3.25-2.68 (m, 8H, H_β), **Ala, Ala:** 4.17-4.10 (m, 1H, H_α), 3.94 (q, *J* = 7.0 Hz, 1H, H_α), 1.35 (d, *J* = 7.1 Hz, 3H, CH₃), 1.10-1.01 (m, 3H, CH₃), **Lys:** 4.17-4.10 (m, 1H, H_α), 3.25-2.68 (m, 2H, H_ε), 1.81-1.70 (m, 1H, H_β), 1.58-1.45 (3H, H_β, 2H_δ), 1.10-1.01 (m, 2H, H_γ), ppm. ESI-LC-MS *m/z* 478.5 [M + 2H]²⁺; HRMS (ESI-MS) calcd. for C₅₁H₆₃N₁₂O₇ [M + H]⁺ 955.4943 found 955.4964.

LCE00243: H-Inp-D-2-Nal-D-2-Nal-Phe-Lys(4-FB)-NH₂ (4-FB-G-7039)

Preparative HPLC (35-80% MeCN + 0.1% TFA) furnished the title compound as a white solid (5.90 mg, 6%): ¹H-NMR (400 MHz, (CD₃)₂SO); δ 8.50 (d, *J* = 8.2 Hz, 1H, NH),

8.45 (t, $J = 5.5$ Hz, 1H, NH), 8.39 (s, 1H, NH), 8.15-8.09 (m, 2H, NH), 8.04 (d, $J = 8.4$ Hz, 1H, NH), 7.86-7.82 (m, 2H, F-ArH), 7.82-7.76 (m, 2H, ArH), 7.75-7.66 (m, 4H, ArH), 7.58 (s, 1H, ArH), 7.48 (s, 1H, ArH), 7.45-7.38 (m, 4H, ArH), 7.31 (dd, $J = 8.5, 1.5$ Hz, 1H, ArH), 7.28 (s, 1H, ArH), 7.26 (s, 1H, NH), 7.24-7.17 (m, 5H, ArH), 7.15-7.08 (m, 2H, ArH), 7.04 (s, 1H, NH), 4.66-4.60 (m, 1H, H_α), 4.60-4.53 (m, 2H, H_α), 4.20-4.14 (m, 1H, Lys- H_α), 3.25-3.14 (m, 2H, \underline{CH}_2), 3.13-3.02 (m, 3H, \underline{CH}_2), 2.98-2.91 (m, 1H, \underline{CH}_2), 2.90-2.83 (m, 1H, \underline{CH}_2), 2.81-2.56 (m, 5H, \underline{CH}_2), 2.30-2.22 (m, 1H, Inp- H_α), 1.75-1.65 (m, 1H, \underline{CH}_2), 1.62-1.55 (m, 1H, \underline{CH}_2), 1.54-1.43 (m, 6H, \underline{CH}_2), 1.38-1.19 (m, 2H, \underline{CH}_2), ppm. ESI-LC-MS m/z 452.5 $[M + 4H - F]^{2+}$; HRMS (ESI-MS) calcd. for $C_{54}H_{59}FN_7O_6$ $[M + H]^+$ 920.4511 found 920.4529.

LCE00244: H-Inp-D-2-Nal-D-2-Nal-1-Nal-Lys-NH₂ (MMF-01-113-G)

Peptide purification by preparative HPLC (25-80% MeCN + 0.1% TFA) delivered a white powder (24.9 mg, 23%): ¹H-NMR (400 MHz, CD₃OD); δ 8.12 (d, $J = 8.4$ Hz, 1H, ArH), 7.84 (d, $J = 7.8$ Hz, 1H, ArH), 7.78-7.72 (m, 2H, ArH), 7.68 (d, $J = 8.5$ Hz, 3H, ArH), 7.62-7.46 (m, 5H, ArH), 7.43-7.35 (m, 5H, ArH), 7.30 (d, $J = 6.4$ Hz, 1H, ArH), 7.27-7.21 (m, 2H, ArH), 7.02 (dd, $J = 8.4, 1.5$ Hz, 1H, ArH), 4.69 (dd, $J = 9.4, 5.4$ Hz, 1H, H_α), 4.65-4.55 (m, 2H, H_α), 4.32 (dd, $J = 9.4, 4.8$ Hz, 1H, Lys- H_α), 3.65 (dd, $J = 14.4, 5.4$ Hz, 1H, \underline{CH}_2), 3.20-3.10 (m, 2H, \underline{CH}_2), 3.05-2.94 (m, 3H, \underline{CH}_2), 2.92-2.80 (m, 5H, \underline{CH}_2), 2.76-2.62 (m, 2H, \underline{CH}_2), 2.30-2.23 (m, 1H, Inp- H_α), 1.92-1.81 (m, 1H, \underline{CH}_2), 1.75-1.29 (m, 9H, \underline{CH}_2), ppm. ESI-LC-MS m/z 424.8 $[M + 2H]^{2+}$; HRMS (ESI-MS) calcd. for $C_{51}H_{58}N_7O_5$ $[M + H]^+$ 848.4499, found 848.4501.

LCE00245: H-Inp-D-2-Nal-D-2-Nal-Phe-Lys-NH₂ (G-7039)

Purification of the peptide proceeded through preparative HPLC (25-80% MeCN + 0.1% TFA). The title compound was obtained as a white powder (6.70 mg, 7%): ¹H-NMR (400 MHz, CD₃OD); 7.80-7.76 (m, 1H, ArH), 7.74 (dd, $J = 6.1, 2.2$ Hz, 2H, ArH), 7.70 (dd, $J = 8.5, 3.5$ Hz, 3H, ArH), 7.56 (s, 1H, ArH), 7.50 (s, 1H, ArH), 7.46-7.35 (m, 4H, ArH), 7.26 (dd, $J = 8.5, 1.5$ Hz, 1H, ArH), 7.20-7.10 (m, 6H, ArH), 4.66-4.56 (m, 2H, H_α), 4.50 (dd, $J = 9.3, 5.4$ Hz, 1H, H_α), 4.30 (dd, $J = 9.5, 4.7$ Hz, 1H, Lys- H_α), 3.20-2.80 (m, 10H,

CH_2), 2.78-2.64 (m, 2H, CH_2), 2.33-2.24 (m, 1H, Inp- H_α), 1.92-1.82 (m, 1H, CH_2), 1.74-1.65 (m, 1H, CH_2), 1.64-1.44 (m, 5H, CH_2), 1.44-1.24 (m, 3H, CH_2), ppm. ESI-LC-MS m/z 399.8 $[\text{M} + 2\text{H}]^{2+}$; HRMS (ESI-MS) calcd. for $\text{C}_{47}\text{H}_{56}\text{N}_7\text{O}_5$ $[\text{M} + \text{H}]^+$ 798.4343 found 798.4339.

LCE00246: H-Inp-His-D-2-Nal-D-2-Thi-Lys(4-FB)-NH₂ (Inp-Thi-4-FB-Ipamorelin)

The title peptide was prepared by automated peptide synthesis and purified by preparative HPLC (20-80% MeCN + 0.1% TFA). This furnished a white powder (14.0 mg, 13%): ¹H-NMR (400 MHz, CD₃OD); **His, D-2-Nal, D-2-Thi, 4-FB:** δ 8.23 (s, 1H, His H _{ϵ}), 7.86-7.81 (m, 2H, F-ArH), 7.80-7.77 (m, 1H, ArH), 7.73 (dd, $J = 8.8, 3.3$ Hz, 2H, ArH), 7.59 (s, 1H, ArH), 7.45-7.39 (m, 2H, ArH), 7.27 (dd, $J = 8.5, 1.6$ Hz, 1H, ArH), 7.22 (dd, $J = 5.0, 1.2$ Hz, 1H, Thi-ArH), 7.15-7.08 (m, 2H, F-ArH), 6.92 (s, 1H, His H _{δ}), 6.91-6.85 (m, 2H, Thi-ArH), 4.61 (dd, $J = 10.3, 4.4$ Hz, 1H, H _{α}), 4.53-4.47 (m, 2H, H _{α}), 4.22 (dd, $J = 9.8, 4.2$ Hz, 1H, Lys-H _{α}), 3.39-3.29 (m, 6H, CH_2), 3.26-3.22 (m, 1H, CH_2), 3.01-2.80 (m, 5H, CH_2), 2.53-2.44 (m, 1H, Inp- H_α), 1.87-1.50 (m, 8H, CH_2), 1.35-1.22 (m, 2H, CH_2), ppm. ESI-LC-MS m/z 433.8 $[\text{M} + 2\text{H}]^{2+}$; HRMS (ESI-MS) calcd. for $\text{C}_{45}\text{H}_{53}\text{FN}_9\text{O}_6\text{S}$ $[\text{M} + \text{H}]^+$ 866.3824 found 866.3850.

LCE00267: H-Aib-His-D-2-Nal-D-2-Thi-Lys(4-FB)-NH₂ (Thi-4-FB-Ipamorelin)

The title peptide was synthesized by automated peptide synthesis and purified by preparative HPLC (20-80% MeCN + 0.1% TFA). This furnished a white solid (4.20 mg, 4%): ¹H-NMR (400 MHz, (CD₃)₂SO); δ 8.83 (s, 1H, ArH), 8.59 (d, $J = 8.1$ Hz, 1H, NH), 8.42 (t, $J = 5.6$ Hz, 1H, NH), 8.29 (d, $J = 9.3$ Hz, 1H, NH), 8.20 (d, $J = 8.2$ Hz, 1H, NH), 8.09 (d, $J = 8.9$ Hz, 1H, NH), 7.99 (s, 2H, NH), 7.86-7.81 (m, 2H, F-ArH), 7.79-7.75 (m, 1H, ArH), 7.72 (dd, $J = 8.7, 3.7$ Hz, 2H, ArH), 7.65 (s, 1H, ArH), 7.41-7.37 (m, 2H, ArH), 7.35-7.31 (m, 2H, ArH, NH), 7.26 (dd, $J = 4.8, 1.5$ Hz, 1H, Thi-H), 7.22-7.16 (m, 2H, F-ArH), 7.05 (s, 2H, NH, ArH), 6.88-6.84 (m, 2H, Thi-H), 4.73-4.66 (m, 1H, H _{α}), 4.62-4.51 (m, 2H, H _{α}), 4.19-4.12 (m, 1H, Lys-H _{α}), 3.21-3.12

(m, 4H, 2H_ε, 2H_β), 3.06-2.96 (m, 1H, H_β), 2.87-2.77 (m, 2H, H_β), 2.62-2.49 (m, 1H, H_β), 1.66-1.56 (m, 1H, Lys-H_β), 1.50-1.36 (m, 3H, Lys-H_β, 2H_δ), 1.26 (s, 3H, CH₃), 1.20-1.10 (m, 2H, H_γ), 1.16 (s, 3H, CH₃), ppm. ESI-LC-MS *m/z* 420.8 [M + 2H]²⁺; HRMS (ESI-MS) calcd. for C₄₃H₅₁FN₉O₆S [M + H]⁺ 840.3667 found 840.3693.

LCE00268: H-Inp-His-D-2-Nal-D-Phe-Lys(4-FB)-NH₂ (Inp-4-FB-Ipamorelin)

The title peptide was synthesized *via* automated peptide synthesis and purified by preparative HPLC (20-70% MeCN + 0.1% TFA). The title compound was acquired as a white solid (6.30 mg, 6%): ¹H-NMR (400 MHz, (CD₃)₂SO); δ 8.79 (s, 1H, His H_ε), 8.72 (s, 1H, NH), 8.44 (dd, *J* = 10.8, 6.4 Hz, 2H, NH), 8.19 (d, *J* = 7.8 Hz, 1H, NH), 8.17-8.10 (m, 2H, NH), 7.87-7.81 (m, 2H, F-ArH), 7.80-7.76 (m, 1H, ArH), 7.71 (d, *J* = 7.9 Hz, 2H, ArH), 7.63 (s, 1H, ArH), 7.42-7.35 (m, 2H, ArH), 7.33-7.29 (m, 2H, NH), 7.22-7.18 (m, 6H, ArH), 7.17-7.11 (m, 2H, F-ArH), 7.06 (s, 1H, NH), 6.96 (s, 1H, His H_δ), 4.64-4.56 (m, 1H, H_α), 4.55-4.44 (m, 2H, H_α), 4.15-4.07 (m, 1H, Lys-H_α), 3.19-3.07 (m, 5H, CH₂), 2.94 (dd, *J* = 13.6, 5.9 Hz, 1H, CH₂), 2.87-2.67 (m, 5H, CH₂), 2.58-2.48 (m, 1H, CH₂), 2.38-2.29 (m, 1H, H_α), 1.67-1.34 (m, 8H, CH₂), 1.15-1.00 (m, 2H, CH₂), ppm. ESI-LC-MS *m/z* 430.9 [M + 2H]²⁺; HRMS (ESI-MS) calcd. for C₄₇H₅₅FN₉O₆ [M + H]⁺ 860.4259 found 860.4284.

LCE00269: H-Inp-His-D-2-Nal-D-2-Nal-Lys(4-FB)-NH₂ (MMF-01-140-H)

The title peptide was made by automated peptide synthesis and purified by preparative HPLC (20-80% MeCN + 0.1% TFA). This delivered a white solid (11.3 mg, 10%): ¹H-NMR (400 MHz, (CD₃)₂SO); δ 8.77 (s, 1H, His H_ε), 8.51 (d, *J* = 7.5 Hz, 2H, NH), 8.36 (t, *J* = 5.5 Hz, 1H, NH), 8.19-8.10 (m, 2H, NH), 8.05 (d, *J* = 8.7 Hz, 1H, NH), 7.85-7.79 (m, 3H, 2F-ArH, ArH), 7.79-7.74 (m, 3H, ArH), 7.73 (s, 1H, ArH), 7.70 (s, 1H, ArH), 7.68 (d, *J* = 2.4 Hz, 2H, ArH), 7.59 (s, 1H, ArH), 7.43-7.35 (m, 5H, ArH), 7.31-7.27 (m, 2H, NH), 7.20-7.13 (m, 2H, F-ArH), 7.05 (s, 1H, NH), 6.93 (s, 1H, His H_δ), 4.67-4.60 (m, 2H, H_α), 4.52-4.44 (m, 1H, H_α), 4.16-4.08 (m, 1H, Lys-H_α), 3.17-

2.93 (m, 7H, CH_2), 2.88-2.66 (m, 4H, CH_2), 2.53-2.47 (m, 1H, CH_2), 2.34-2.25 (m, 1H, H_α), 1.63-1.34 (m, 6H, CH_2), 1.32-1.23 (m, 2H, CH_2), 1.07-0.95 (m, 2H, CH_2), ppm. ESI-LC-MS m/z 455.9 $[\text{M} + 2\text{H}]^{2+}$; HRMS (ESI-MS) calcd. for $\text{C}_{51}\text{H}_{57}\text{FN}_9\text{O}_6$ $[\text{M} + \text{H}]^+$ 910.4416 found 910.4400.

LCE00270: H-Inp-D-2-Nal-D-2-Nal-1-Nal-Lys(4-FB)-NH₂ (MMF-01-115-H)

The product was purified by preparative HPLC (25-90% MeCN + 0.1% TFA) which yielded a white powder (9.80 mg, 9%): $^1\text{H-NMR}$ (400 MHz, $(\text{CD}_3)_2\text{SO}$); δ 8.64 (d, $J = 8.3$ Hz, 1H, NH), 8.46 (t, $J = 5.5$ Hz, 1H, NH), 8.33 (s, 1H, NH), 8.25 (d, $J = 8.4$ Hz, 1H, ArH), 8.13 (d, $J = 8.0$ Hz, 1H, NH), 8.09 (d, $J = 7.5$ Hz, 1H, NH), 8.03 (d, $J = 8.5$ Hz, 1H, NH), 8.01-7.97 (m, 1H, NH), 7.89 (d, $J = 8.2$ Hz, 1H, ArH), 7.86-7.80 (m, 2H, F-ArH), 7.79-7.72 (m, 3H, ArH), 7.71-7.66 (m, 2H, ArH), 7.58-7.50 (m, 4H, ArH), 7.44 (d, $J = 6.9$ Hz, 1H, ArH), 7.42-7.34 (m, 5H, ArH), 7.31-7.25 (m, 2H, ArH), 7.21-7.15 (m, 3H, 2F-ArH, ArH), 7.07 (s, 1H, NH), 7.02 (d, $J = 8.4$ Hz, 1H, ArH), 4.72-4.65 (m, 1H, H_α), 4.62-4.50 (m, 2H, H_α), 4.19 (dd, $J = 13.3, 8.4$ Hz, 1H, Lys- H_α), 3.61 (dd, $J = 14.3, 3.9$, 1H, CH_2), 3.24-3.00 (m, 5H, CH_2), 2.97-2.89 (m, 1H, CH_2), 2.82-2.49 (m, 5H, CH_2), 2.29-2.19 (m, 1H, Inp- H_α), 1.78-1.66 (m, 1H, CH_2), 1.66-1.54 (m, 1H, CH_2), 1.53-1.40 (m, 5H, CH_2), 1.40-1.16 (m, 2H, CH_2), ppm. ESI-LC-MS m/z 477.4 $[\text{M} + 4\text{H} - \text{F}]^{2+}$; HRMS (ESI-MS) calcd. for $\text{C}_{58}\text{H}_{61}\text{FN}_7\text{O}_6$ $[\text{M} + \text{H}]^+$ 970.4667 found 970.4693.

LCE00272: H-His-D-Trp-Ala-Trp-D-Phe-Lys(4-FB)-NH₂ (4-FB-GHRP-6)

The product was purified by preparative HPLC (15-80% MeCN + 0.1% TFA). This yielded a white powder (9.60 mg, 7%): $^1\text{H-NMR}$ (400 MHz, CD_3OD); **His, D-Trp, Trp, D-Phe, 4-FB**: δ 8.50 (s, 1H, His H_ϵ), 7.88-7.80 (m, 2H, F-ArH), 7.57 (d, $J = 7.9$ Hz, 1H, ArH), 7.49 (d, $J = 7.8$ Hz, 1H, ArH), 7.30 (t, $J = 8.2$ Hz, 2H, ArH), 7.26-6.95 (m, 14H, 13ArH, His H_δ), 4.53-4.46 (m, 2H, H_α), 4.37-4.30 (m, 2H, H_α), 3.26-3.04 (m, 6H, H_β), 2.87 (d, $J = 8.0$ Hz, 2H, H_β), **Lys**: 4.04 (dd, $J = 10.2, 4.0$ Hz, 1H, H_α), 3.26-

3.04 (m, 2H, H_ε), 1.81-1.70 (m, 1H, H_β), 1.58-1.43 (m, 3H, 2H_δ, H_β), 1.06-0.97 (m, 2H, H_γ), **Ala**: 3.94 (q, *J* = 7.3 Hz, 1H, H_α), 0.87 (d, *J* = 7.3 Hz, 3H, CH₃) ppm. ESI-LC-MS *m/z* 498.4 [M + 2H]²⁺; HRMS (ESI-MS) calcd. for C₅₃H₅₉FN₁₂O₇Na [M + Na]⁺ 1017.4511 found 1017.4522.

LCE00281: H-His-D-Trp-Ala-Trp-D-Phe-Dpr(4-FB)-NH₂ (Dpr-4-FB-GHRP-6)

Preparative HPLC (25-70% MeCN + 0.1% TFA) gave the title compound as a white solid (19.8 mg, 14%): ¹H-NMR (400 MHz, CD₃OD); **His, D-Trp, Trp, D-Phe, 4-FB**: δ 8.58 (d, *J* = 1.3 Hz, 1H, His H_ε), 7.82-7.75 (m, 2H, F-ArH), 7.52 (d, *J* = 7.9 Hz, 1H, ArH), 7.40 (d, *J* = 7.9 Hz, 1H, ArH), 7.27 (dd, *J* = 8.6, 1.5 Hz, 2H, ArH), 7.15-7.07 (m, 5H, ArH), 7.06-6.98 (m, 6H, ArH), 6.97-6.89 (m, 3H, 2ArH, His H_δ), 4.54-4.45 (m, 1H, H_α), 4.44-4.30 (m, 3H, H_α), 3.22-2.98 (m, 6H, H_β), 2.93-2.74 (m, 2H, H_β), **Dpr**: 4.54-4.45 (m, 1H, H_α), 3.67 (dd, *J* = 13.8, 5.6 Hz, 1H, H_β), 3.54 (dd, *J* = 13.8, 7.8 Hz, 1H, H_β), **Ala**: 3.93 (q, *J* = 7.3 Hz, 1H, H_α), 0.86 (d, *J* = 7.3 Hz, 3H, CH₃) ppm. ESI-LC-MS *m/z* 477.4 [M + 2H]²⁺; HRMS (ESI-MS) calcd. for C₅₀H₅₄FN₁₂O₇ [M + H]⁺ 953.4223 found 953.4237.

LCE00282: H-D-Ala-D-2-Nal-Ala-Trp-D-Phe-Lys-NH₂ (GHRP-2)

Purification by preparative HPLC (25-70% MeCN + 0.1% TFA) delivered the title peptide as a white powder (19.7 mg, 17%): ¹H-NMR (400 MHz, CD₃OD); **D-2-Nal, Trp, D-Phe**: δ 7.76 (d, *J* = 9.2 Hz, 2H, ArH), 7.73 (s, 1H, ArH), 7.65 (s, 1H, ArH), 7.51-7.47 (m, 1H, ArH), 7.44-7.37 (m, 2H, ArH), 7.35 (dd, *J* = 8.4, 1.7 Hz, 1H, ArH), 7.25-7.14 (m, 4H, ArH), 7.09-7.01 (m, 4H, ArH), 7.00 (s, 1H, ArH), 4.77 (dd, *J* = 10.9, 4.6 Hz, 1H, H_α), 4.49 (t, *J* = 6.8 Hz, 1H, H_α), 4.36 (t, *J* = 7.6 Hz, 1H, H_α), 3.11 (t, *J* = 6.7 Hz, 2H, H_β), 3.07 (d, *J* = 4.5 Hz, 1H, H_β), 2.88-2.70 (m, 3H, H_β), **D-Ala, Ala**: 4.23 (q, *J* = 7.1 Hz, 1H, H_α), 3.79 (q, *J* = 7.0 Hz, 1H, H_α), 1.27 (d, *J* = 7.2 Hz, 3H, CH₃), 1.00 (d, *J* = 7.1 Hz, 3H, CH₃), **Lys**: 4.16 (dd, *J* = 10.3, 4.1 Hz, 1H, H_α), 2.88-2.70 (m, 2H, H_ε), 1.82-1.72 (m, 1H, H_β), 1.56-1.43 (m, 3H, H_β, 2H_δ), 1.07-0.96 (m, 2H, H_γ), ppm. ESI-LC-MS *m/z* 409.9 [M

+ 2H]²⁺; HRMS (ESI-MS) calcd. for C₄₅H₅₅N₉O₆Na [M + Na]⁺ 840.4204 found 840.4173.

LCE00295: H-Inp-D-2-Nal-D-2-Nal-Phe-Lys(2-FP)-NH₂ (2-FP-G-7039)

The product was purified by preparative HPLC (30-80% MeCN + 0.1% TFA). This yielded a white powder (12.9 mg, 13 %): ¹H-NMR (400 MHz, CD₃OD); δ 8.22-8.17 (m, 2H, amide NH), 8.11 (d, *J* = 7.5 Hz, 2H, amide NH), 8.05 (dd, *J* = 7.9, 2.0 Hz, 1H, amide NH), 7.79-7.66 (m, 6H, ArH), 7.58 (s, 1H, ArH), 7.48 (s, 1H, ArH), 7.44-7.34 (m, 4H, ArH), 7.28 (d, *J* = 8.4 Hz, 1H, ArH), 7.16-7.06 (m, 6H, ArH), 4.96-4.90 (m, 0.5H, HC-F), 4.82-4.77 (m, 0.5H, HC-F), 4.68-4.56 (m, 2H, H_α), 4.55-4.48 (m, 1H, H_α), 4.28-4.21 (m, 1H, Lys-H_α), 3.22-3.13 (m, 4H, CH₂), 3.12-2.64 (m, 8H, CH₂), 2.34-2.26 (m, 1H, Inp-H_α), 1.89-1.78 (m, 1H, CH₂), 1.76-1.64 (m, 1H, CH₂), 1.60-1.23 (m, 11H, 8CH₂, CH₃), ppm. ESI-LC-MS *m/z* 872.5 [M + H]⁺; HRMS (ESI-MS) calcd. for C₅₀H₅₉FN₇O₆ [M + H]⁺ 872.4511 found 872.4516.

LCE00297: H-Inp-D-2-Nal-D-2-Nal-1-Nal-Lys(2-FP)-NH₂ (MMF-03-59-H)

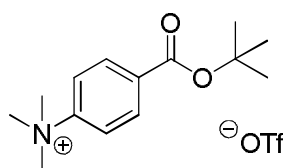
The title peptide was purified by preparative HPLC (35-80% MeCN + 0.1% TFA). This furnished a white powder (7.5 mg, 7 %): ¹H-NMR (400 MHz, CD₃OD); 8.11 (d, *J* = 8.4 Hz, 1H, ArH), 7.82 (d, *J* = 8.0 Hz, 1H, ArH), 7.75-7.62 (m, 5H, ArH), 7.59-7.42 (m, 5H, ArH), 7.41-7.32 (m, 5H, ArH), 7.29-7.23 (m, 2H, ArH), 7.21-7.12 (m, 1H, ArH), 6.99 (d, *J* = 8.4 Hz, 1H, ArH), 4.96-4.89 (m, 0.5H, HC-F), 4.83-4.74 (m, 0.5H, HC-F), 4.73-4.66 (m, 1H, H_α), 4.66-4.54 (m, 2H, H_α), 4.26 (dd, *J* = 9.5, 4.8 Hz, 1H, Lys-H_α), 3.65 (dd, *J* = 14.5, 4.9 Hz, 1H, CH₂), 3.23-3.10 (m, 5H, CH₂), 3.03-2.93 (m, 2H, CH₂), 2.90-2.81 (m, 2H, CH₂), 2.78-2.62 (m, 2H, CH₂), 2.33-2.23 (m, 1H, Inp-H_α), 1.89-1.78 (m, 1H, CH₂), 1.75-1.64 (m, 1H, CH₂), 1.58-1.23 (m, 11H, 8CH₂, CH₃), ppm. ESI-LC-MS *m/z* 922.5 [M + H]⁺; HRMS (ESI-MS) calcd. for C₅₄H₆₁FN₇O₆ [M + H]⁺ 922.4667 found 922.4651.

LCE00298: H-His-D-Trp-Ala-Trp-D-Phe-Dpr-NH₂ (Dpr-GHRP-6)

Purification by preparative HPLC (15-80% MeCN + 0.1% TFA) furnished the title peptide as a white powder (4.7 mg, 3 %): ¹H-NMR (400 MHz, CD₃OD); 8.49 (s, 1H His H_c), 7.55 (d, *J* = 7.9 Hz, 1H, ArH), 7.46 (d, *J* = 7.9 Hz, 1H, ArH), 7.30 (t, *J* = 8.6 Hz, 2H, ArH), 7.21-7.12 (m, 3H, ArH), 7.11-7.04 (m, 3H, ArH), 7.02-6.92 (m, 5H, ArH), 6.89 (d, *J* = 1.0 Hz, 1H, His H_δ), 4.62 (t, *J* = 6.8 Hz, 1H, H_α), 4.52 (t, *J* = 7.9 Hz, 1H, H_α), 4.42-4.33 (m, 2H, H_α), 4.28 (t, *J* = 6.7 Hz, 1H, Dpr-H_α), 4.00 (q, *J* = 7.3 Hz, 1H, Ala-H_α), 3.24-3.11 (m, 3H, CH₂), 3.12-2.92 (m, 5H, CH₂), 2.89-2.76 (m, 2H, CH₂), 0.94 (d, *J* = 7.3 Hz, 3H, Ala-CH₃), ppm. ESI-LC-MS *m/z* 831.4 [M + H]⁺; HRMS (ESI-MS) calcd. for C₄₃H₅₁N₁₂O₆ [M + H]⁺ 831.4055 found 831.4070.

4.2.6 Synthesis of Small Molecule Triflate Salt

4-(*Tert*-butoxycarbonyl)-*N,N,N*-trimethylbenzenammonium triflate salt



4-dimethylaminobenzoic acid (1.00 g, 6.05 mmol, 1.0 eq.) was added to THF (50 ml) and the resultant mixture stirred and cooled to 0°C. After 15 minutes, trifluoroacetic anhydride (1.85 ml, 13.3 mmol, 2.2 eq.) was added dropwise and the consequent blue solution stirred (35 mins). Addition of ^tBuOH (11.4 ml, 119 mmol, 19.7 eq.) was followed by further stirring at room temperature (2 hrs). The solution was then poured into saturated NaHCO₃ (250 ml) and extracted with DCM (3x 100 ml, 3x 50 ml). The combined organic layers were dried (MgSO₄), filtered by gravity and residual solvent removed by rotary evaporation. This delivered a black oil which was eluted through a silica pad (DCM, 60 ml) and solvent removed by concentration *in vacuo*. The final yellow oil (1.12 g, crude) was then re-dissolved in DCM (dry, 30 ml) and cooled to 0°C under a blanket of N₂. This was followed by the addition of MeOTf (0.86 ml, 7.61 mmol, 1.5 eq.) and stirring at 0°C (1 hr). The reaction mixture was then poured into an ice-cold solution of Et₂O (200 ml) which caused instant precipitation of the product salt as a white crystalline solid (740 mg, 38%): ¹H-NMR (400 MHz, CD₃COCD₃); δ 8.24 (d, *J* = 9.3 Hz, 2H), 8.18 (d, *J* = 9.3 Hz, 2H), 3.91 (s, 9H, NMe₃), 1.60 (s, 9H, OC(CH₃)₃); ¹³C-

NMR (100 MHz, CD₃COCD₃); δ 205.5 (CO) 163.6 (ArC), 133.7 (ArC), 131.0 (ArC), 120.9 (ArC), 81.7, 56.9, 27.3 (CH₃CO) ppm. ESI-MS m/z 165.1 [C₁₀H₁₃O₂]⁺; HRMS (ESI-MS) calcd for C₁₄H₂₂NO₂ [M-CF₃O₃S]⁺ 236.1651, found 236.1658.

4.3 Calcium Flux Dose-Response Assay

This assay was carried out for both lead compounds [1-Nal⁴,Lys⁵(4-FB)]G-7039 and [Lys⁵(2-FP)]G-7039 by the EMD Millipore GPCRProfiler® service. Samples of both compounds were dissolved in DMSO (1 ml) at a concentration of 250 μ M and solubility tested in the recommended buffer (Hanks balanced salt solution: 1.26 mM CaCl₂, 0.493 mM MgCl₂·6H₂O, 0.407 mM MgSO₄·7H₂O, 5.33 mM KCl, 0.441 mM KH₂PO₄, 4.17 mM NaHCO₃, 137.9 mM NaCl, 0.338 mM Na₂HPO₄, 5.56 mM D-Glucose with 20 mM HEPES, pH = 7.4 and final concentration of 1.2 % DMSO). If the compound remained soluble 15 minutes after addition, samples were shipped to the EMD Millipore Corporation (15 Research Park Drive, St. Charles, MO 63304, USA). The assay service calculated EC₅₀ values for both peptidomimetics as well as the ghrelin control in terms of intracellular Ca²⁺ release. Human recombinant ghrelin receptor calcium-optimized stable cell lines (chem-1 cells) were loaded with a fluorescent calcium dye (Fluo-8 NW from ABD Bioquest 21080) and calcium flux detected in response to the agonists by a Molecular Devices FLIPR^{TETRA} instrument. The agonist assay was performed for a total of 180 seconds. Each assay and assay concentration was performed in duplicate.

4.4 Computation of Partition Coefficient (LogP)

The *n*-octanol/water partition coefficients for all peptidomimetics were calculated using two different types of computational software. The first was the ACD/LogP prediction software from ACD/ChemSketch (Freeware) version 14.01.¹¹³ Here, calculated values were based on an experimental data set of over 18,000 logP measurements using an additive-constitutive algorithm that took into account contributions from individual atoms, fragments and fragment-based intramolecular interactions.^{112, 113} The second tool was XLOGP3 version 3.2.2.¹¹⁴ Starting from the known logP value of a structurally similar reference compound, the logP value of the desired compound was determined

using a knowledge-based atom-additive model which utilized two correction factors as well as 87 atom/group types.¹¹⁴ This model was calibrated using a training set of 8199 organic compounds and evaluated with two test sets comprising 406 organic compounds and 219 oligopeptides respectively.¹¹⁴ All sets contained experimentally determined log*P* values obtained from Hansch and co-workers compilation.^{114, 121}

4.5 Radiochemistry

4.5.1 General Information

Analytical HPLC runs for radioactive and non-radioactive compounds were performed on a Sunfire™ LCC-012 RP C-18 column (4.6 x 150 mm). Purification of the radioactive compounds was carried out on a Sunfire™ LCC-013 C-18 semi-preparative column (10 x 150 mm). Breeze™ software v.3.30 (2002 Waters Corporation) was used to analyse peptidomimetic and small molecule chromatograms and radio-chromatograms.

4.5.2 Production of [¹⁸F]Fluoride

The [¹⁸F] anion was produced by the PET cyclotron (St. Joseph's Health Care London Ontario, Canada) as a result of the ¹⁸O(p,n)¹⁸F reaction involving proton bombardment of [¹⁸O]H₂O. A Waters Sep-Pak® Accell™ Plus Light (46 mg) QMA Carbonate cartridge was pre-activated by slowly treating with Milli-Q® water (10 ml) and then flushing with air. The radioactive [¹⁸F] anion was then trapped by drawing up the [¹⁸O]H₂O solution containing it through the Sep-Pak.® The left-over enriched water was kept in a separate vial for storage and the initial radioactivity of the cartridge measured on a dose calibrator.

4.5.3 Synthesis of [¹⁸F]FBA

To potassium carbonate (2.0 mg, 0.014 mmol, 2.5 eq.) and Kryptofix 222 (6.0 mg, 0.016 mmol, 2.8 eq.) was added water (200 µl) and anhydrous MeCN (800 µl) and the resulting solution used to elute the Sep-Pak® containing [¹⁸F]fluoride into a glass vial. After measuring the radioactivity of the vial, the mixture was dried azeotropically (50 °C). The drying step was repeated twice more after the drop-wise addition of anhydrous MeCN (1 ml). A diagonal vial was charged with 4-(*tert*-butoxycarbonyl)-*N,N,N*-

trimethylbenzenammonium triflate salt (2.0 mg, 0.0057 mmol, 1.0 eq.) and the aforementioned mixture in DMSO (400 μ l). The solution was heated (without stirring) at 120 °C. After 10 minutes, 5M HCl (1 ml) was added and heating continued for an additional 5 minutes. The reaction mixture was then diluted (water, 2 ml) and the crude [18 F]FBA was trapped in a Sep-Pak[®] Light tC-18 cartridge (pre-treated with 10 ml of ethanol and water) before being extracted with ethanol (0.5 ml) into a reaction vial. The ethanol was then removed by the V10 evaporator (36 °C) and the radioactivity measured. A co-injection of the cold 4-[19 F]-FBA and hot [18 F]-FBA 1:1 mixture diluted in water (10 μ l, 25-90% MeCN + 0.1% TFA gradient system) was used to confirm that the desired product had been acquired. This was used in the next step without further purification.

4.5.4 Attempted Coupling of [18 F]FBA to [1-Nal⁴]G-7039

The peptide cold standard [1-Nal⁴,Lys⁵(4-FB)]G-7039 (0.5 mg) was dissolved in a mixture of MeCN (2.5 ml) and water (7.5 ml). This solution was used to check the retention time of the cold standard by HPLC (10 μ l, gradient system 25-90% MeCN + 0.1% TFA). [1-Nal⁴]G-7039 (1.5 mg, 0.0014 mmol, 1.0 eq.) in DMF (200 μ l) along with HATU in DMF (30 μ l, 7.0×10^{-4} mmol, 0.5 eq.), DIPEA in DMF (10 μ l, 4.8% solution) were added to the [18 F]FBA from the previous step and the consequent solution allowed to stand at room temperature. After 20 minutes, an analytical HPLC was run in order to check the progress of the reaction (25-90% MeCN + 0.1% TFA). As no product had formed, DIPEA/DMF (10 μ l, 4.8%) and HATU/DMF (30 μ l) were added. As this also did not yield a fluorobenzoylated product after 20 minutes, this coupling procedure was abandoned.

4.5.5 Synthesis of [18 F]SFB

The crude [18 F]FBA was synthesized as described previously. However, trapping of the radioactive compound in a Sep-Pak[®] Light tC-18 cartridge (pre-treated with 10 ml of ethanol and 10 ml of water) was followed by elution with MeCN (500 μ l) into a mixture of EDC (35.0 mg, 0.23 mmol.) and NHS (20.0 mg, 0.17 mmol.) The resultant solution was allowed to stand at room temperature. After 10 minutes, the reaction mixture was diluted with H₂O + 0.1 % TFA (1 ml) and purified by semi-preparative HPLC (35-60%

MeCN + 0.1% TFA gradient system, $R_t = 9.3$ mins) to furnish the prosthetic group [^{18}F]SFB (25-90% MeCN + 0.1% TFA, $R_t = 5.7$ mins) in a radiochemical yield of 59 % and radiochemical purity > 99 %. This radioactive compound was dried on the V10 evaporator (36 °C) before being coupled to the peptidomimetic precursor agonist [1-Nal⁴]G-7039.

4.5.6 Synthesis of [1-Nal⁴, Lys⁵(4-[^{18}F]-FB)]G-7039

To [1-Nal⁴]G-7039 (1.0 mg, 9.29×10^{-4} mmol., 1.0 eq.) was consecutively added [^{18}F]SFB in a 1:1 mixture of MeCN/H₂O (200 μl) and DIPEA (5 μl). The consequent reaction mixture was heated to 50-70 °C (without stirring). After 15 minutes, crude ^{18}F -radiolabelled peptidomimetic began to precipitate out of solution as a white solid. The solvent was subsequently removed and the solid re-dissolved stepwise with DMF (200 μl), H₂O (400 μl) and MeCN (100 μl). This solution was purified by preparative HPLC (35-60% MeCN + 0.1% TFA gradient system, $R_t = 12.2$ mins) and delivered the title ^{18}F -radiolabelled peptidomimetic GHS-R1a agonist [1-Nal⁴,Lys⁵(4-[^{18}F]-FB)]G-7039 (45-55% MeCN + 0.1% TFA gradient system, $R_t = 6.7$ mins) in a decay correct radiochemical yield of 52 %, radiochemical purity > 98% and specific activity of 116 MBq/ μmol .

5 References

- (1) Hoffman, J. M.; Gambhir, S. S. *Radiology* **2007**, *244*, 39-47.
- (2) James, M. L.; Gambhir, S. S. *Physiol. Rev.* **2012**, *92*, 897-965.
- (3) Massoud, T. F.; Gambhir, S. S. *Genes Dev.* **2003**, *17*, 545-580.
- (4) Fani, M.; Maecke, H. R.; Okarvi, S. M. *Theranostics* **2012**, *2*, 481-501.
- (5) Alauddin, M. M. *Am. J. Nucl. Med. Mol. Imaging* **2012**, *2*, 55-76.
- (6) Lu, C.; McFarland, M. S.; Nesbitt, R.; Williams, A. K.; Chan, S.; Gomez-Lemus, J.; Autran-Gomez, A. M.; Al-Zahrani, A.; Chin, J. L.; Izawa, J. I.; Luyt, L. G.; Lewis, J. D. *The Prostate* **2012**, *72*, 825-833.
- (7) The Canadian Cancer Society, Canadian Prostate Cancer Statistics.
<http://www.cancer.ca/en/cancer-information/cancer-type/prostate/statistics/?region=on> (accessed March 22nd, 2014).
- (8) The Canadian Cancer Society, Prostate Cancer Risks.
<http://www.cancer.ca/en/cancer-information/cancer-type/prostate/risks/?region=on> (accessed May 25th, 2013).
- (9) McNeal, J. E. *Prostate* **1981**, *2*, 35-49.
- (10) Seitz, M.; Shukla-Dave, A.; Bjartell, A.; Touijer, K.; Sciarra, A.; Bastian, P. J.; Stief, C.; Hricak, H.; Graser, A. *Eur. Urol.* **2009**, *55*, 801-814.
- (11) The Canadian Cancer Society, Anatomy and Physiology of the Prostate.
<http://www.cancer.ca/en/cancer-information/cancer-type/prostate/anatomy-and-physiology/?region=on> (accessed February 21st, 2014).
- (12) Kattan, M. W.; Eastham, J. A.; Stapleton, A. M.; Wheeler, T. M.; Scardino, P. T. *J. Natl. Cancer. Inst.* **1998**, *90*, 766-771.

- (13) Eifler, J. B.; Feng, Z.; Lin, B. M.; Partin, M. T.; Humphreys, E. B.; Han, M.; Epstein, J. I.; Walsh, P. C.; Trock, B. J.; Partin, A. W. *BJU Int.* **2013**, *111*, 22-29.
- (14) D'Amico, A. V.; Whittington, R.; Malkowicz, S. B.; Schultz, D.; Blank, K.; Broderick, G. A.; Tomaszewski, J. E.; Renshaw, A. A.; Kaplan, I.; Beard, C. J.; Wein, A. *Jama* **1998**, *280*, 969-974.
- (15) Gupta, R. T.; Kauffman, C. R.; Polascik, T. J.; Taneja, S. S.; Rosenkrantz, A. B. *Oncology (Williston Park)* **2013**, *27*, 262-270.
- (16) Turkbey, B.; Mani, H.; Shah, V.; Rastinehad, A. R.; Bernardo, M.; Pohida, T.; Pang, Y.; Daar, D.; Benjamin, C.; McKinney, Y. L.; Trivedi, H.; Chua, C.; Bratslavsky, G.; Shih, J. H.; Linehan, W. M.; Merino, M. J.; Choyke, P. L.; Pinto, P. A. *J. Urol.* **2011**, *186*, 1818-1824.
- (17) Thormer, G.; Otto, J.; Reiss-Zimmermann, M.; Seiwerts, M.; Moche, M.; Garnov, N.; Franz, T.; Do, M.; Stolzenburg, J.; Horn, L.; Kahn, T.; Busse, H. *Eur. Radiol.* **2012**, *22*, 1820-1828.
- (18) Schwarzenboeck, S.; Souvatzoglou, M.; Krause, B. J. *Theranostics* **2012**, *2*, 318-330.
- (19) Casciani, E.; Gualdi, G. F. *Abdom. Imaging* **2006**, *31*, 490-499.
- (20) Ido, T.; Wan, C. N.; Casella, V.; Fowler, J. S.; Wolf, A. P.; Reivich, M.; Kuhl, D. E. *J. Labelled Compd. Radiopharm.* **1978**, *14*, 175-183.
- (21) Langner, J. Whole body PET image. http://commons.wikimedia.org/wiki/File:PET-MIPS_anim_frame.PNG (accessed March 22nd, 2014).
- (22) Warburg, O. *Science* **1956**, *123*, 309-314.
- (23) Jadvar, H. *J. Nucl. Med.* **2011**, *52*, 81-89.
- (24) Fanti, S.; Nanni, C.; Ambrosini, V.; Gross, M. D.; Rubello, D.; Farsad, M. *J. Nucl. Med. Mol. Imaging* **2007**, *51*, 260-271.

- (25) Kato, T.; Tsukamoto, E.; Kuge, Y.; Takei, T.; Shiga, T.; Shinohara, N.; Katoh, C.; Nakada, K.; Tamaki, N. *Eur. J. Nucl. Med. Mol. Imaging* **2002**, *29*, 1492-1495.
- (26) Shiiba, M.; Ishihara, K.; Kimura, G.; Kuwako, T.; Yoshihara, H.; Yoshihara, N.; Sato, H.; Kondo, Y.; Tsuchiya, S.; Kumita, S. *Ann. Nucl. Med.* **2012**, *26*, 138-145.
- (27) Liu, Y.; Hu, X.; Liu, H.; Bu, L.; Ma, X.; Cheng, K.; Li, J.; Tian, M.; Zhang, H.; Cheng, Z. *J. Nucl. Med.* **2013**, *54*, 2132-2138.
- (28) Kroll, C.; Mansi, R.; Braun, F.; Dobitz, S.; Maecke, H. R.; Wennemers, H. *J. Am. Chem. Soc.* **2013**, *135*, 16793-16796.
- (29) Wieser, G.; Mansi, R.; Grosu, A. L.; Schultze-Seemann, W.; Dumont-Walter, R. A.; Meyer, P. T.; Maecke, H. R.; Reubi, J. C.; Weber, W. A. *Theranostics* **2014**, *4*, 412-419.
- (30) Cheng, Z.; Zhang, L.; Graves, E.; Xiong, Z.; Dandekar, M.; Chen, X.; Gambhir, S. *S. J. Nucl. Med.* **2007**, *48*, 987-994.
- (31) Hausner, S. H.; Marik, J.; Gagnon, M. K. J.; Sutcliffe, J. L. *J. Med. Chem.* **2008**, *51*, 5901-5904.
- (32) Bejot, R.; Gouverneur, V. *Mol. Med. Med. Chem.* **2012**, *6*, 335-382.
- (33) Lasne, M.; Perrio, C.; Rouden, J.; Barre, L.; Roeda, D.; Dolle, F.; Crouzel, C. *Topics in current chemistry* **2002**, *222*, 201-258.
- (34) Jacobson, O.; Zhu, L.; Ma, Y.; Weiss, I. D.; Sun, X.; Niu, G.; Kiesewetter, D. O.; Chen, X. *Bioconjug. Chem.* **2011**, *22*, 422-428.
- (35) Schottelius, M.; Wester, H. *Methods (Amsterdam, Neth.)* **2009**, *48*, 161-177.
- (36) Vlieghe, P.; Lisowski, V.; Martinez, J.; Khrestchatsky, M. *Drug Discovery Today* **2010**, *15*, 40-56.
- (37) Markwalder, R.; Reubi, J. C. *Cancer Res.* **1999**, *59*, 1152-1159.

- (38) Jeffery, P. L.; Herington, A. C.; Chopin, L. K. *J. Endocrinol.* **2002**, *172*, R7-R11.
- (39) Bowers, C. Y.; Chang, J.; Momany, F.; Folkers, K. *Mol. Endocrinol. Proc.* **1977**, 287-292.
- (40) Bowers, C. Y.; Momany, F. A.; Reynolds, G. A.; Hong, A. *Endocrinology* **1984**, *114*, 1537-1545.
- (41) Bowers, C. Y. *J. Pediatr. Endocrinol.* **1993**, *6*, 21-31.
- (42) Ilson, B. E.; Jorkasky, D. K.; Curnow, R. T.; Stote, R. M. *J. Clin. Endocrinol. Metab.* **1989**, *69*, 212-214.
- (43) Moulin, A.; Ryan, J.; Martinez, J.; Fehrentz, J. *ChemMedChem* **2007**, *2*, 1242-1259.
- (44) Akman, M. S.; Girard, M.; O'Brien, L. F.; Ho, A. K.; Chik, C. L. *Endocrinology* **1993**, *132*, 1286-1291.
- (45) Nakagawa, T.; Ukai, K.; Ohyama, T.; Koida, M.; Okamura, H. *Life Sci.* **1996**, *59*, 705-712.
- (46) Isidro, M. L.; Cordido, F. *Comb. Chem. High Throughput Screening* **2006**, *9*, 175-180.
- (47) Smith, R. G.; Cheng, K.; Schoen, W., R.; Pong, S. S.; Hickey, G.; Jacks, T.; Butler, B.; Chan, W. W. S.; Chaung, L. Y. P.; et al *Science* **1993**, *260*, 1640-1643.
- (48) Jacks, T.; Hickey, G.; Judith, F.; Taylor, J.; Chen, H.; Krupa, D.; Feeney, W.; Schoen, W.; Ok, D.; Fisher, M.; et al *J Endocrinol.* **1994**, *143*, 399-406.
- (49) Patchett, A. A.; Nargund, R. P.; Tata, J. R.; Chen, M. -.; Barakat, K. J.; Johnston, D. B. R.; Cheng, K.; Chan, W. W.; Butler, B.; et al *Proc. Natl. Acad. Sci.* **1995**, *92*, 7001-7005.
- (50) Conley, L. K.; Giustina, A.; Imbimbo, B. P.; Stagg, L. C.; Deghenghi, R.; Wehrenberg, W. B. *Endocrine* **1994**, *2*, 691-695.

- (51) Deghenghi, R.; Cananzi, M. M.; Torsello, A.; Battisti, C.; Muller, E. E.; Locatelli, V. *Life Sci.* **1994**, *54*, 1321-1328.
- (52) Elias, K.; Ingle, G.; Burnier, J.; Hammonds, R.; Mcdowell, R.; Rawson, T.; Somers, T.; Stanley, M.; Cronin, M. *Endocrinology* **1995**, *136*, 5694-5699.
- (53) Howard, A. D.; Feighner, S. D.; Cully, D. F.; Arena, J. P.; Liberator, P. A.; Rosenblum, C. I.; Hamelin, M.; Hreniuk, D. L.; Palyha, O. C.; et al *Science* **1996**, *273*, 974-977.
- (54) Smith, R. G.; Van Der Ploeg, L. H. T.; Howard, A. D.; Feighner, S. D.; Cheng, K.; Hickey, G. J.; Wyratt, M. J., Jr.; Fisher, M. H.; Nargund, R. P.; Patchett, A. A. *Endocr. Rev.* **1997**, *18*, 621-645.
- (55) Muccioli, G.; Broglio, F.; Tarabra, E.; Ghigo, E. *Endocr. Updates* **2004**, *23*, 27-45.
- (56) Lefkowitz, R. J. *Angew. Chem. Int. Ed.* **2013**, *52*, 6366-6378.
- (57) Kojima, M.; Hosoda, H.; Date, Y.; Nakazato, M.; Matsuo, H.; Kangawa, K. *Nature* **1999**, *402*, 656-660.
- (58) Heppner, K. M.; Mueller, T. D.; Tong, J.; Tschoep, M. H. *Methods Enzymol.* **2012**, *514*, 249-260.
- (59) Dezaki, K.; Sone, H.; Yada, T. *Pharmacol. Ther.* **2008**, *118*, 239-249.
- (60) Ogiso, K.; Asakawa, A.; Amitani, H.; Inui, A. *J. Gastroenterol. Hepatol.* **2011**, *26*, 67-72.
- (61) Bednarek, M. A.; Feighner, S. D.; Pong, S.; McKee, K. K.; Hreniuk, D. L.; Silva, M. V.; Warren, V. A.; Howard, A. D.; Van der Ploeg, L. H. Y.; Heck, J. V. *J. Med. Chem.* **2000**, *43*, 4370-4376.
- (62) Torsello, A.; Ghe, C.; Bresciani, E.; Catapano, F.; Ghigo, E.; Deghenghi, R.; Locatelli, V.; Muccioli, G. *Endocrinology* **2002**, *143*, 1968-1971.

- (63) Ye, Z.; Gao, Y.; Bakshi, R. K.; Chen, M.; Rohrer, S. P.; Feighner, S. D.; Pong, S.; Howard, A. D.; Blake, A.; Birzin, E. T.; Locco, L.; Parmar, R. M.; Chan, W. W. -.; Schaeffer, J. M.; Smith, R. G.; Patchett, A. A.; Nargund, R. P. *Bioorg. Med. Chem. Lett.* **2000**, *10*, 5-8.
- (64) Li, J. J.; Wang, H.; Li, J.; Qu, F.; Swartz, S. G.; Hernandez, A. S.; Biller, S. A.; Robl, J. A.; Tino, J. A.; Slusarchyk, D.; Seethala, R.; Slep, P.; Yan, M.; Grover, G.; Flynn, N.; Murphy, B. J.; Gordon, D. *Bioorg. Med. Chem. Lett.* **2008**, *18*, 2536-2539.
- (65) Tokunaga, T.; Hume, W. E.; Nagamine, J.; Kawamura, T.; Taiji, M.; Nagata, R. *Bioorg. Med. Chem. Lett.* **2005**, *15*, 1789-1792.
- (66) Xin, Z.; Zhao, H.; Serby, M. D.; Liu, B.; Schaefer, V. G.; Falls, D. H.; Kaszubska, W.; Colins, C. A.; Sham, H. L.; Liu, G. *Bioorg. Med. Chem. Lett.* **2005**, *15*, 1201-1204.
- (67) Raun, K.; Hansen, B. S.; Johansen, N. L.; Thogersen, H.; Madsen, K.; Ankersen, M.; Andersen, P. H. *Eur. J. Endocrinol.* **1998**, *139*, 552-561.
- (68) Ankersen, M.; Johansen, N. L.; Madsen, K.; Hansen, B. S.; Raun, K.; Nielsen, K. K.; Thogersen, H.; Hansen, T. K.; Peschke, B.; Lau, J.; Lundt, B. F.; Andersen, P. H. *J. Med. Chem.* **1998**, *41*, 3699-3704.
- (69) Hansen, T. K.; Ankersen, M.; Hansen, B. S.; Raun, K.; Nielsen, K. K.; Lau, J.; Peschke, B.; Lundt, B. F.; Thogersen, H.; Johansen, N. L.; Madsen, K.; Andersen, P. H. *J. Med. Chem.* **1998**, *41*, 3705-3714.
- (70) Ankersen, M.; Hansen, B. S.; Hansen, T. K.; Lau, J.; Peschke, B.; Madsen, K.; Johansen, N. L. *Eur. J. Med. Chem.* **1999**, *34*, 783-790.
- (71) Hansen, B.; Raun, K.; Nielsen, K.; Johansen, P.; Mansen, T.; Peschke, B.; Lau, J.; Andersen, P.; Ankersen, M. *Eur. J. Endocrinol.* **1999**, *141*, 180-189.

- (72) Peschke, B.; Ankersen, M.; Hansen, B.; Hansen, T.; Johansen, N.; Lau, J.; Madsen, K.; Petersen, H.; Thogersen, H.; Watson, B. *Eur. J. Med. Chem.* **1999**, *34*, 363-380.
- (73) Peschke, B.; Hansen, B. S. *Bioorg. Med. Chem. Lett.* **1999**, *9*, 1295-1298.
- (74) Ankersen, M.; Nielsen, K. K.; Hansen, T. K.; Raun, K.; Hansen, B. S. *Eur. J. Med. Chem.* **2000**, *35*, 487-497.
- (75) Peschke, B.; Ankersen, M.; Hansen, T. K.; Hansen, B. S.; Lau, J.; Nielsen, K. K.; Raun, K. *Eur. J. Med. Chem.* **2000**, *35*, 599-618.
- (76) Hansen, T.; Ankersen, M.; Raun, K.; Hansen, B. *Bioorg. Med. Chem. Lett.* **2001**, *11*, 1915-1918.
- (77) Peschke, B.; Ankersen, M.; Bauer, M.; Hansen, T. K.; Hansen, B. S.; Nielsen, K. K.; Raun, K.; Richter, L.; Westergaard, L. *Eur. J. Med. Chem.* **2002**, *37*, 487-501.
- (78) Reubi, J. C.; Maecke, H. R. *J. Nucl. Med.* **2008**, *49*, 1735-1738.
- (79) Reubi, J. C. *Endocr. Rev.* **2003**, *24*, 389-427.
- (80) Patrick, G. L. *An introduction to medicinal chemistry*; Oxford University Press: Oxford, 2005; , pp 87.
- (81) Wild, D.; Fani, M.; Behe, M.; Brink, I.; Rivier, J. E. F.; Reubi, J. C.; Maecke, H. R.; Weber, W. A. *J. Nucl. Med.* **2011**, *52*, 1412-1417.
- (82) Feighner, S.; Howard, A.; Prendergast, K.; Palyha, O.; Hreniuk, D.; Nargund, R.; Underwood, D.; Tata, J.; Dean, D.; Tan, C.; McKee, K.; Woods, J.; Patchett, A.; Smith, R.; Van der Ploeg, L. *Molecular Endocrinology* **1998**, *12*, 137-145.
- (83) Huang, P.; Loew, G.; Funamizu, H.; Mimura, M.; Ishiyama, N.; Hayashida, M.; Okuno, T.; Shimada, O.; Okuyama, A.; Ikegami, S.; Nakano, J.; Inoguchi, K. *J. Med. Chem.* **2001**, *44*, 4082-4091.

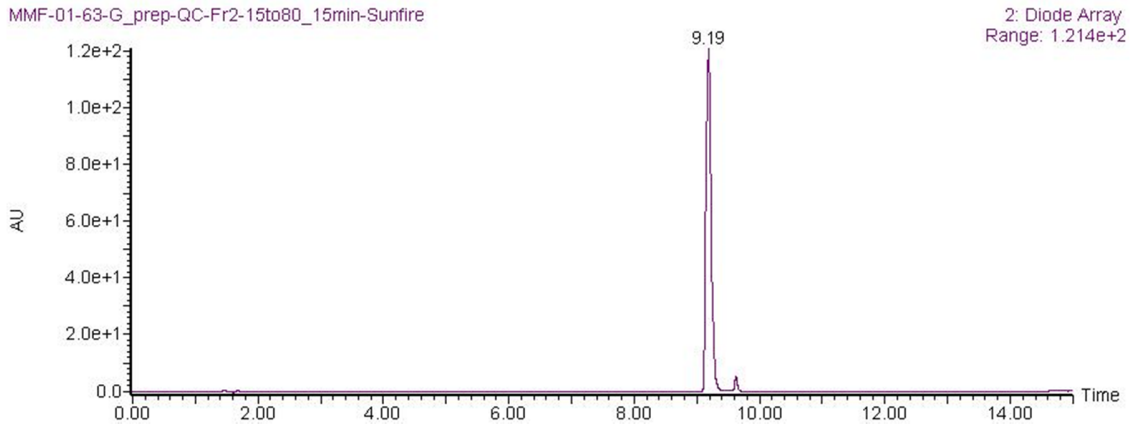
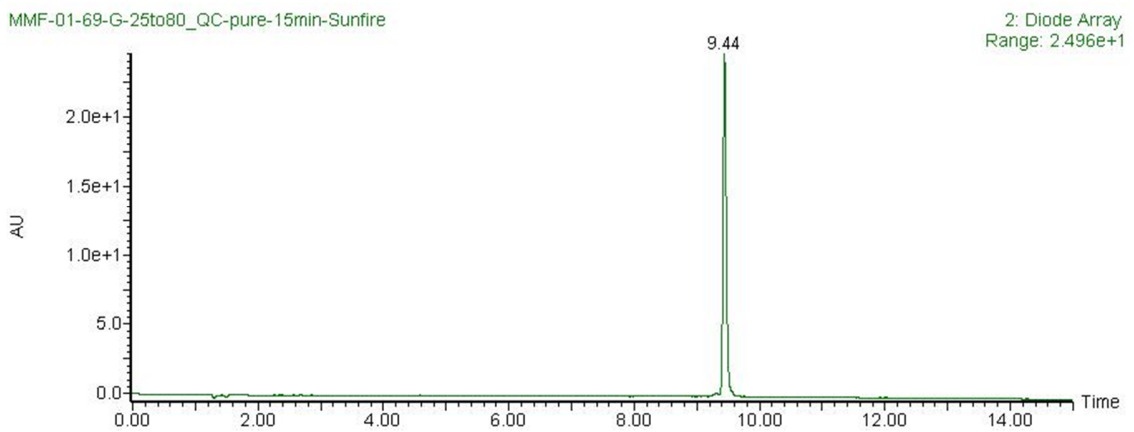
- (84) Pedretti, A.; Villa, M.; Pallavicini, M.; Valoti, E.; Vistoli, G. *J. Med. Chem.* **2006**, *49*, 3077-3085.
- (85) Pedretti, A.; Vistoli, G. *Bioorg. Med. Chem.* **2007**, *15*, 3054-3064.
- (86) Martin-Pastor, M.; De Capua, A.; Alvarez, C. J. P.; Diaz-Hernandez, M. D.; Jimenez-Barbero, J.; Casanueva, F. F.; Pazos, Y. *Bioorg. Med. Chem.* **2010**, *18*, 1583-1590.
- (87) Grossauer, J.; Kosol, S.; Schrank, E.; Zangger, K. *Bioorg. Med. Chem.* **2010**, *18*, 5483-5488.
- (88) Conner, A.; Wheatley, M.; Poyner, D. R. *G Protein-Coupled Recept.* **2010**, 275-288.
- (89) Simms, J. *G Protein-Coupled Recept.* **2010**, 251-273.
- (90) Schoen, W. R.; Pisano, J. M.; Prendergast, K.; Wyvratt, M. J., Jr.; Fisher, M. H.; Cheng, K.; Chan, W. W. -.; Butler, B.; Smith, R. G.; Ball, R. G. *J. Med. Chem.* **1994**, *37*, 897-906.
- (91) Strader, C. D.; Candelore, M. R.; Hill, W. S.; Dixon, R. A. F.; Sigal, I. S. *J. Biol. Chem.* **1989**, *264*, 16470-16477.
- (92) Probst, W. C.; Snyder, L. A.; Schuster, D. I.; Brosius, J.; Sealfon, S. C. *DNA Cell Biol.* **1992**, *11*, 1-20.
- (93) Huang, P.; Kim, S.; Loew, G. J. *Comput. -Aided Mol. Des.* **1997**, *11*, 21-28.
- (94) Resh, M. D. *Biochim. Biophys. Acta, Mol. Cell Res.* **1999**, *1451*, 1-16.
- (95) Banerjee, S. R.; Pullambhatla, M.; Byun, Y.; Nimmagadda, S.; Green, G.; Fox, J. J.; Horti, A.; Mease, R. C.; Pomper, M. G. *J. Med. Chem.* **2010**, *53*, 5333-5341.
- (96) Hickey, J. L.; Lim, S. C.; Hayne, D. J.; Paterson, B. M.; White, J. M.; Villemagne, V. L.; Roselt, P.; Binns, D.; Cullinane, C.; Jeffery, C. M.; Price, R. I.; Barnham, K. J.; Donnelly, P. S. *J. Am. Chem. Soc.* **2013**, *135*, 16120-16132.

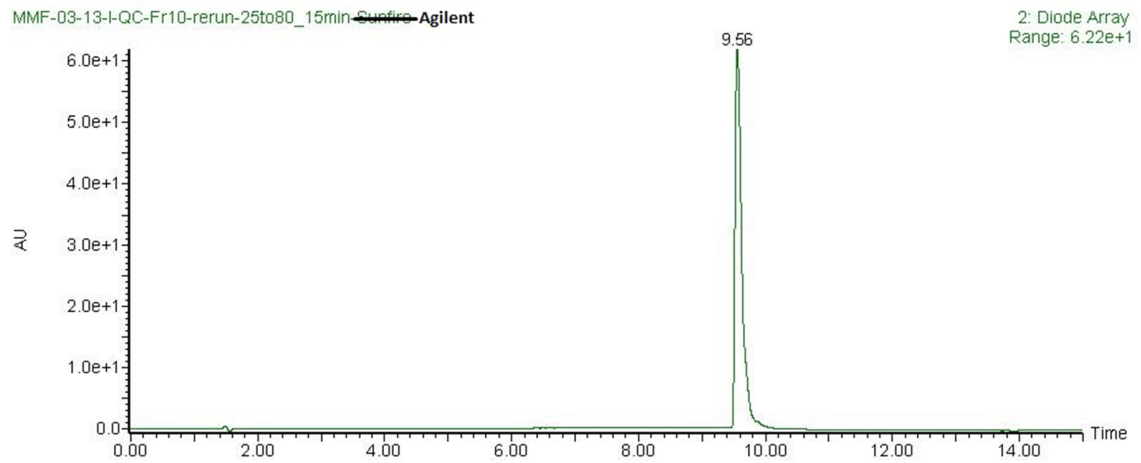
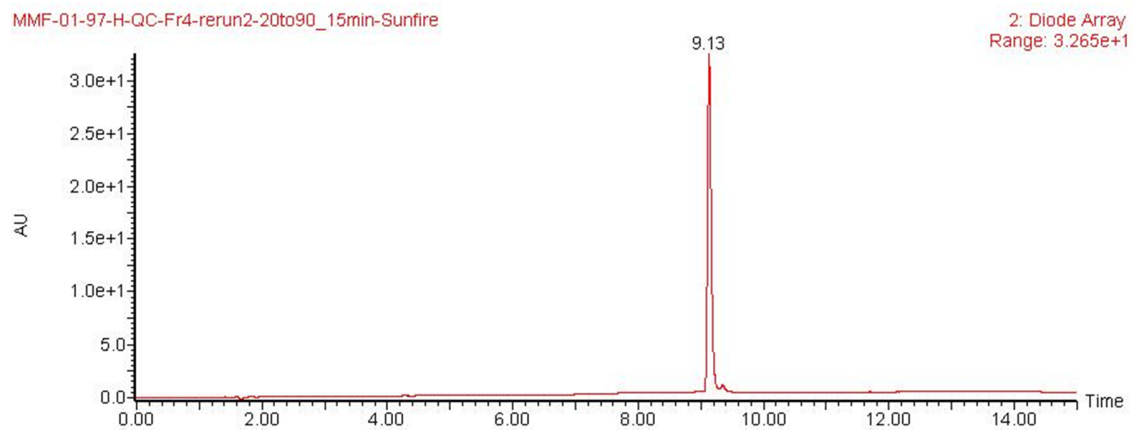
- (97) White, J. B.; Hausner, S. H.; Carpenter, R. D.; Sutcliffe, J. L. *Appl. Radiat. Isot.* **2012**, *70*, 2720-2729.
- (98) Wust, F.; Hultsch, C.; Bergmann, R.; Johannsen, B.; Henle, T. *Appl. Radiat. Isot.* **2003**, *59*, 43-48.
- (99) Maeding, P.; Fuechtner, F.; Wuest, F. *Appl. Radiat. Isot.* **2005**, *63*, 329-332.
- (100) Kuchar, M.; Pretze, M.; Kniess, T.; Steinbach, J.; Pietzsch, J.; Loeser, R. *Amino Acids* **2012**, *43*, 1431-1443.
- (101) Kaiser, E.; Colescot, R.; Bossing, C.; Cook, P. *Anal. Biochem.* **1970**, *34*, 595-&.
- (102) Lipton, M. *In Palladium-catalyzed deprotection of allyl-based protecting groups.* Physical Organic Chemistry; 2002; Vol. 2, pp 1901-1911.
- (103) Zhang, H. X.; Guibe, F.; Balavoine G *Tetrahedron Lett.* **1988**, *29*, 623-626.
- (104) Pearson, D. A.; Blanchette, M.; Baker, M. L.; Guindon, C. A. *Tetrahedron Lett.* **1989**, *30*, 2739-2742.
- (105) Dessolin, M.; Guillerez, M.; Thieriet, N.; Guibe, F.; Loffet, A. *Tetrahedron Lett.* **1995**, *36*, 5741-5744.
- (106) Pinyot, A.; Nikolovski, Z.; Bosch, J.; Segura, J.; Gutiérrez-Gallego, R. *Anal. Biochem.* **2010**, *399*, 174-181.
- (107) Hunt, I. Resonance Energy.
<http://www.chem.ucalgary.ca/courses/351/Carey5th/useful/resenergy.html> (accessed February 17th, 2014).
- (108) Somers, T. C.; Elias, K. A.; Clark, R. G.; Mcdowell, R. S.; Stanley, M. S.; Burnier, J. P.; Rawson, T. E. Patent, WO9615148, 1996.
- (109) Arnott, J. A.; Planey, S. L. *Expert Opin. Drug Discovery* **2012**, *7*, 863-875.

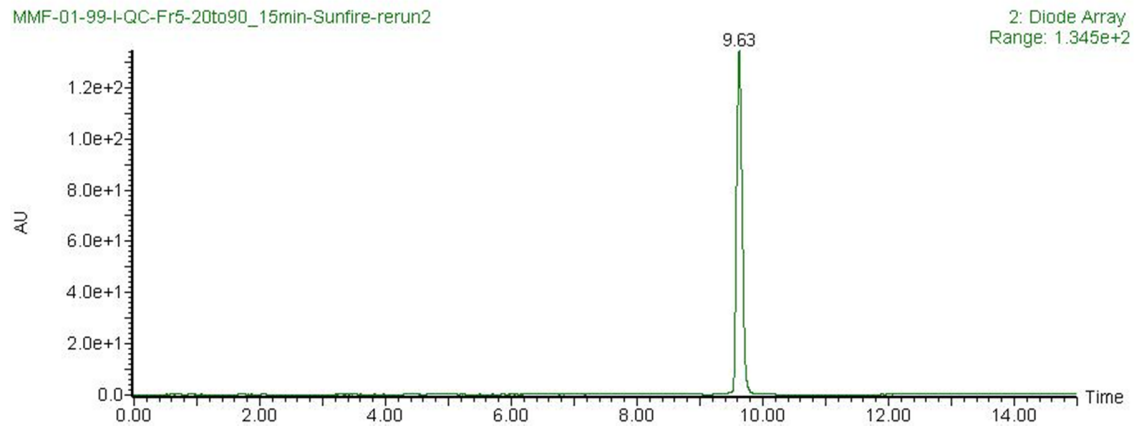
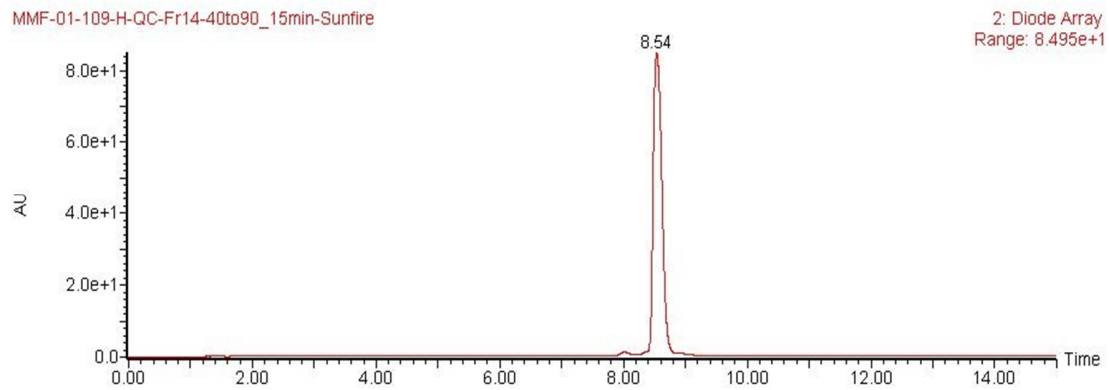
- (110) Zhao, M.; Li, Z.; Wu, Y.; Tang, Y.; Wang, C.; Zhang, Z.; Peng, S. *Eur. J. Med. Chem.* **2007**, *42*, 955-965.
- (111) Thompson, S. J.; Hattotuwigama, C. K.; Holliday, J. D.; Flower, D. R. *Bioinformatics* **2006**, *1*, 237-241.
- (112) Spessard, G. O. *J. Chem. Inf. Comput. Sci.* **1998**, *38*, 1250-1253.
- (113) ACD/ChemSketch (Freeware), version 14.01, Advanced Chemistry Development, Inc., Toronto, ON, Canada, www.acdlabs.com, **2012**.
- (114) Cheng, T.; Zhao, Y.; Li, X.; Lin, F.; Xu, Y.; Zhang, X.; Li, Y.; Wang, R.; Lai, L. *J. Chem. Inf. Model.* **2007**, *47*, 2140-2148.
- (115) Behnam Azad, B. Development of Single and Multimodality Imaging Probes for PET, SPECT and Fluorescence Imaging, University of Western Ontario - Electronic Thesis and Dissertation Repository, 2011.
- (116) Kaptj, J.; Kniess, T.; Wuest, F.; Mercer, J. R. *Appl. Radiat. Isot.* **2011**, *69*, 1218-1225.
- (117) Richter, S.; Bouvet, V.; Wuest, M.; Bergmann, R.; Steinbach, J.; Pietzsch, J.; Neundorf, I.; Wuest, F. *Nucl. Med. Biol.* **2012**, *39*, 1202-1212.
- (118) Yan, Y.; Chen, K.; Yang, M.; Sun, X.; Liu, S.; Chen, X. *Amino Acids* **2011**, *41*, 439-447.
- (119) Haskali, M. B.; Roselt, P. D.; Karas, J. A.; Noonan, W.; Wichmann, C. W.; Katsifis, A.; Hicks, R. J.; Hutton, C. A. *J. Labelled Compd. Radiopharm.* **2013**, *56*, 726-730.
- (120) World Health Organization, Worldwide Cancer Statistics.
http://globocan.iarc.fr/Pages/fact_sheets_cancer.aspx (accessed March 20th, 2014).

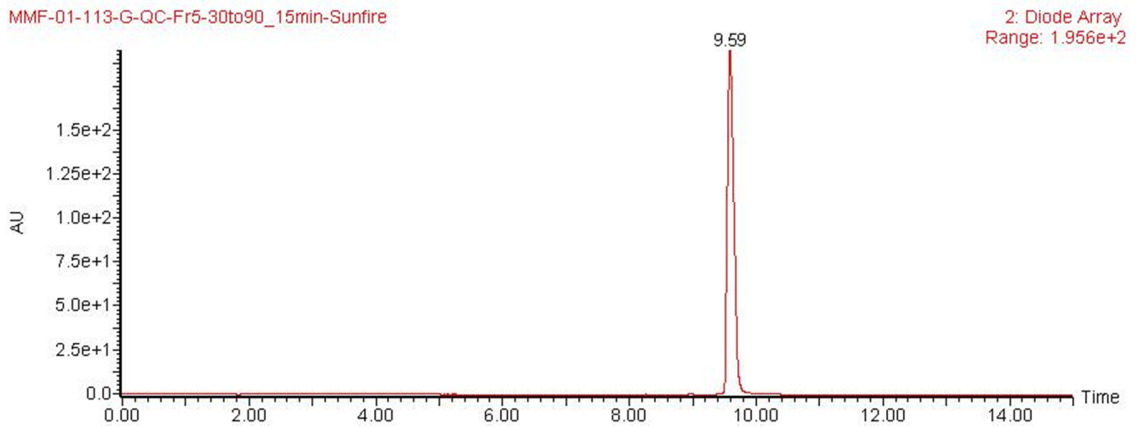
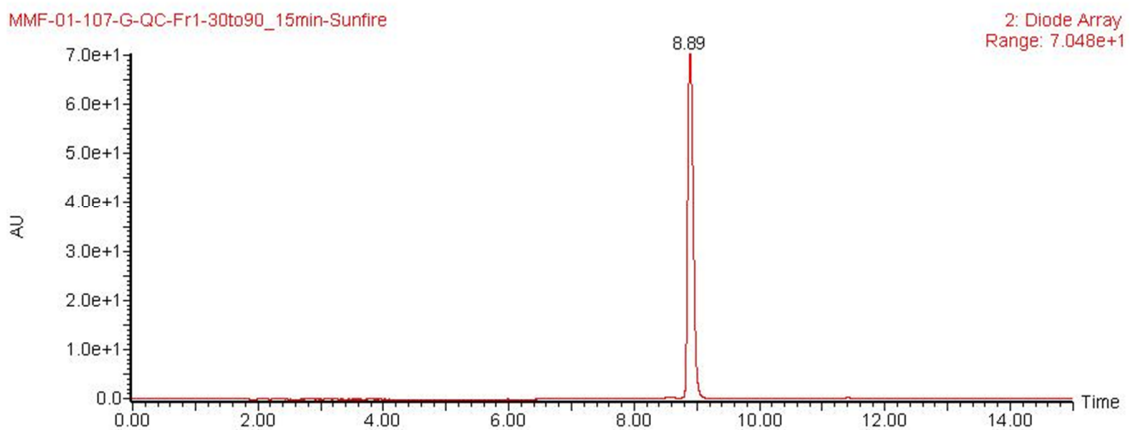
- (121) Hansch, C.; Leo, A.; Hoekman, D. In *Exploring QSAR, Hydrophobic Electronic and Steric Constants*; American Chemical Society: Washington DC, 1995; Vol. 2, pp 3-193.

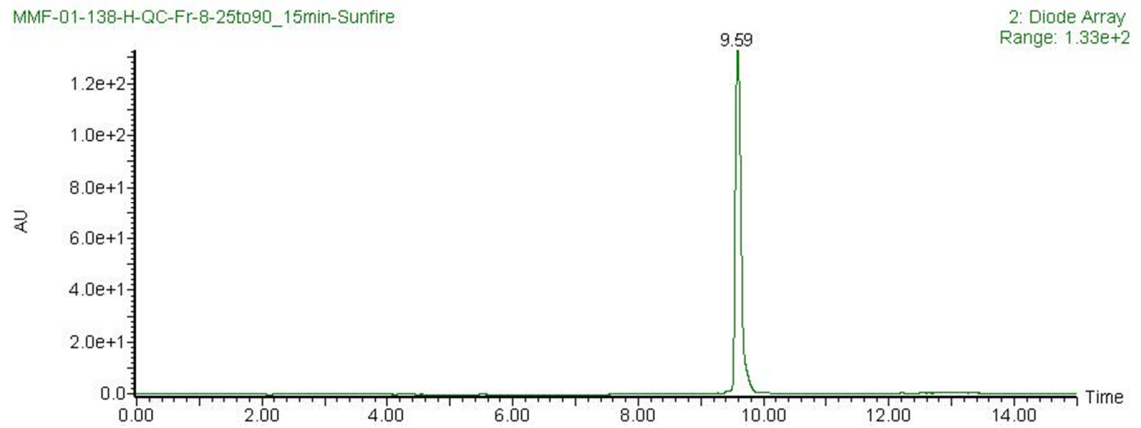
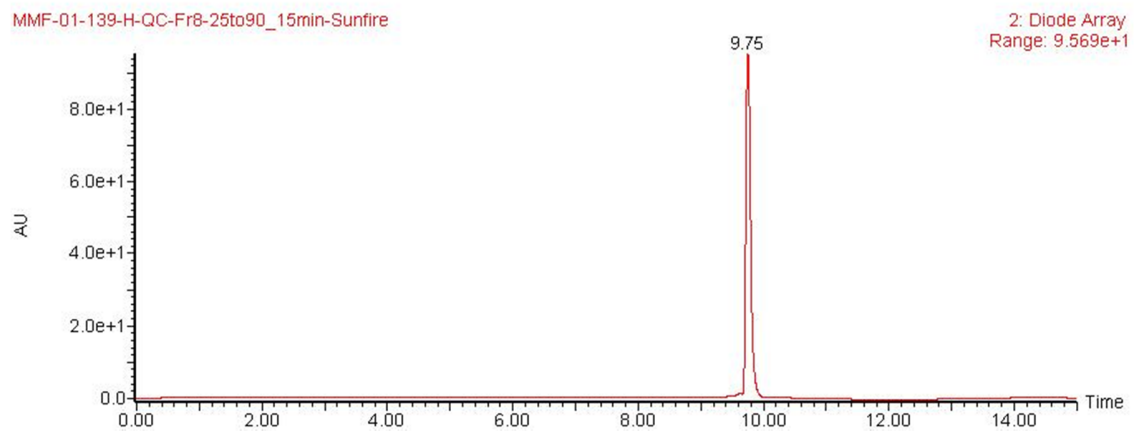
Appendix A: Peptidomimetic Chromatograms

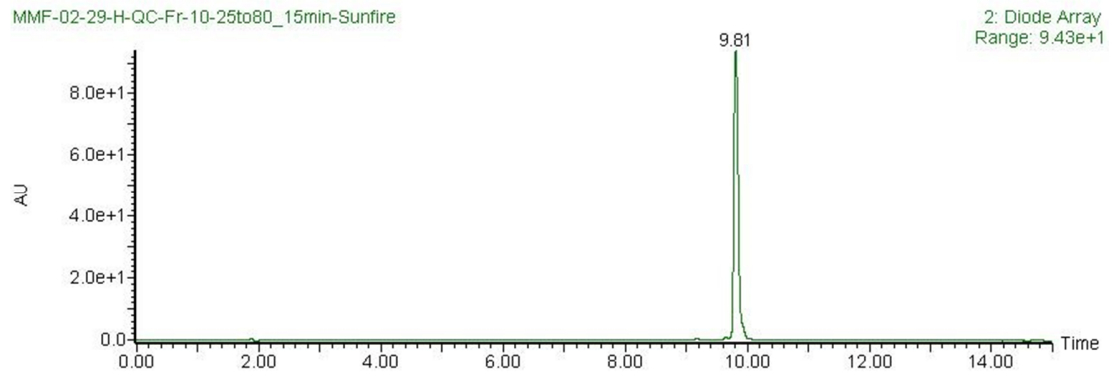
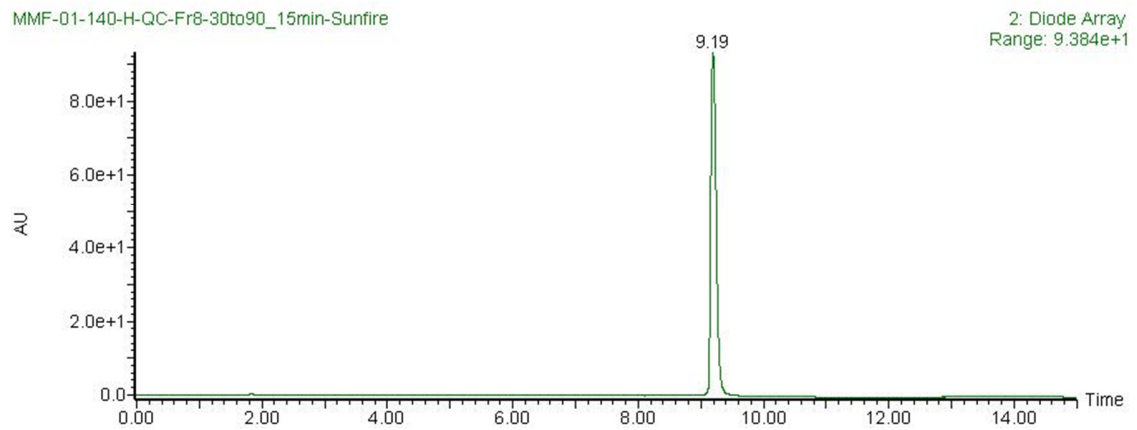
LCE00210: H-Aib-His-D-2-Nal-D-Phe-Lys-NH₂**LCE00211: H-Aib-His-D-2-Nal-D-Phe-Lys(4-FB)-NH₂**

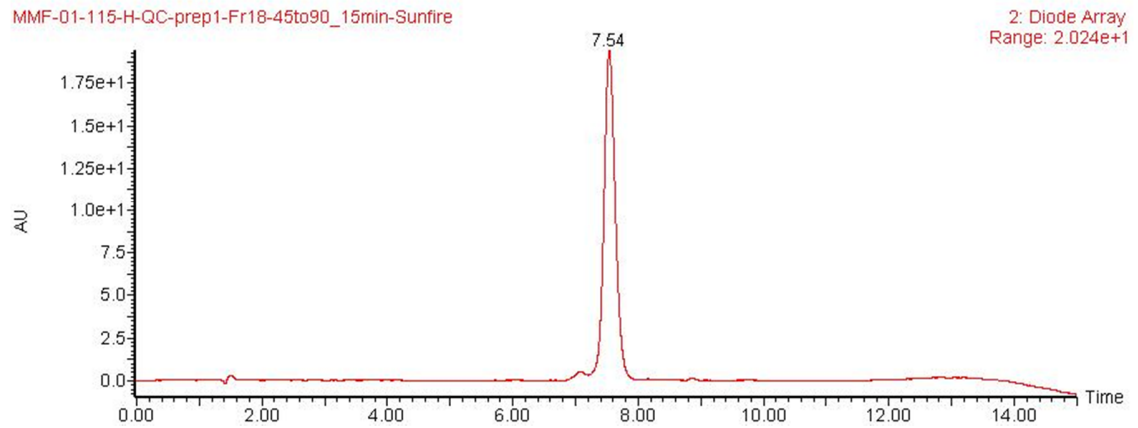
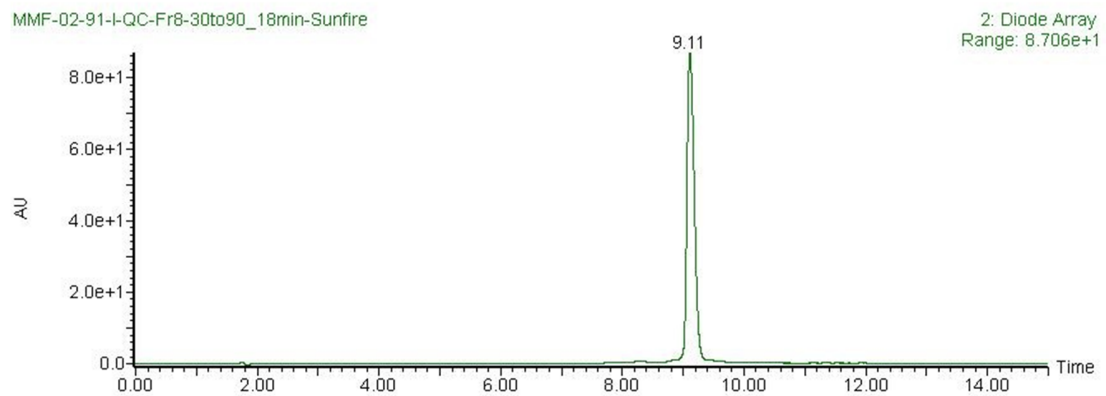
LCE00217: H-Aib-His-D-2-Nal-D-Phe-Lys(AEEA-4-FB)-NH₂**LCE00239: H-His-D-Trp-Ala-Trp-D-Phe-Lys-NH₂**

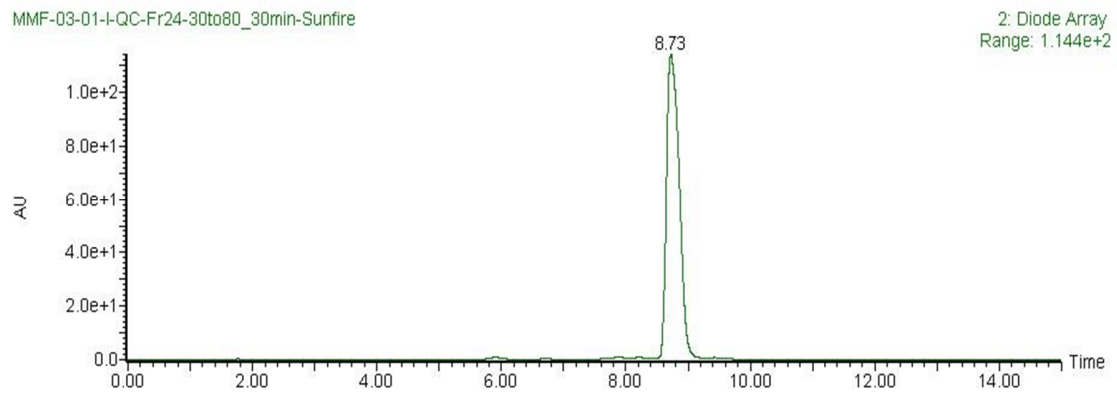
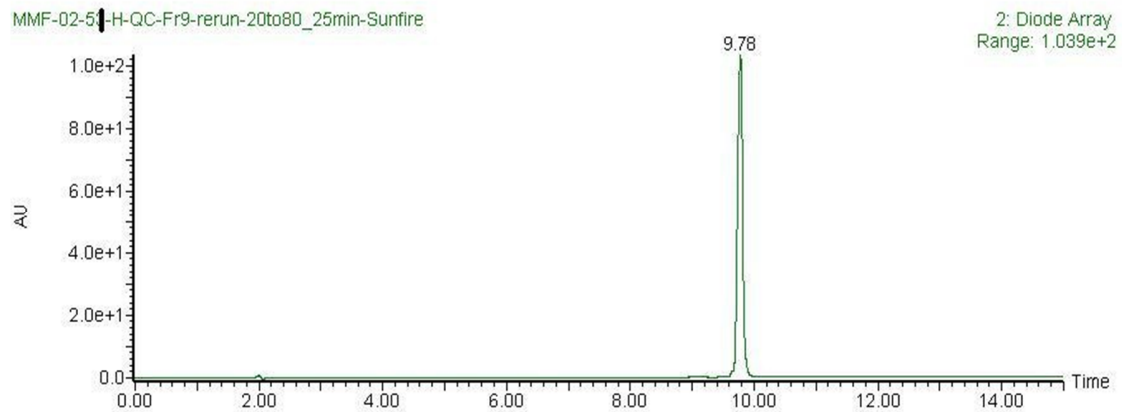
LCE00240: H-Ala-His-D-2-Nal-Ala-Trp-D-Phe-Lys-NH₂**LCE00243: H-Inp-D-2-Nal-D-2-Nal-Phe-Lys(4-FB)-NH₂**

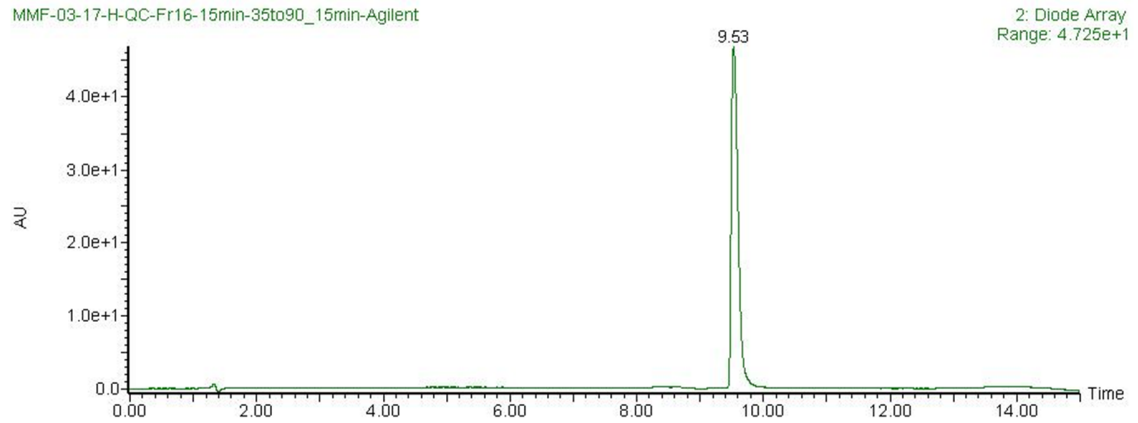
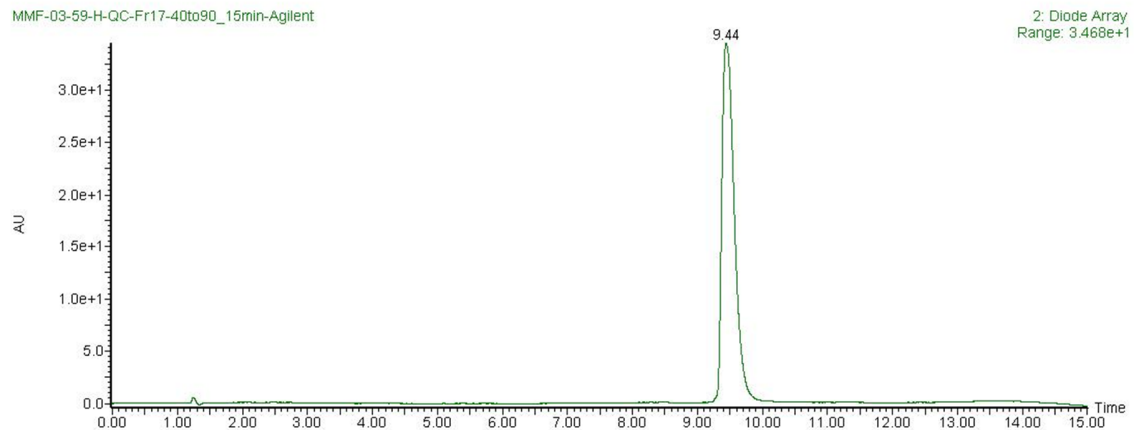
LCE00244: H-Inp-D-2-Nal-D-2-Nal-1-Nal-Lys-NH₂**LCE00245: H-Inp-D-2-Nal-D-2-Nal-Phe-Lys-NH₂**

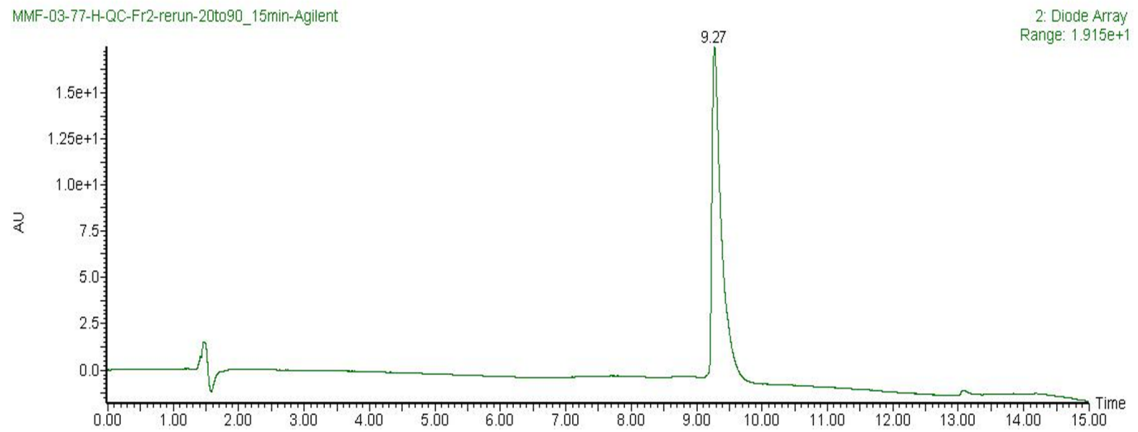
LCE00246: H-Inp-His-D-2-Nal-D-2-Thi-Lys(4-FB)-NH₂**LCE00267: H-Aib-His-D-2-Nal-D-2-Thi-Lys(4-FB)-NH₂**

LCE00268: H-Inp-His-D-2-Nal-D-Phe-Lys(4-FB)-NH₂**LCE00269: H-Inp-His-D-2-Nal-D-2-Nal-Lys(4-FB)-NH₂**

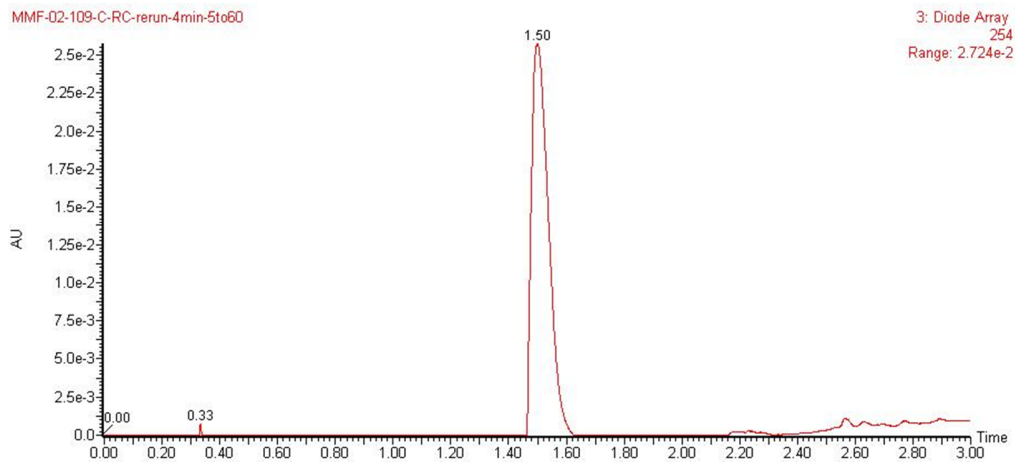
LCE00270: H-Inp-D-2-Nal-D-2-Nal-1-Nal-Lys(4-FB)-NH₂**LCE00272: H-His-D-Trp-Ala-Trp-D-Phe-Lys(4-FB)-NH₂**

LCE00281: H-His-D-Trp-Ala-Trp-D-Phe-Dpr(4-FB)-NH₂**LCE00282: H-D-Ala-D-2-Nal-Ala-Trp-D-Phe-Lys-NH₂**

LCE00295: H-Inp-D-2-Nal-D-2-Nal-Phe-Lys(2-FP)-NH₂**LCE00297: H-Inp-D-2-Nal-D-2-Nal-1-Nal-Lys(2-FP)-NH₂**

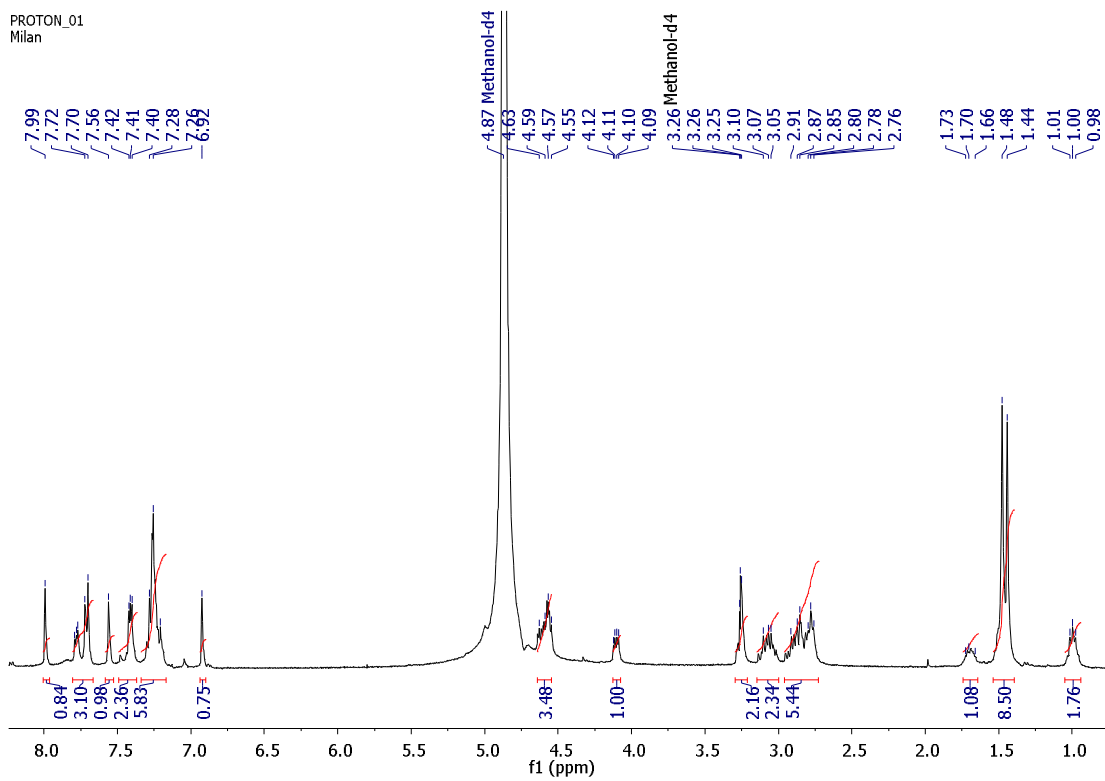
LCE00298: H-His-D-Trp-Ala-Trp-D-Phe-Dpr-NH₂

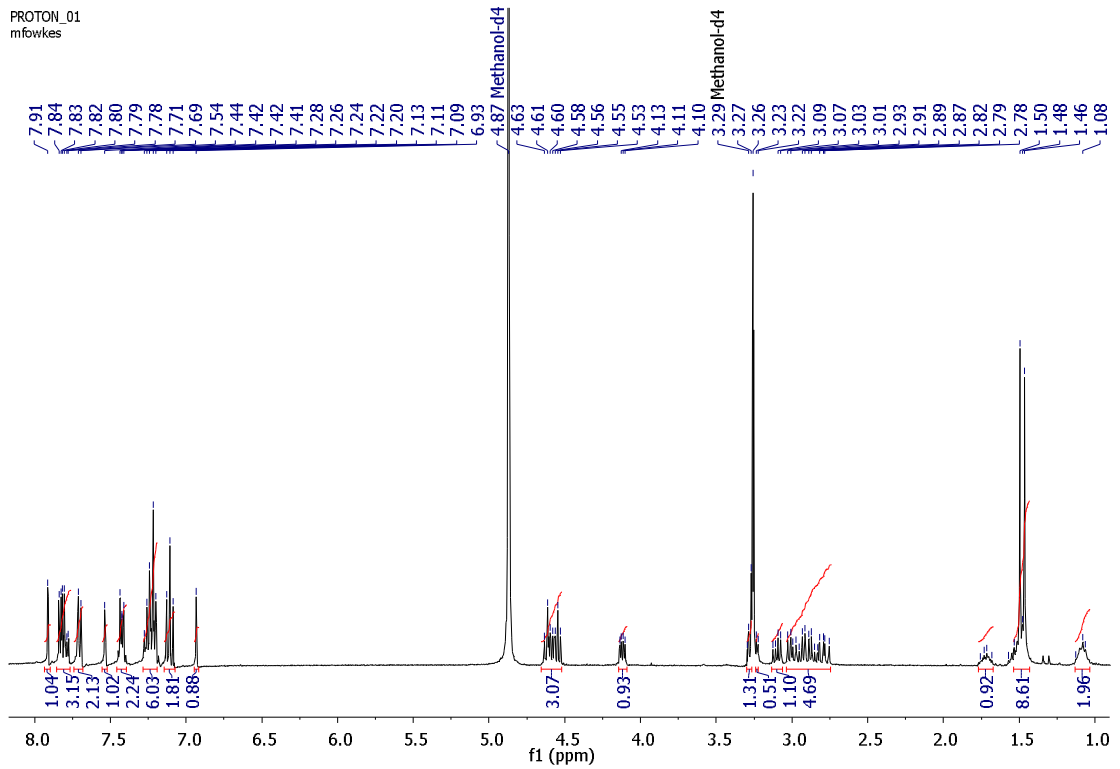
Appendix B: Triflate Salt UHPLC Chromatogram

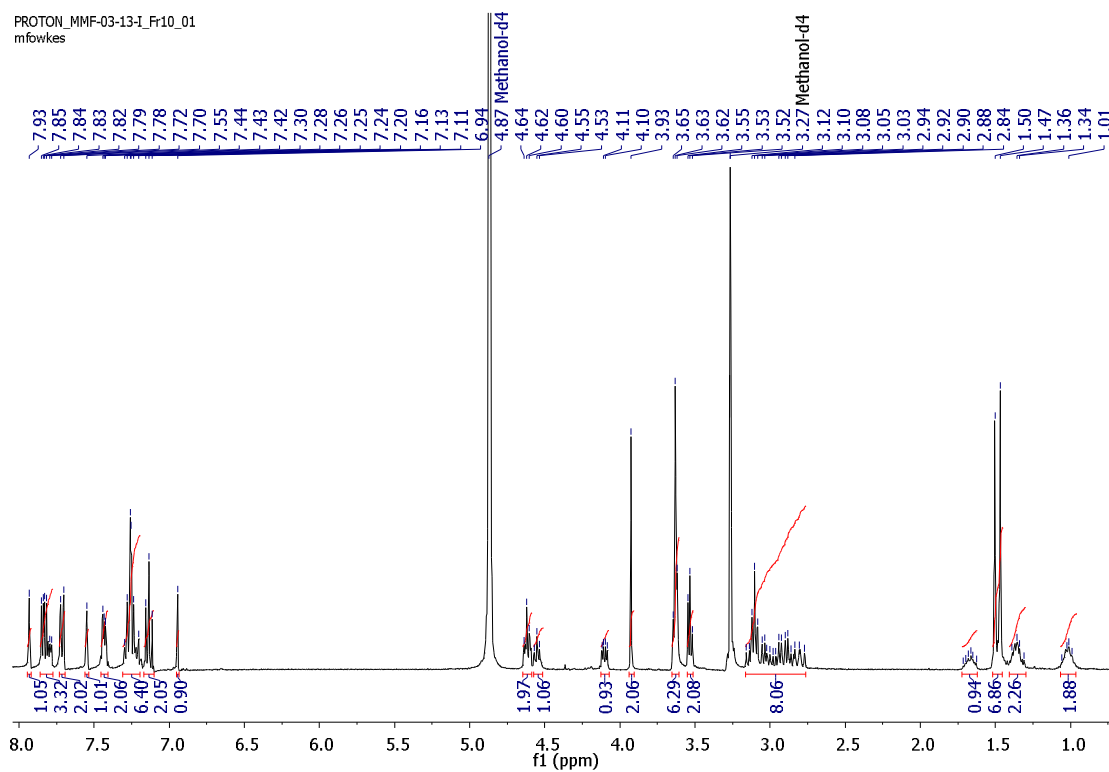


Appendix C: Peptidomimetic $^1\text{H-NMR}$ Spectra

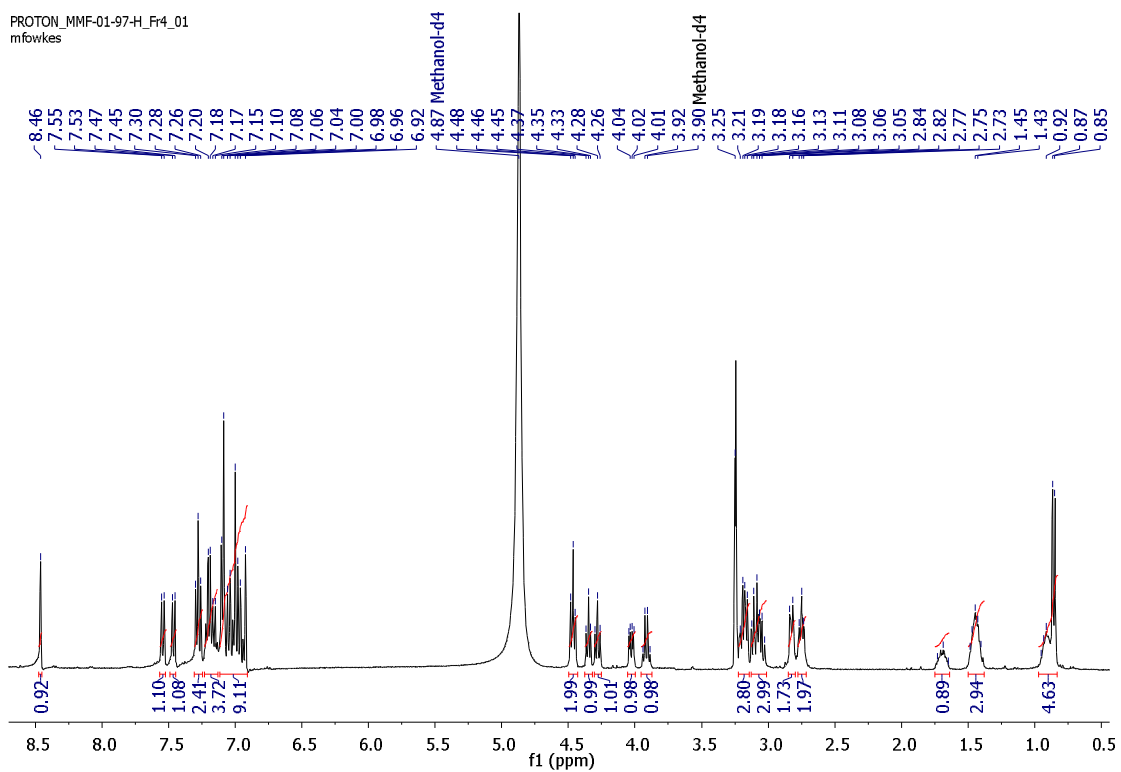
LCE00210: H-Aib-His-D-2-Nal-D-Phe-Lys-NH₂



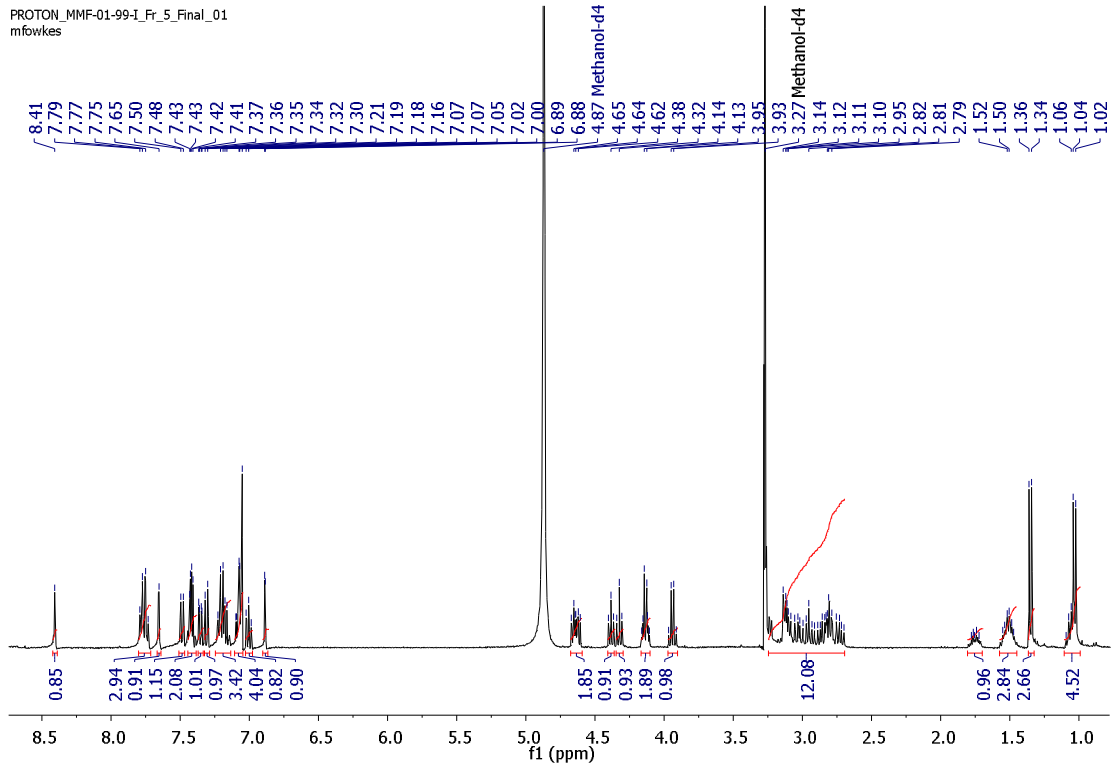
LCE00211: H-Aib-His-D-2-Nal-D-Phe-Lys(4-FB)-NH₂

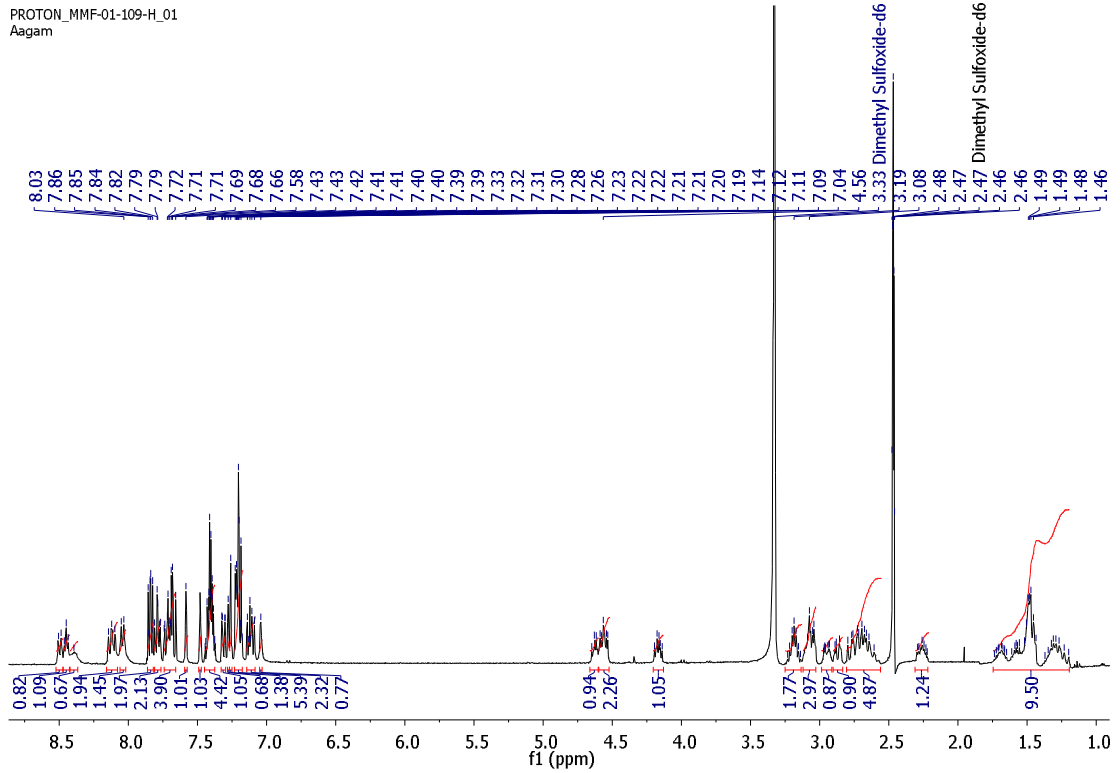
LCE00217: H-Aib-His-D-2-Nal-D-Phe-Lys(AEEA-4-FB)-NH₂

LCE00239: H-His-D-Trp-Ala-Trp-D-Phe-Lys-NH₂

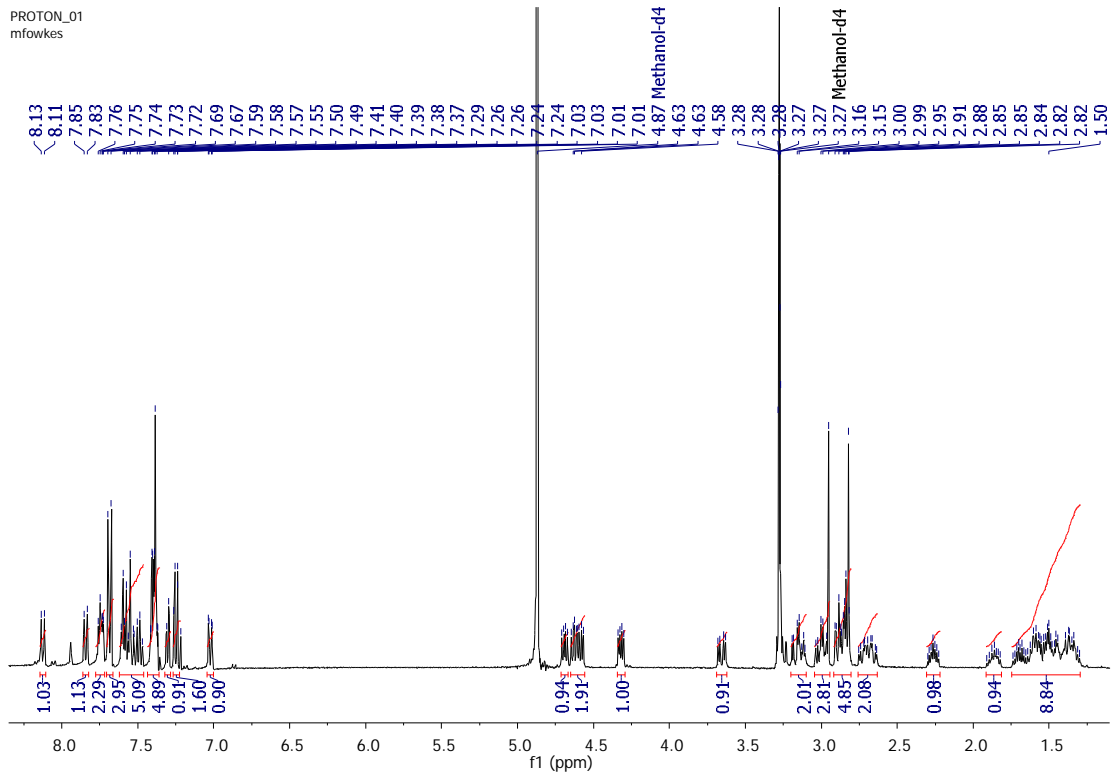


LCE00240: H-Ala-His-D-2-Nal-Ala-Trp-D-Phe-Lys-NH₂

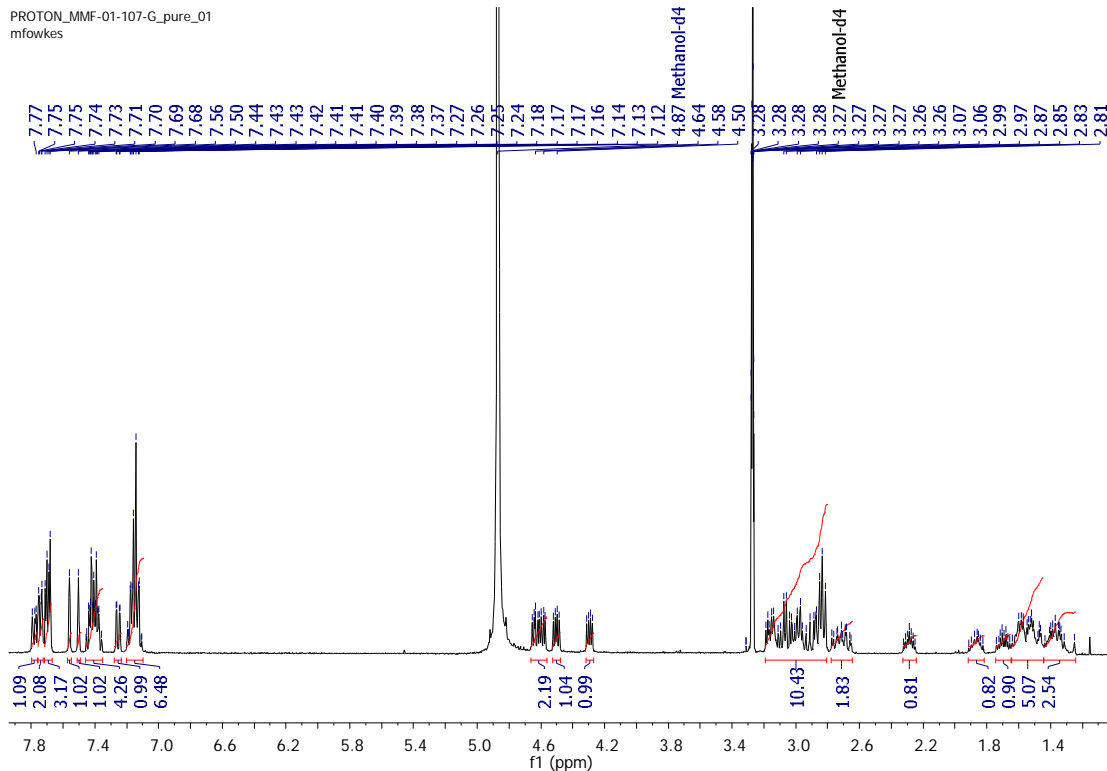


LCE00243: H-Inp-D-2-Nal-D-2-Nal-Phe-Lys(4-FB)-NH₂

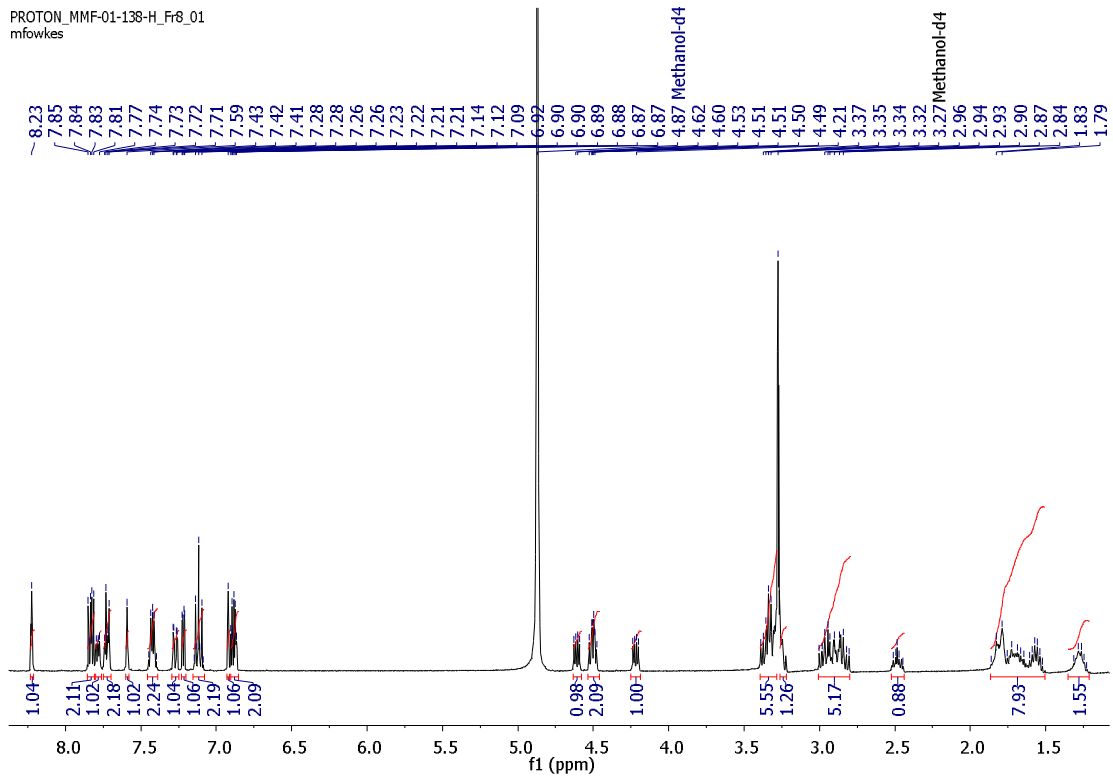
LCE00244: H-Inp-D-2-Nal-D-2-Nal-1-Nal-Lys-NH₂

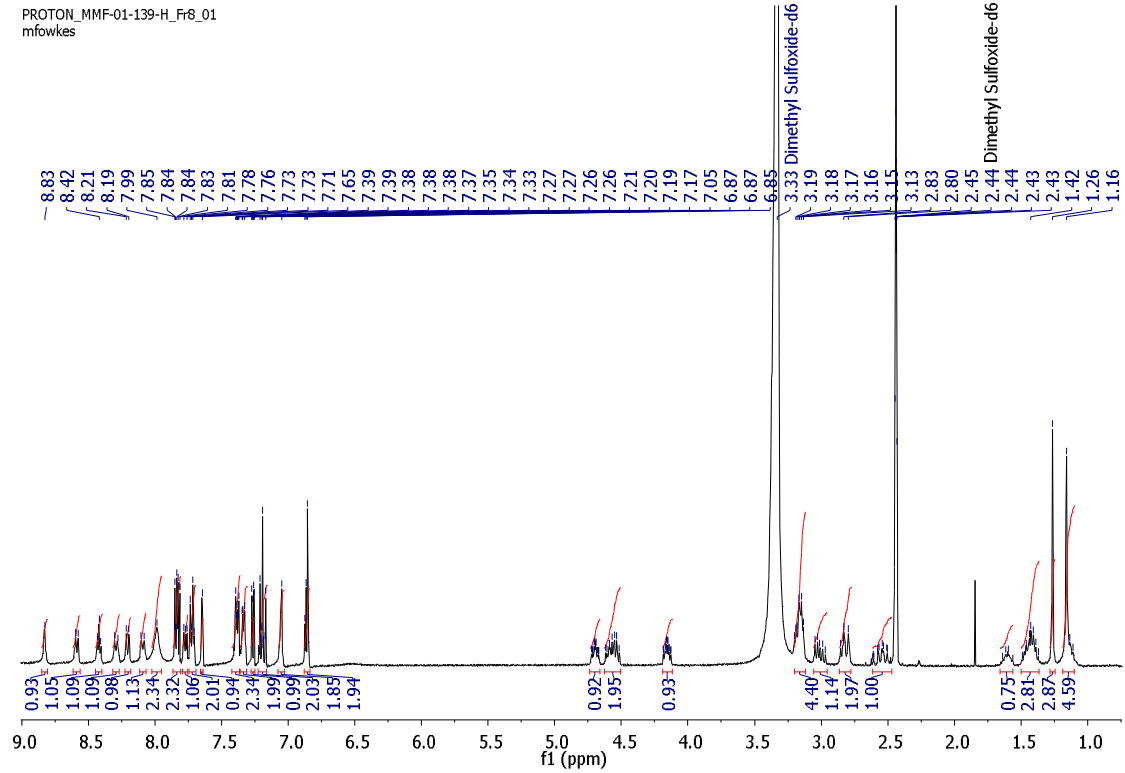


LCE00245: H-Inp-D-2-Nal-D-2-Nal-Phe-Lys-NH₂



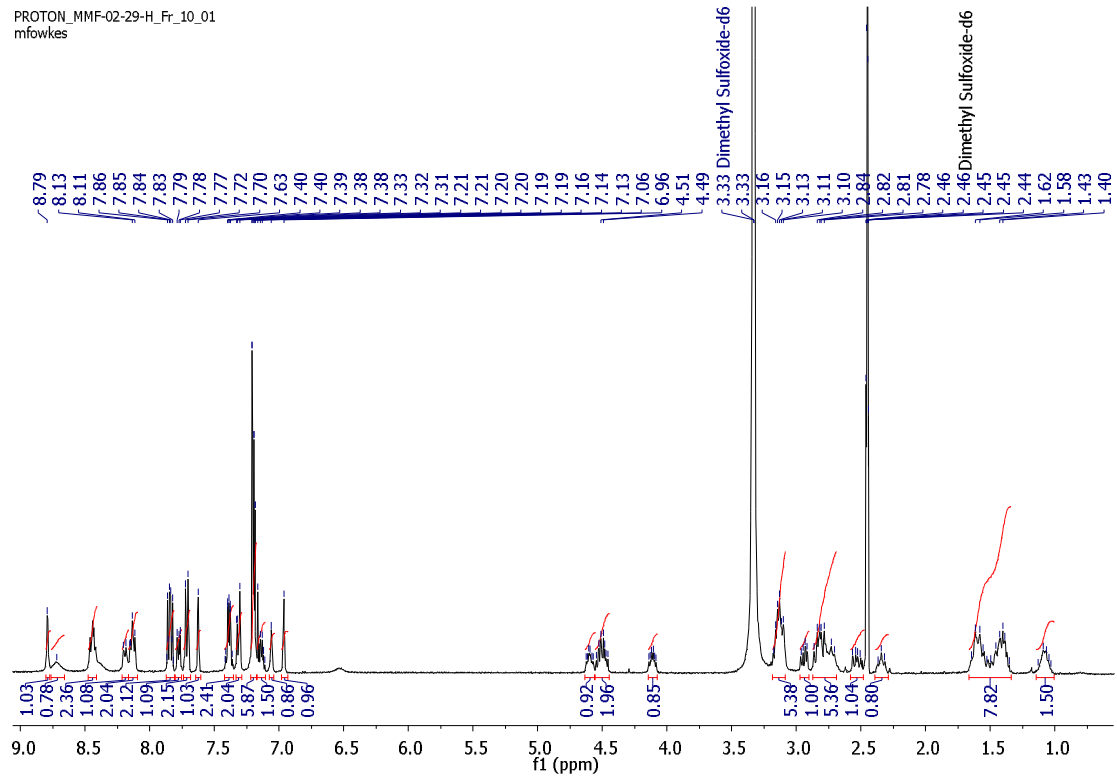
LCE00246: H-Inp-His-D-2-Nal-D-2-Thi-Lys(4-FB)-NH₂



LCE00267: H-Aib-His-D-2-Nal-D-2-Thi-Lys(4-FB)-NH₂

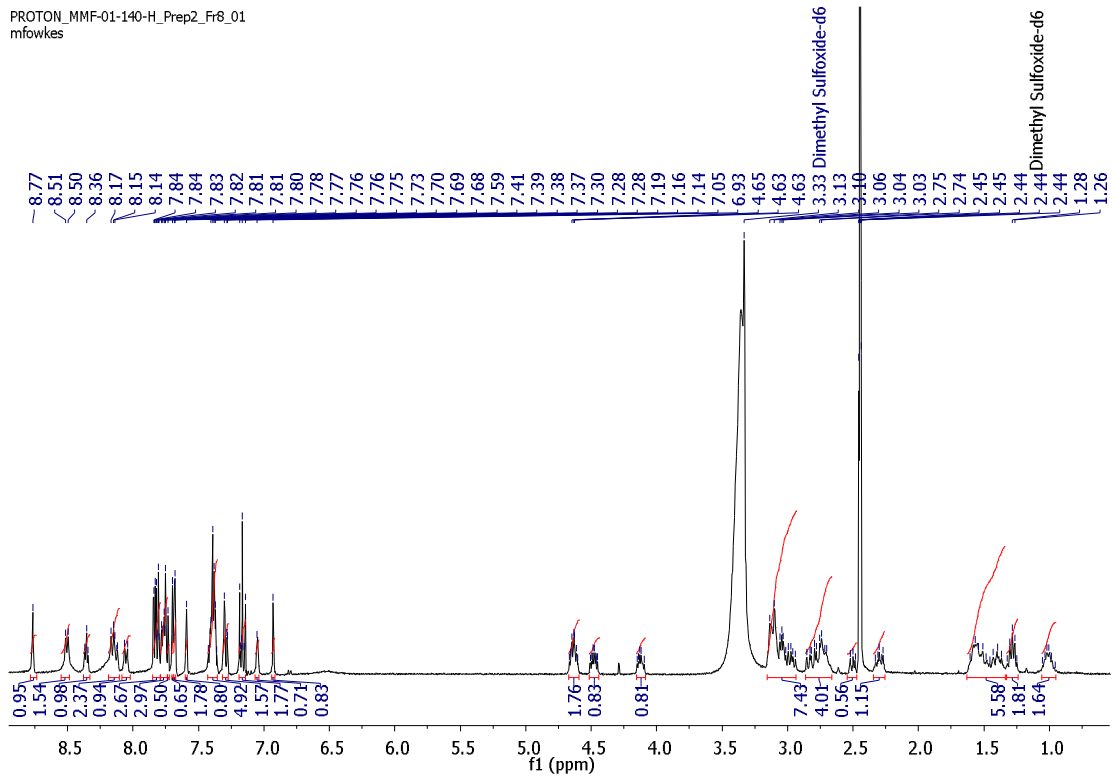
LCE00268: H-Inp-His-D-2-Nal-D-Phe-Lys(4-FB)-NH₂

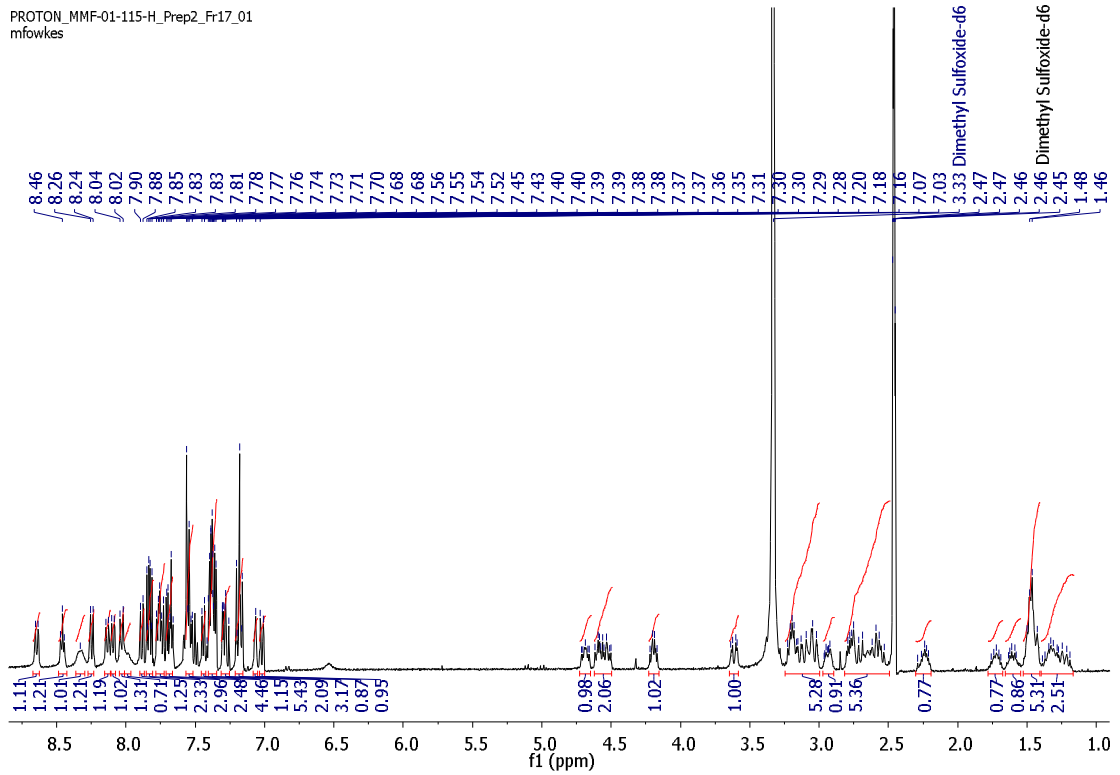
PROTON_MMF-02-29-H_Fr_10_01
mfowkes

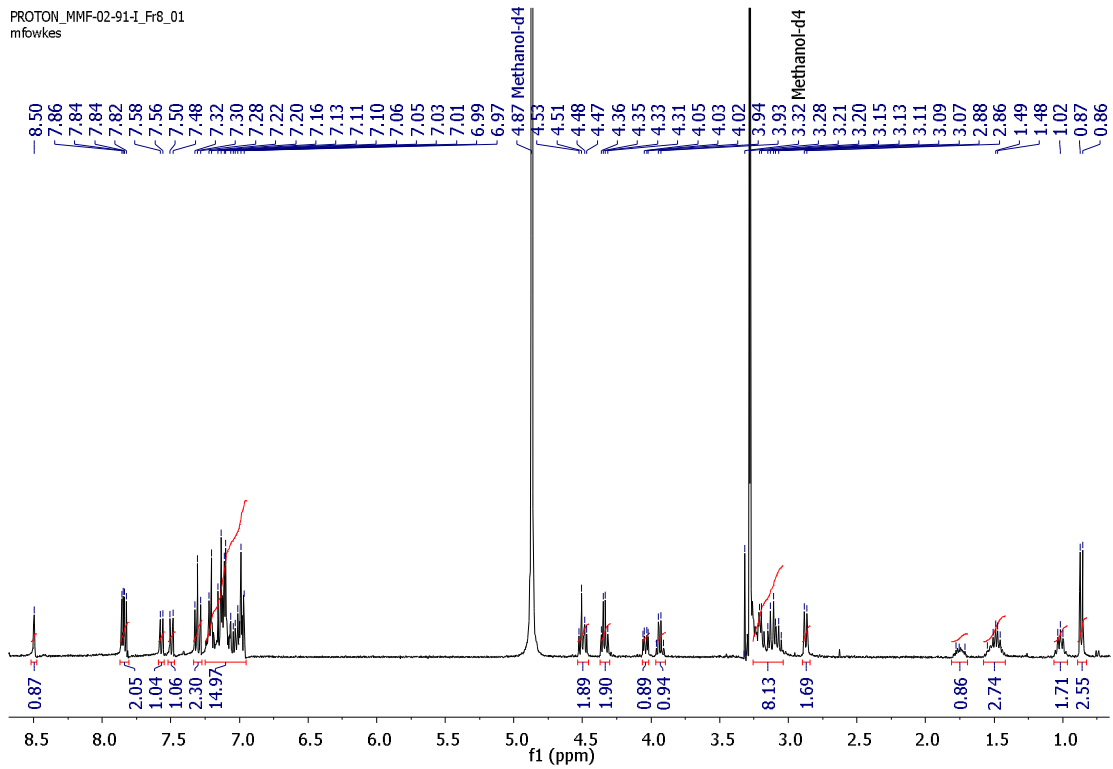


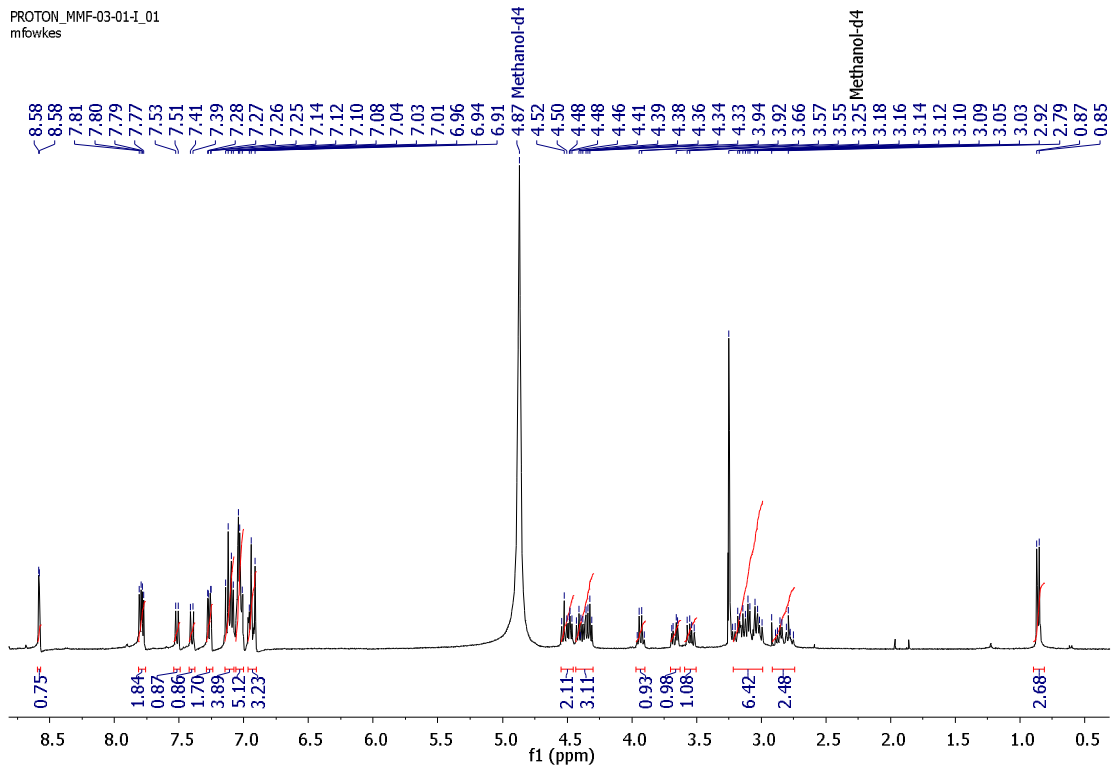
LCE00269: H-Inp-His-D-2-Nal-D-2-Nal-Lys(4-FB)-NH₂

PROTON_MMF-01-140-H_Prep2_Fr6_01
mfowkes

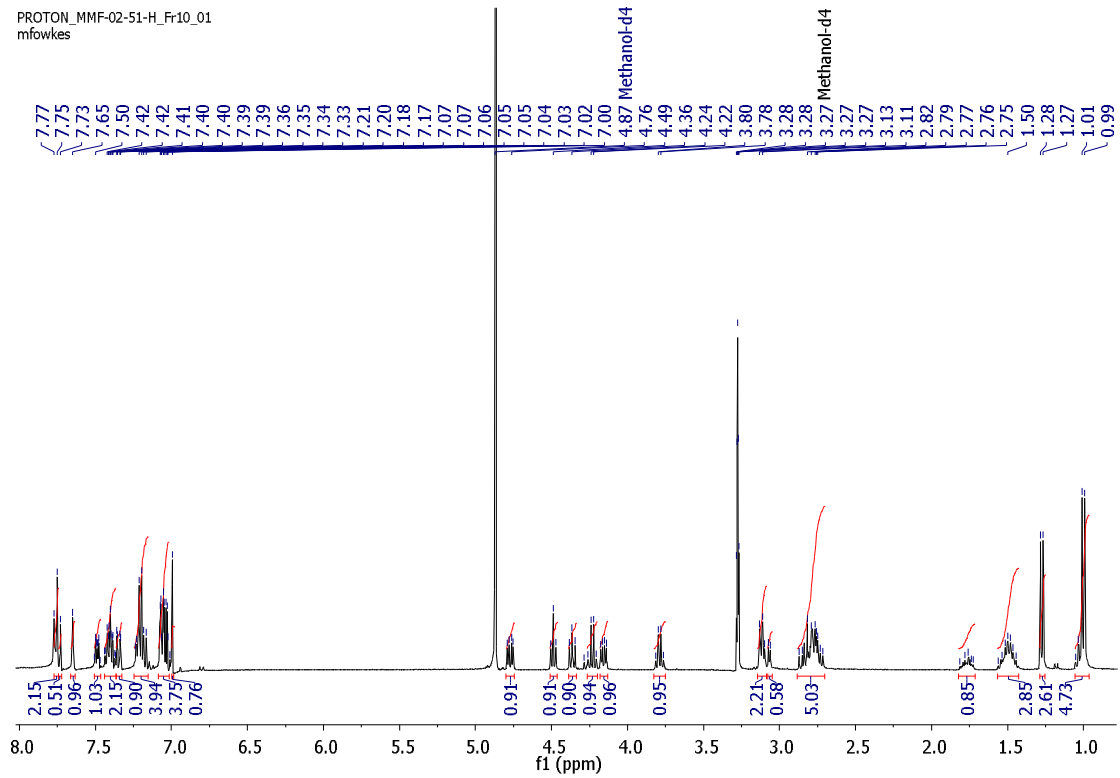


LCE00270: H- Inp-D-2-Nal-D-2-Nal-1-Nal-Lys(4-FB)-NH₂PROTON_MMF-01-115-H_Prep2_Fr17_01
mfowkes

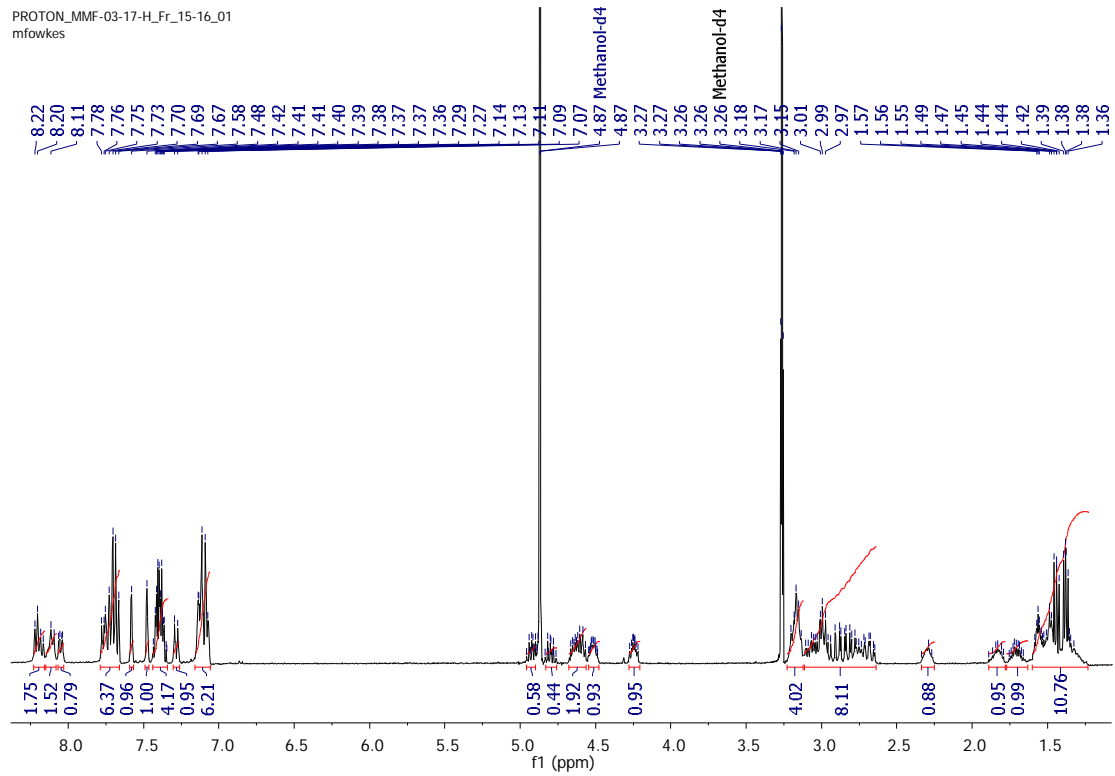
LCE00272: H-His-D-Trp-Ala-Trp-D-Phe-Lys(4-FB)-NH₂

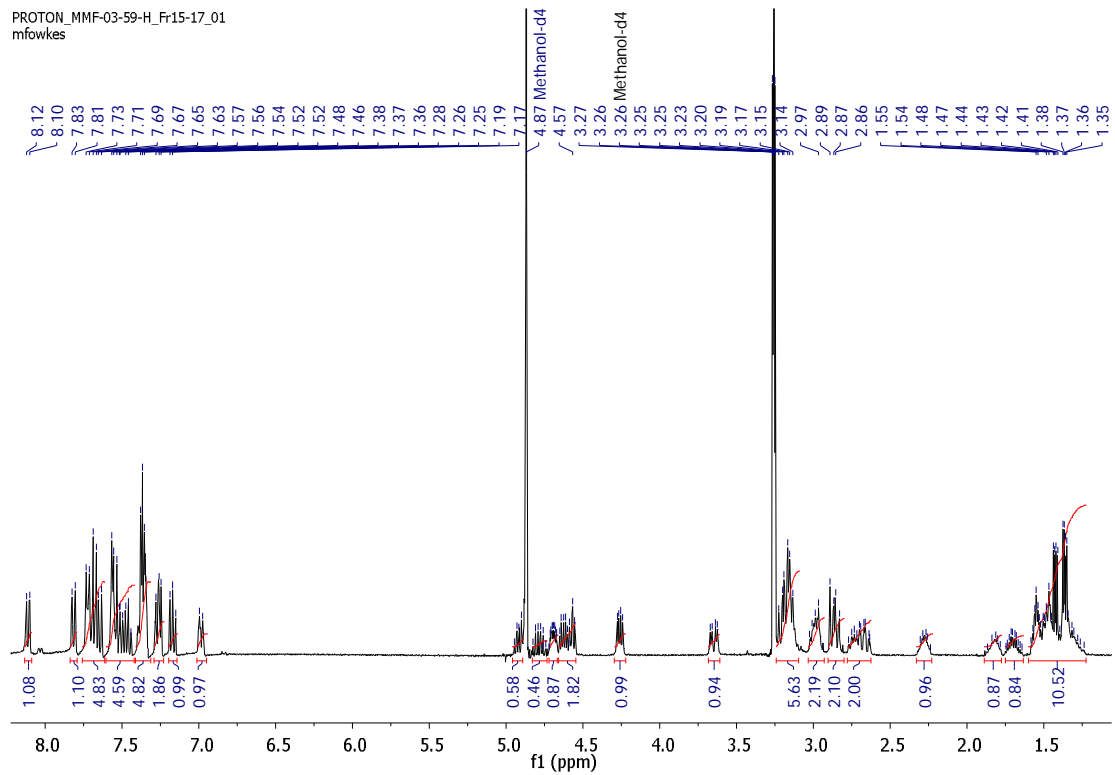
LCE00281: H-His-D-Trp-Ala-Trp-D-Phe-Dpr(4-FB)-NH₂

LCE00282: H-D-Ala-D-2-Nal-Ala-Trp-D-Phe-Lys-NH₂

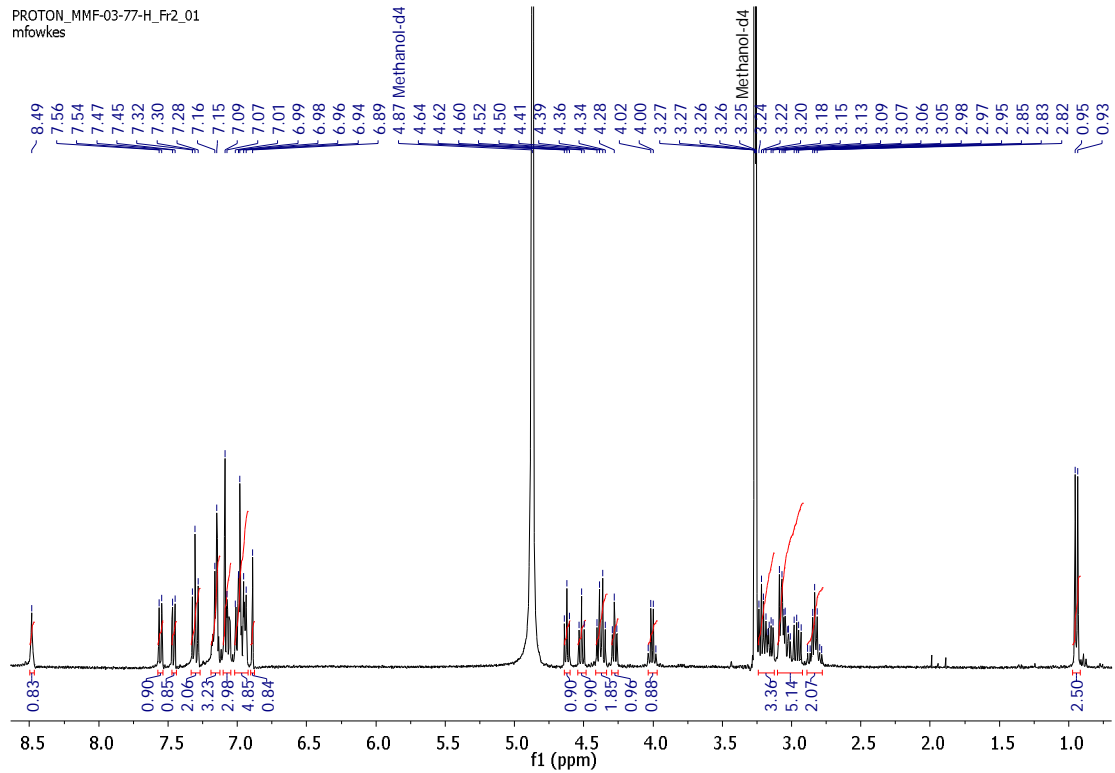


LCE00295: H-Inp-D-2-Nal-D-2-Nal-Phe-Lys(2-FP)-NH₂



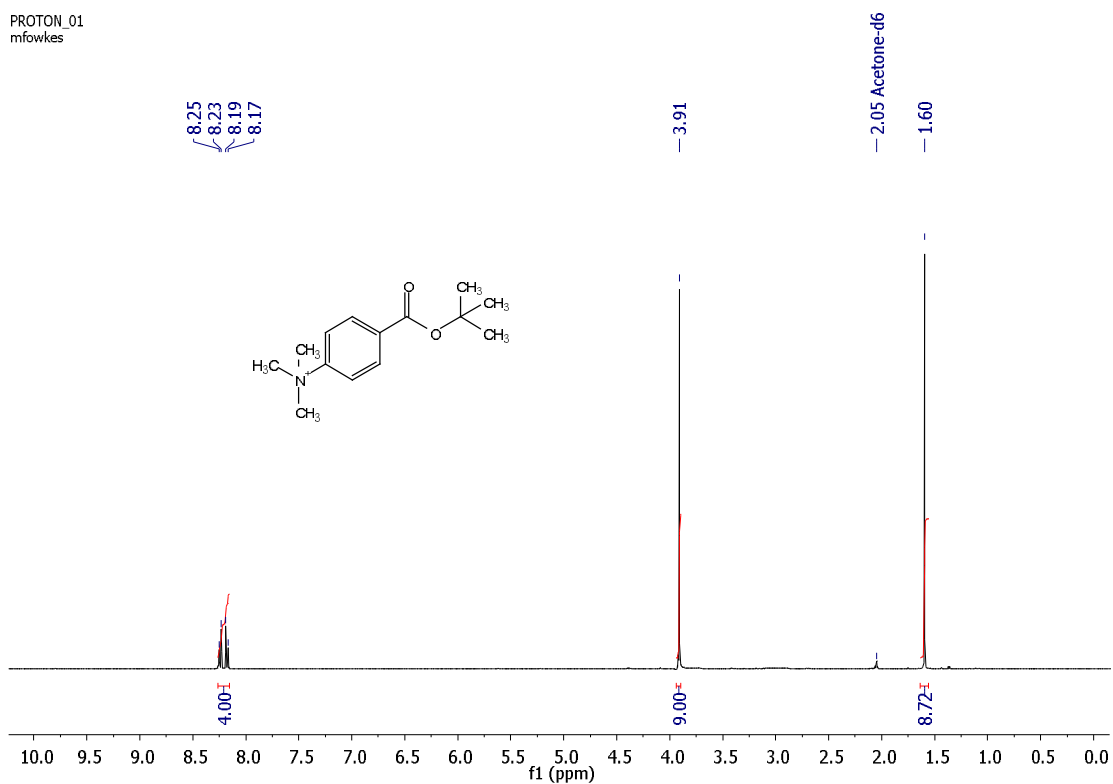
LCE00297: H-Inp-D-2-Nal-D-2-Nal-1-Nal-Lys(2-FP)-NH₂

LCE00298: H-His-D-Trp-Ala-Trp-D-Phe-Dpr-NH₂



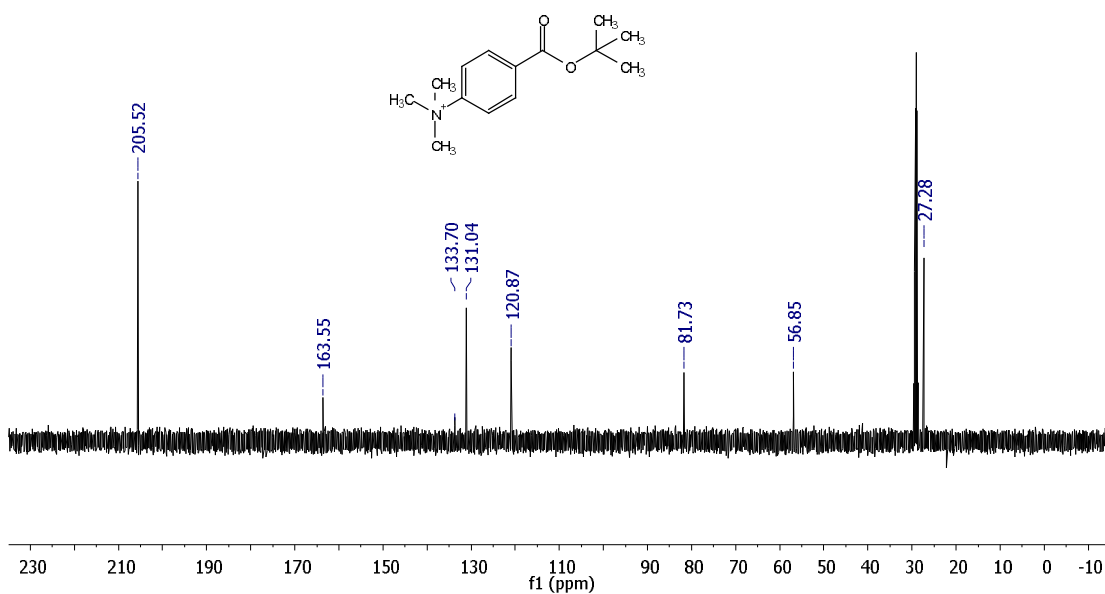
Appendix D: Triflate Salt ^1H -NMR and ^{13}C -NMR Spectra

$^1\text{H-NMR}$ Spectrum of 4-(*tert*-butoxycarbonyl)-*N,N,N*-trimethylbenzenammonium triflate salt



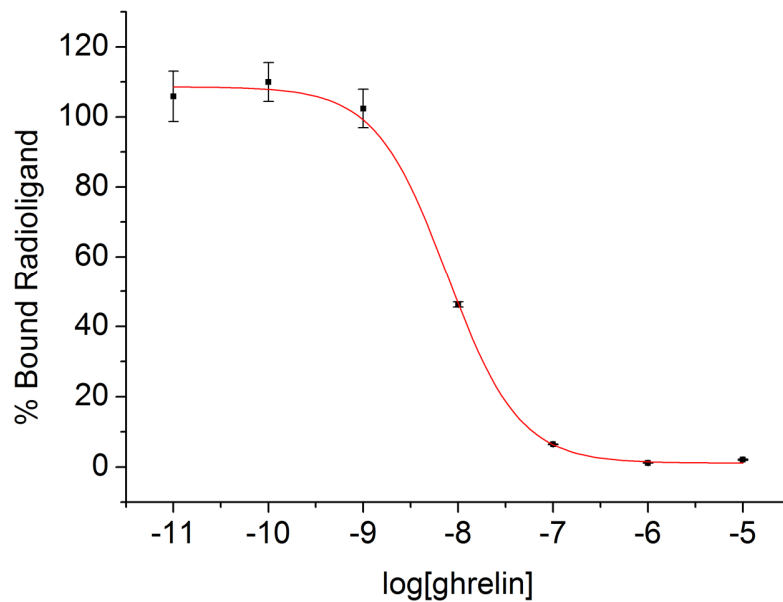
^{13}C -NMR Spectrum of 4-(*tert*-butoxycarbonyl)-*N,N,N*-trimethylbenzenammonium triflate salt

CARBON_01
mfowkes

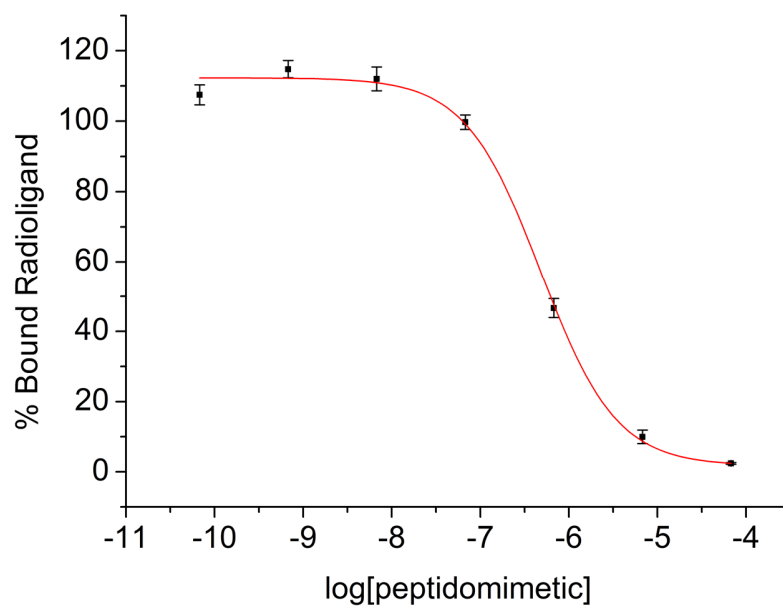


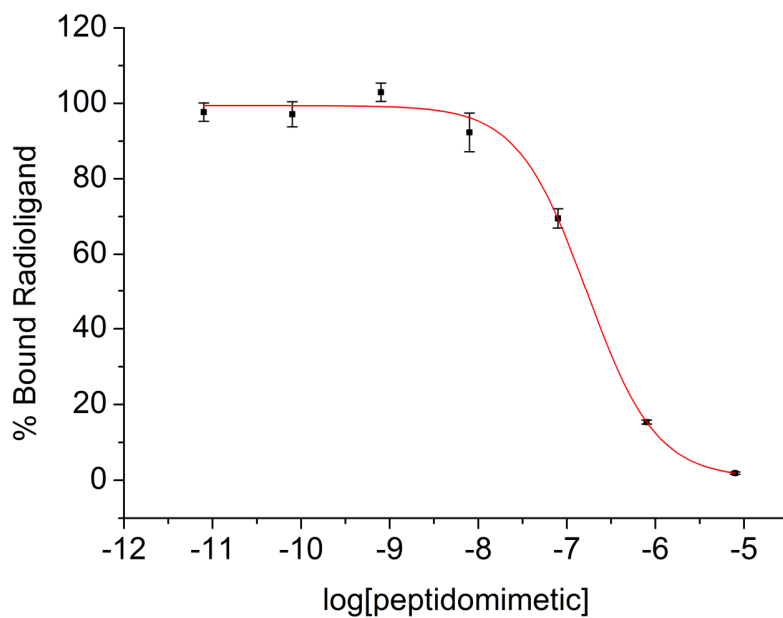
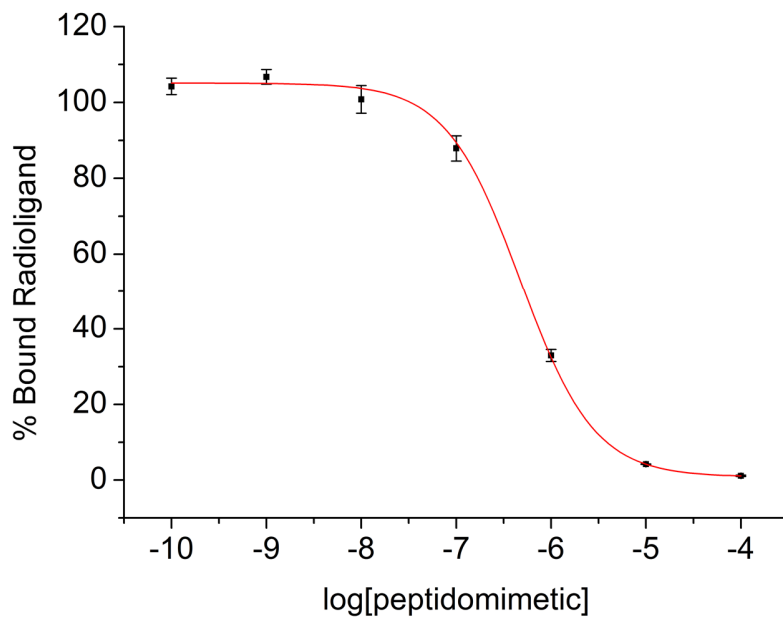
Appendix E: Peptidomimetic Displacement Curves

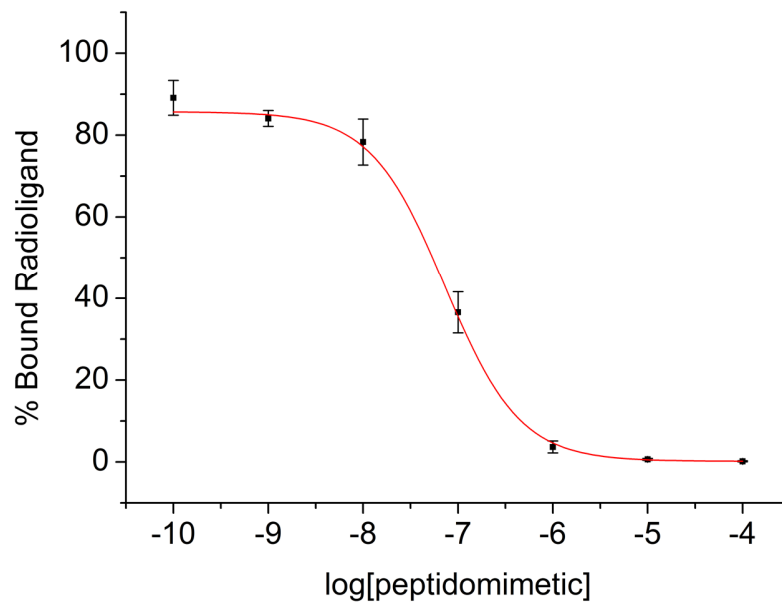
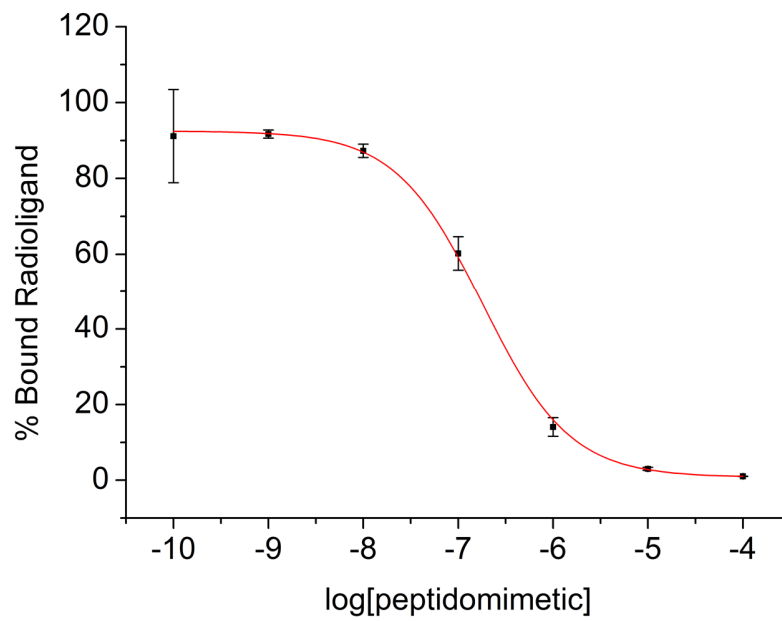
Ghrelin 1-28

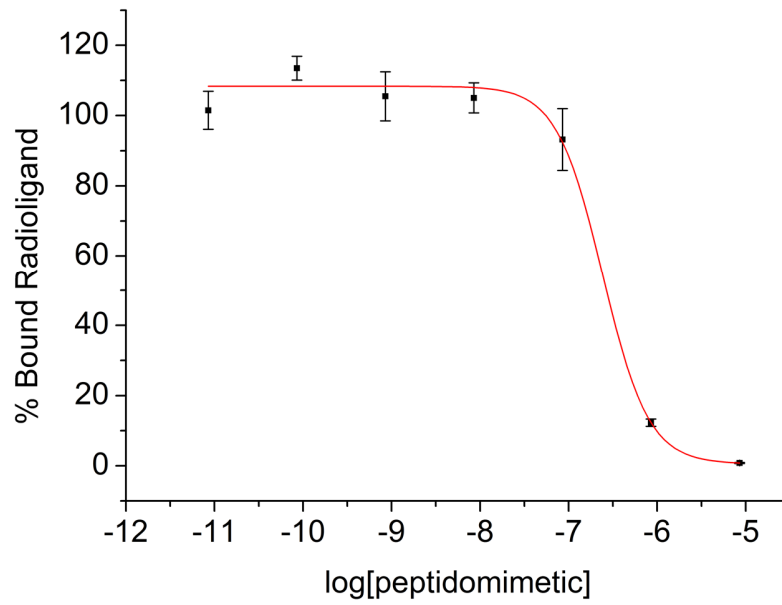
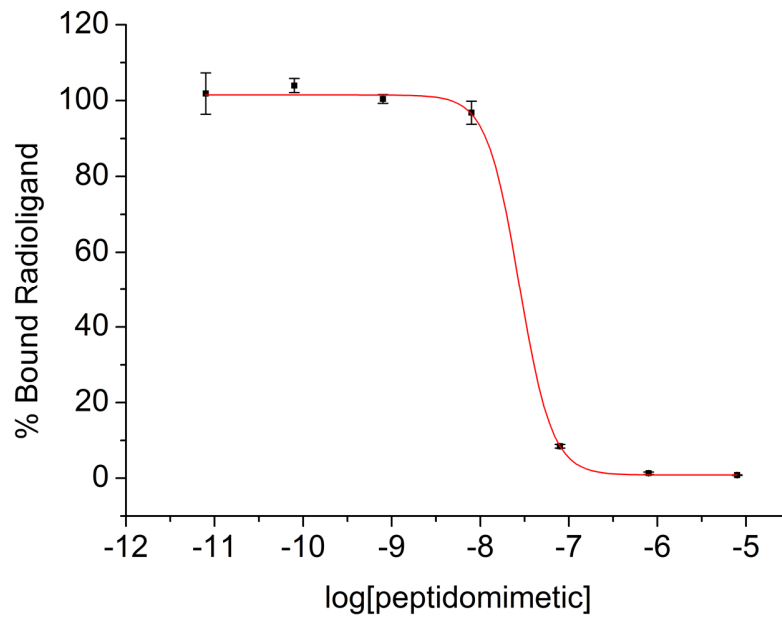


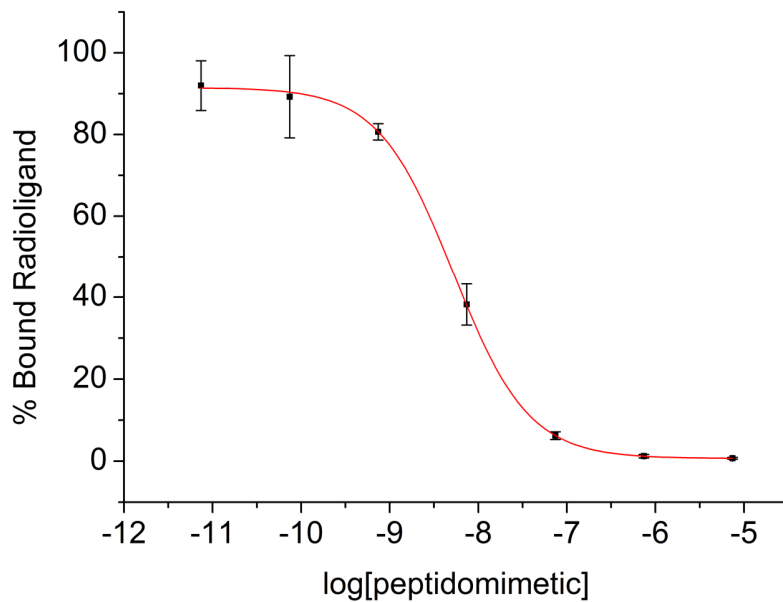
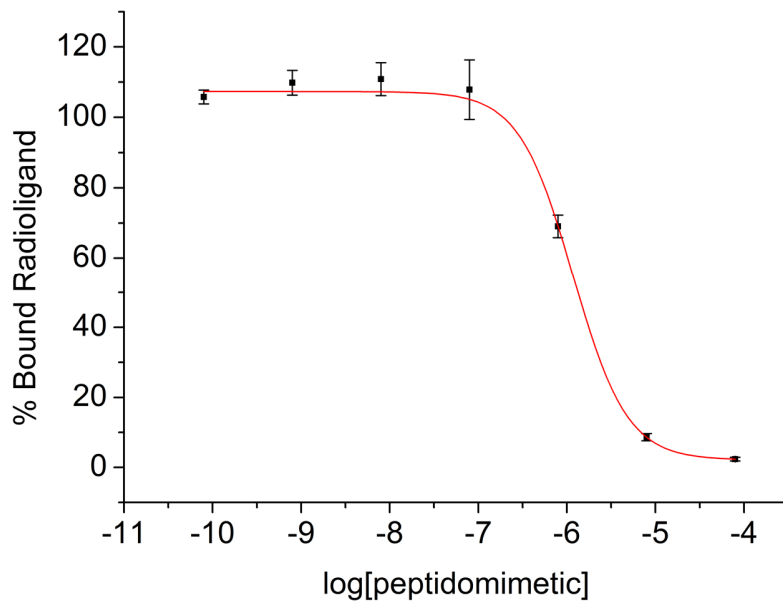
LCE00210

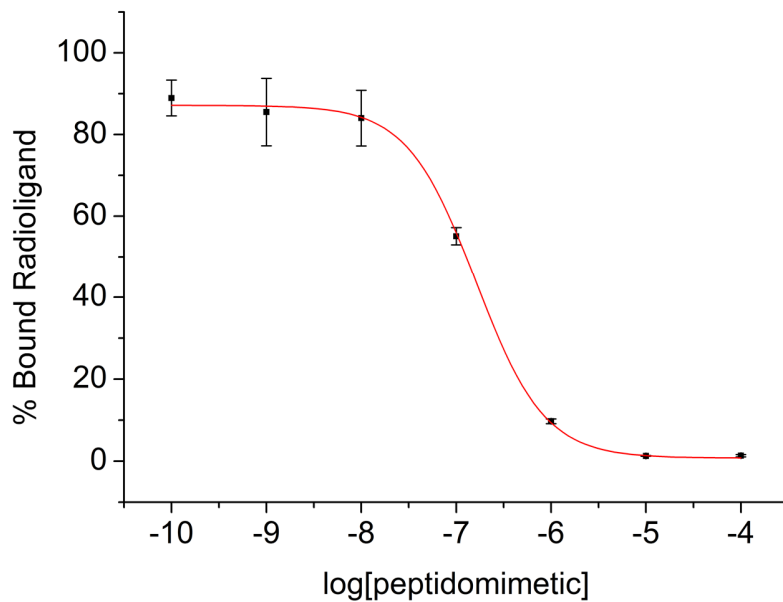
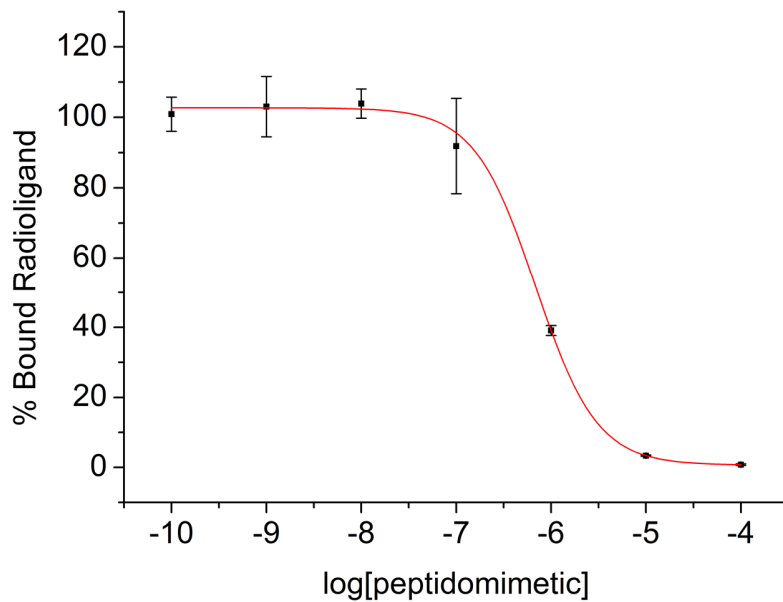


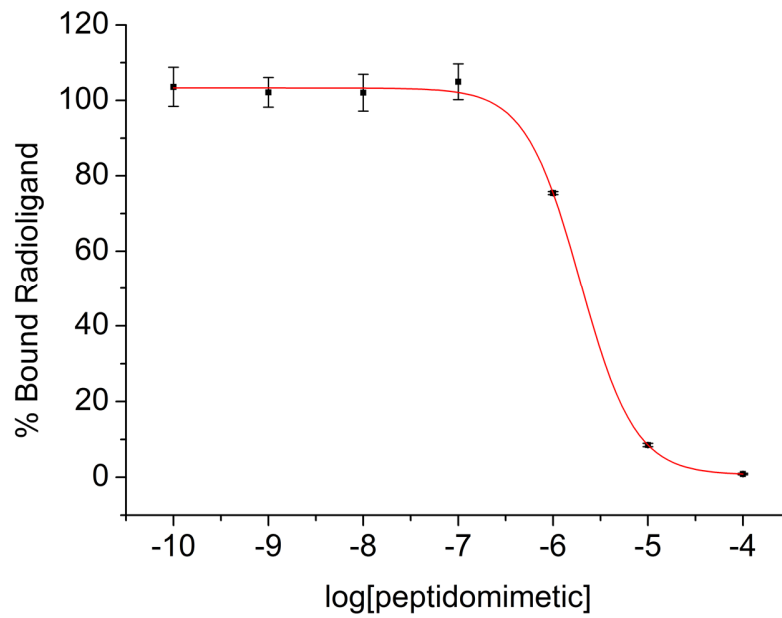
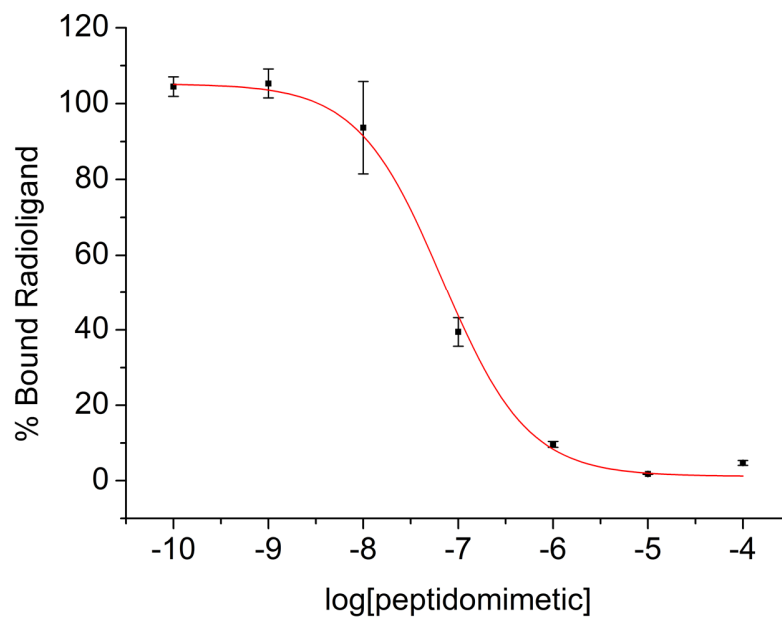
LCE00211**LCE00217**

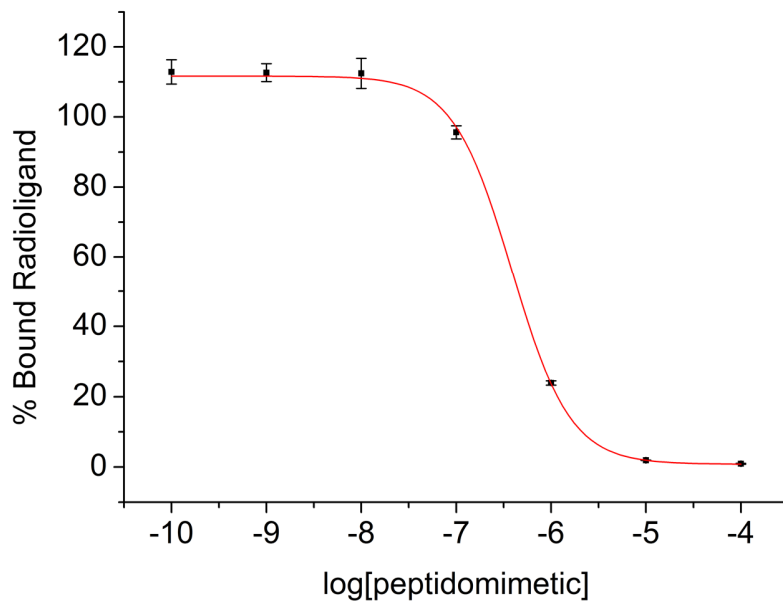
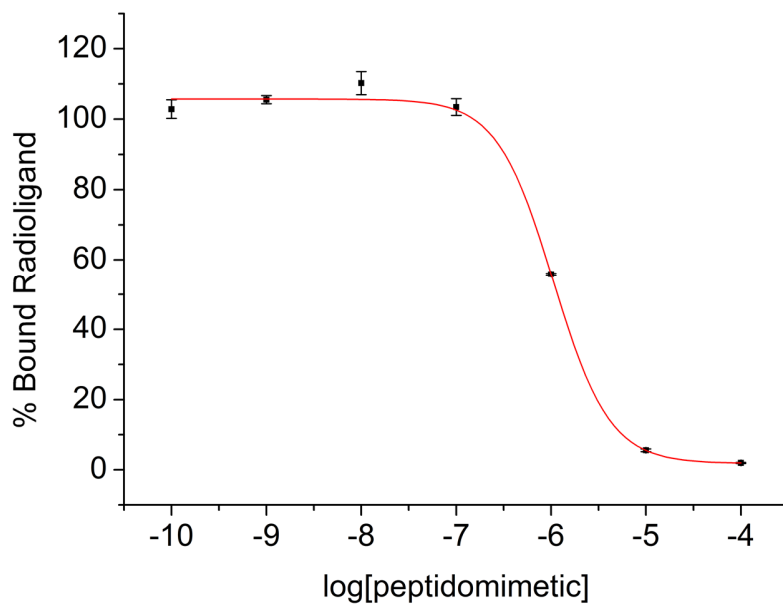
LCE00239**LCE00240**

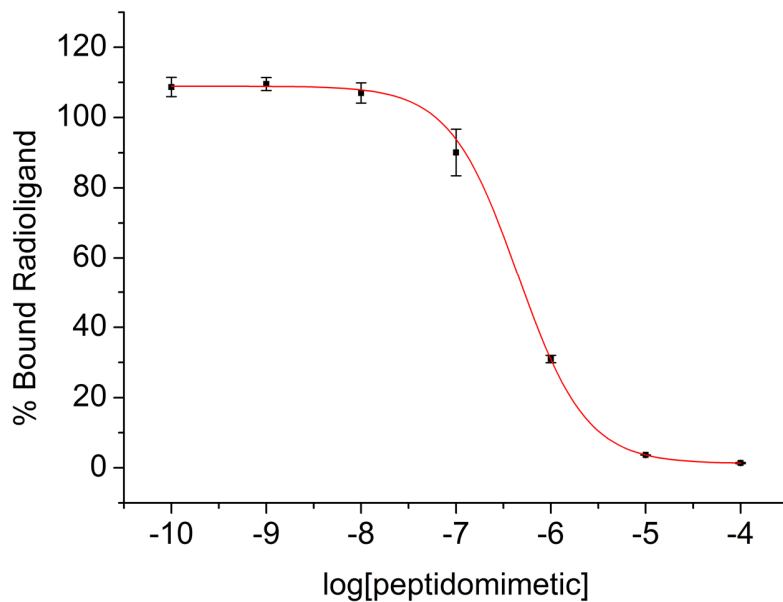
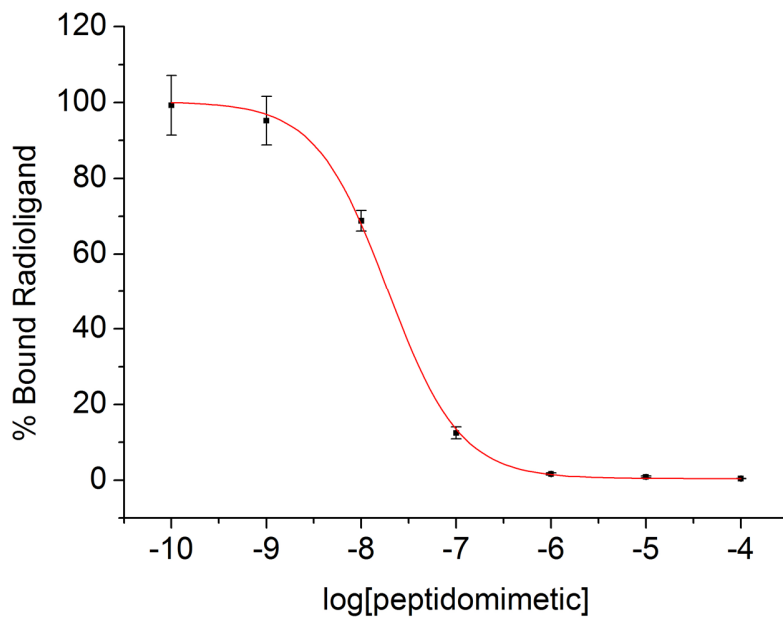
LCE00243**LCE00244**

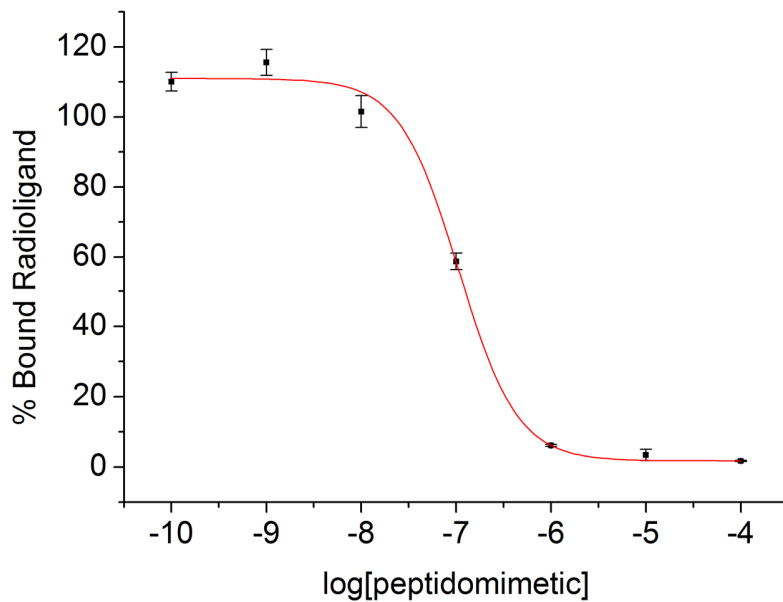
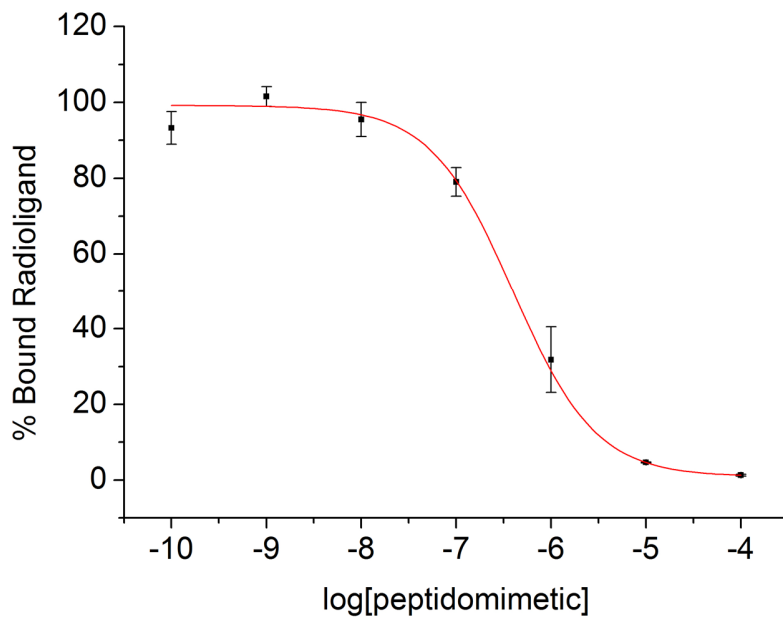
LCE00245**LCE00246**

LCE00267**LCE00268**

LCE00269**LCE00270**

LCE00272**LCE00281**

LCE00282**LCE00295**

LCE00297**LCE00298**

Curriculum Vitae

Milan Mrázek Fowkes

Educational Qualifications:

2012-2014 Western University (Ontario, Canada)

- Candidate for Master of Science (M.Sc.) degree in Chemistry (Molecular Imaging).

2007-2011: University of Warwick (Coventry, England)

- Master of Chemistry, MChem (First class honours).
- Final year modules: *Synthetic Chemistry I-III, Electrochemistry and Nanotechnology.*
- Final year project: *Bond Rotation and Radical Cyclisation Studies of N-alkenyl-N-2-bromobenzyl Acetamides.*

Research Experience:

- 2010-11 (20 weeks): Research project on “*Bond Rotation and Radical Cyclisation Studies of N-alkenyl-N-2-bromobenzyl Acetamides*” (Supervisor: Dr. Andrew Clark).

Course Work

- Mechanistic Organic Chemistry 9553A (Autumn 2012, 90%).
- Molecular Imaging 9518B (Winter 2012, 95%).
- Chemistry 9658 Seminar (Winter 2013, 94%).

Abstracts

- Fowkes M.M., McGirr R., Dhanvantari S., Luyt, L.G. *Peptidomimetic GHS-R1a Agonists as PET Imaging Agents for Prostate Cancer*, CIHR-STP in Cancer Research & Technology Transfer Research and Education Day 2013 [poster presentation].
- Fowkes, M.M. Dhanvantari, S. Kovacs, M. Luyt, L.G. *Peptidomimetic GHS-R1a Agonists as PET Imaging Agents for Prostate Cancer*, 97th

Canadian Chemistry Conference and Exhibition (CSC), Vancouver, B.C.,
Canada, June 1-5th 2014 [oral presentation].

Teaching Experience

- 2012-2014: Teaching Assistant for Chemistry 2213a.
- 2013-2014: Teaching Assistant for Chemistry 2273a and 2283g.

Honours and Awards

- 2012 Western Graduate Research Scholarship.
- 2013 Western Graduate Research Scholarship.
- 2013 Nominated for a Graduate Student Teaching Assistant (GSTA) Award.